Utrecht University
Copernicus Institute of Sustainable Development

Master Thesis Energy Science
GEO4-2510
30 ECT

Towards a zero-emission construction site by utilizing a fuel cell-battery system and renewable energy

Peter Bakker
7042744
14-7-2023

EMMETT GREEN

Supervisors:
dr. Madeleine Gibescu (Utrecht University)
ir. drs. Michiel Wildschut (Emmett Green)

Second Reader:
dr. Hamed Aslannejad (Utrecht University)

Abstract

The construction sector is a large energy consumer, contributes to the global GHG emissions significantly, and is a conservative sector where positive change goes slowly. In addition to that, current diesel-fuelled construction sites have additional negative impacts such as the emission of nitrogen and PM_x, as well as excessive noise. Although technical solutions for electrification and increasing energy efficiency are available, however, several socio-techno-economic barriers limit their implementation. This study examined five potential configurations for electrifying a pilot construction site utilizing the Dutch electricity grid, an LFP battery, and a PEM fuel cell (FCPB-system) in different sizes. The results indicate that the electricity grid and a battery are currently the cheapest option; while PEM fuel cells and green hydrogen are very expensive. However, green hydrogen is the most environmentally friendly option compared to the Dutch electricity grid now and in the future. The yearly energy costs from the FCPB-system are significantly higher compared to the fuel costs of current diesel machinery. The LCOS and LCOE of the LFP battery and PEM fuel cell respectively, are mostly sensitive to a change in efficiency, technical lifetime, and electricity/hydrogen price. From an environmental perspective, the FCPB-system can reduce CO_2 emissions in the conservative construction sector. Additionally, the FCPB-system does not emit any nitrogen due to the absence of combustion and high temperatures which is currently an important benefit for the construction sector in The Netherlands. One additional advantage of the FCPB-system is the capability of utilizing renewable energy. The results indicate that configurations with a battery have the most potential for utilizing renewable energy on construction sites. The energy cost reduction increases with the increase of battery size and use and the use of expensive green hydrogen; while CO_2 emission reduction is mostly found in the grid-connected configurations. Renewable energy is very interesting for reducing energy costs and further a reduction in CO_2 emissions.

TABLE OF CONTENT

1. INTRODUCTION

1.1. SCIENTIFIC AND SOCIAL RELEVANCE

The construction sector is a relatively traditional sector where change and progression go slowly (Palm & Bryngelson, 2023). Globally, the construction sector is witnessing a rise in GHG emissions and energy consumption, a lack of significant progress in implementing new and existing policies, and a decline in the growth of energy-efficiency investments (Global Alliance for Buildings and Construction, 2019; Stokke et al., 2023). According to the IEA data, in 2018 the building and construction sector accounted for 36% of the global final energy consumption and 39% of GHG emissions (IEA, 2022). The contribution of just the construction sector is 6% and 11% respectively. The GHG emissions from these sectors greatly contribute to climate change caused by the greenhouse gas effect, leading to an increased likelihood of extreme weather events, loss of biodiversity, and rising sea levels (IPCC, 2021). The majority of emissions on construction sites come from heavy equipment, primarily powered by diesel (Barati & Shen, 2017). Furthermore, equipment compatibility and efficiency also play an important role in determining emissions per unit of conducted work (Ahn & Lee, 2013). Given the importance of reducing energy consumption and GHG emissions, the construction sector has to make large improvements. Nevertheless, energy efficiency at construction sites is so far an under-researched topic (Palm & Bryngelson, 2023).

Besides the GHG emissions from diesel combustion, it also results in the release of NO_x, NH_3, small particles (PM_x), and noise pollution in urban areas. As for now, the emission of nitrogen is a large problem for the Netherlands as it currently limits the opportunity to build new projects which is extremely delaying the plans of the Dutch government to build approximately 1.000.000 residential homes by 2030 (Rijksoverheid, 2021). In the past few years, the Netherlands increased their rate of building new dwellings up to approximately 70.000 dwellings per year (CBS, 2023). However, to reach the 2030 goal the Netherlands must build twice as many buildings per year.

Too much nitrogen emissions can have negative effects on the environment such as the formation of acid rain and it contributes to nutrient pollution which harms sensitive ecosystems such as lakes and forests. Some plant species grow faster as a consequence of the nutrient pollution overgrowing other plant species causing the disappearance of animal species including insects and birds (Soons et al., 2017). In 2021, a new law is introduced to reduce the nitrogen (NO_x, NH_3) deposition below the critical threshold for at least half of the "natura 2000-gebieden" by 2030 (Milieucentraal, n.d.). Construction projects may not exceed the critical threshold of 0,00 mol/ha/year in an area of 25 kilometres around the source of emission (Provincie Noord-Holland, 2020; Rijksoverheid, 2020). Besides the construction sector, other sectors such as industry, aviation, and agriculture must contribute to this 2030 goal and can receive financial aid. The Dutch Economic Institute for the Construction sector (Economisch Instituut voor de Bouw, EIB) concludes that the current legislation is slowing down the process of building new dwellings (EIB, 2023).

Therefore, the Netherlands introduced a subsidy named "Subsidieregeling Schoon en Emissieloos Bouwmaterieel (SSEB)", which is specifically meant for emission-free construction equipment and improvements for the electric infrastructure (RVO, 2022). This subsidy is introduced to aid in the shift towards a future-proof construction sector by increasing the sustainability of construction equipment that emits less NO_x. Additionally, the SSEB subsidy contributes to the climate agreement and the clean air agreement and stimulates the market for emission-free construction equipment (RVO, 2022).

The Global Alliance for Buildings and Construction (GABC, an alliance between the IEA and UN) published a global status report with global roadmap recommendations to improve the transition towards a zero-emissions, efficient and resilient buildings and construction sector (Global Alliance for Buildings and Construction, 2019). These roadmap recommendations are primarily focused on reducing the energy use of existing and new buildings by improving energy systems within the buildings and reducing the impact of materials used in construction. However, no recommendations are made to improve the efficiency or sustainability of heavy construction equipment on the construction site.

Stokke et al., (2023) explored the opportunities and challenges of using green public procurement to achieve zero-emission construction sites. Several barriers and critical success factors (CSF) for successful zero-emission construction sites were found during the study. The main named barriers are a limited market, technology, lack of knowledge, high costs, limited suppliers of electrical machinery, and lack of charging infrastructure (Stokke et al., 2023). According to this study, CSFs for zero-emission construction sites are raising awareness for the market and decision makers, economic and environmental gains, and considering local contractors. Palm and Bryngelson (2023) performed analysed the barriers and drivers for improving energy efficiency at construction sites. Similar barriers were found during this study such as high costs, low electricity prices, lack of regulations, lack of knowledge and information, and conservatism of the industry (Palm & Bryngelson, 2023). Some drivers for improving energy efficiency at construction sites according to Palm & Bryngelson (2023) are support schemes, regulations enforcing energy efficiency, environmental and building certifications, network and education, competitions between construction sites, client demand, and technology. Both studies found several barriers and drivers/CSFs which are related to (available) technology, information, organization, economics, and environment.

There has been significant progress in on-road vehicle electrification. However, the majority of construction equipment (off-road vehicles) is still using diesel engines. So far, research has primarily focused on hybrid electric configurations and fuel replacement (including biofuels) of construction equipment. The possibilities of battery-electric alternatives have not been explored to the same extent as hybrid configurations (Un-Noor et al., 2021). An assessment of the operational feasibility of battery-electric construction equipment was performed by Un-Noor et al., (2021). Results of this study showed that 4 out of 6 equipment categories can be electrified, while the remaining 2 categories are more suitable for hybridization due to high energy demands. The findings of Un-Noor et al., (2021) indicate that a majority of construction equipment can be electrified using battery-electric powertrains.

The National Renewable Energy Laboratory (NREL, 2022) published a report about R&D gaps and opportunities to decarbonize off-road vehicles and energy systems integration. The off-road sector (all sectors using heavy-duty vehicles including the construction sector) has very specific and extreme performance requirements such as high temperatures, restricted and dusty environments, rough operation conditions, and demanding duty cycles, which are not common in lighter-duty vehicles. According to the NREL, this sector must advance multiple technical pathways in search of the best fit for specific applications while meeting specific requirements. Many technical and deployment strategies are possible considering different options for fuel, energy sources, generators, and vehicles (NREL, 2022). However, determining the most suitable technologies requires an understanding of different duty cycles, refuelling/repowering strategies, and finding the optimal fuel and powertrain combinations (NREL, 2022). The NREL considers four key technology areas that are of utmost importance to achieve a carbon-neutral construction: battery-electric and fuel cell vehicles, low-carbon fuels for existing internal combustion engine stock, operational efficiency, and availability of green electricity and hydrogen. Other important factors that complicate the decarbonization of construction sites are the changing power demand across the project period and the fact that projects

are usually temporary, operating from months to a few years (NREL, 2022). Nevertheless, this suggests the opportunity for modular energy systems and energy model systems (EMS).

Multiple technologies can be deployed as modular energy systems such as batteries, flywheels, hydraulic accumulators, and fuel cells. Un-Noor et al., (2021) concluded that large batteries, fast chargers with more capacity, and innovative charging solutions can increase the electrification of construction equipment. Lin et al., (2020) described the development and key technologies of pure electric construction machinery. The results of this study showed that there are still lots of challenges to overcome in order to electrify construction equipment. For a successful deployment of electric machinery, properties like specific energy, costs, safety, and compatibility with the power grid should be improved (Lin et al., 2020).

In the last couple of years, experiments on electrifying construction sites are being done. Such as the employment of a large battery of 2.32 MWh (Bouwmachines.nl, 2023) and a solar aggregate (Volta Energy, n.d.) in the Netherlands, and a hydrogen-fuelled fuel cell in the UK (CNBC, 2020). However, a completely electric construction site seems still a challenge to achieve.

The emphasis of this thesis is to identify the possibilities for a successful implementation of a modular and mobile energy system consisting of a hydrogen-fuelled fuel cell and a battery with limited to zero grid capacity. As modular and mobile energy systems are necessary to further electrify the construction sector, improve its sustainability and make it possible to execute projects with limited grid capacity. Therefore, a pilot initiated by Green Planet will be used as a case study.

1.2. ABOUT THE PILOT

The pilot is an electric construction site for new residential homes in the Netherlands (Greenplanet, n.d.). Instead of using conventional diesel equipment, battery-electric construction equipment will be used for construction activities. The focus of this pilot is to contribute towards a solution for zero-emission construction sites with renewable energy (Greenplanet, n.d.). The pilot is being initiated by the company Green Planet and partners including Emmett Green are contributing towards the realization of an electric construction site.

Since the grid capacity is often limited on construction sites, other technologies are needed to provide enough power and energy. Therefore, a combination of two technologies will be deployed to provide the electrical construction equipment with enough energy. The energy system primarily consists of a hydrogen-fuelled fuel cell (FC) and a battery (also called the FCPB-system) with limited grid capacity. The hydrogen will come from the hydrogen hub Delfzijl which is being transported to the construction site. Hydrogen will be stored and transported by exchangeable storage containers. Since the hydrogen comes from Delfzijl it can be assumed that the construction site is nearby and somewhere in the province of Groningen. The exact location and size of the pilot still have to be clarified yet. Figure 1 shows a schematic example of the electric construction site pilot.
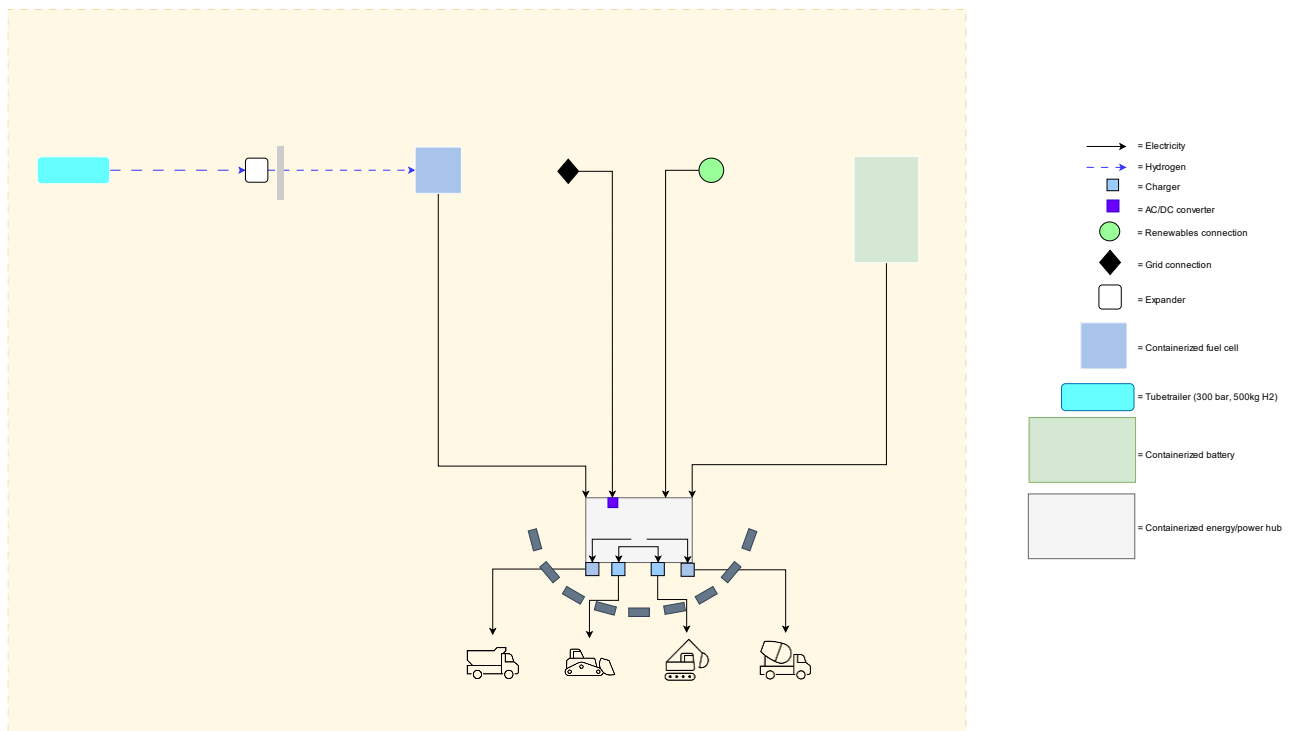
Figure 1 Schematic example of a zero-emission construction site

1.3. RESEARCH SCOPE

The scope of the research is primarily the operational phase of the construction site considering the energy and power demand, energy system and emissions. The technical, economic, and environmental aspects of the energy system will be considered to propose multiple strategies for implementing the FCPB-system on construction sites.

The technical analysis considers the technical specifications of the construction machines which leads to an energy profile. Thereafter, the energy profile is used to determine the minimum required size of the LFP battery, PEM fuel cell and container size. The energy distribution is a result of simulations and the lifetime of both technologies are considered. The results of the technical analysis form the basis for the economic and environmental analysis. The economic analysis considers the investment costs (CAPEX) for the FCPB system including containerizing these technologies, operational costs (OPEX), and the yearly energy costs. Then, the levelized cost of storage and energy (LCOS & LCOE) are calculated for the LFP battery and PEM fuel cell. Finally, a sensitivity analysis is performed to find sensitive parameters of the FCPB-system. For the environmental analysis, a Well-to-Wheel approach is taken into account for calculating the CO2 emissions from energy consumption, which means that the emissions from production and operational-phase are taken into account. Only for the nitrogen emissions (NO_x and NH_3) the on-site emissions are taken into account as these emissions are tested by the law in this way.

The results of the economic and environmental analyses are compared to the Business-As-Usual (BAU) scenario. The utilization of renewable energy for an electric construction site is viewed from both an economic and environmental perspective. In addition to that, future CO_2 emission factors are used to simulate the future CO_2 emissions of the FCPB-system.

Business-As-Usual (BAU)	FCPB-system		
	Technical Analysis	**Economic Analysis**	**Environmental Analysis**
Diesel Consumption	Energy Profile	CAPEX OPEX Energy Costs	NO_x & NH_3
Fuel Costs	Required power, capacity, & container size	LCOS & LCOE	CO_2
CO_2	Energy Distribution	Sensitivity Analysis	Future Emission Factors
NO_x & NH_3	Lifetime FCPB	Renewable Energy	Renewable Energy

Figure 2 Research scope

2. THEORETICAL BACKGROUND

2.1. HYDROGEN TECHNOLOGY

2.1.1. Hydrogen production

Compared to other fuels, hydrogen has some unique characteristics. It can be produced by water and it is the most abundant element in the universe (Jain, 2009). Hydrogen is the lightest chemical element (1 g/mol) and therefore the lightest fuel and has the highest specific energy per mass. Compared to diesel, which is the main fuel being used in heavy-duty vehicles, the lower heating value (LHV) of hydrogen and diesel respectively 120 MJ/kg (= 33.3 kWh/kg) and 42.6 MJ/kg (= 11.83 kWh/kg) (Engineering Toolbox, 2003). However, the energy density of hydrogen per volume is the lowest among fuels. Under ambient conditions, a litre of hydrogen contains only 0.0108 MJ/litre while diesel contains around 36 MJ/litre (Engineering Toolbox, 2003).

Different from fossil fuels, hydrogen is an energy carrier that must be produced from other sources of energy. There are several possibilities of producing hydrogen such as steam methane reforming, coal gasification, biomass gasification, microbial biomass conversion, and thermochemical water splitting cycles (TWSC) (Shadidi et al., 2021). The current industrially established processes for hydrogen production are steam methane reforming and coal gasification due to their relatively low costs (Shadidi et al., 2021). More than 90% of the total hydrogen is produced using the steam methane reforming process (Shadidi et al., 2021). The sustainability of hydrogen is dependent on the production process and energy source, so the current hydrogen (production) cannot be called sustainable yet. Hydrogen produced from fossil fuels is often referred to as "grey hydrogen".

Producing hydrogen in a sustainable way ("green hydrogen") is possible using electrolysis and renewable energy. Electrolysis is the process of splitting water (H_2O) into hydrogen gas (H_2) and oxygen (O_2) using electricity. An electrolyser has an electrochemical cell filled with pure water and has two electrodes which are connected to an external power source (Zoulias et al., 2017). When the critical voltage level is reached, the electrodes start producing hydrogen gas at the negatively biased electrode (cathode) and oxygen at the positively biased cell (anode). By the use of a diaphragm, gas receivers can collect hydrogen and oxygen (Zeng & Zhang, 2010). The amount of gases produced is related to the current (voltage) that flows through the electrochemical cell (Zoulias et al., 2017). Figure 3 shows a schematic overview of an electrochemical cell for hydrogen production.
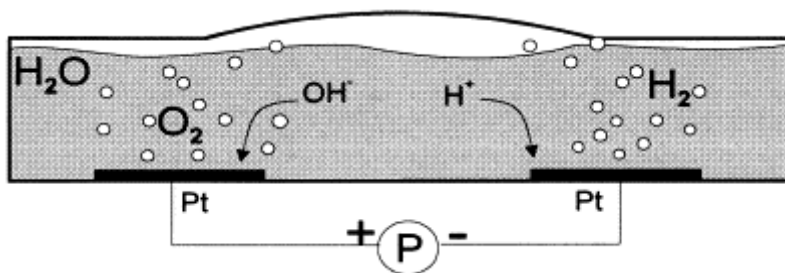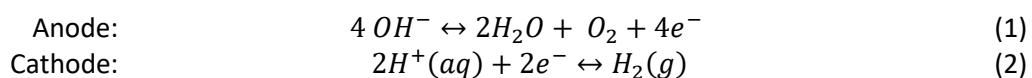

Figure 3 Schematic overview of an electrochemical cell for hydrogen production (Neagu et al., 2000)

Zoulias et al., (2017) described the basic process of water electrolysis. During electrolysis, two chemical reactions can be distinguished:

Anode:	$4\,OH^- \leftrightarrow 2H_2O + O_2 + 4e^-$	(1)
Cathode:	$2H^+(aq) + 2e^- \leftrightarrow H_2(g)$	(2)

The reactions which at the electrodes are slightly different when the water is acidic or basic (Zoulias et al., 2017). There are no side reactions that yields undesired by-products in water electrolysis, therefore the net balance is:

$$2\,H_2O \rightarrow 4e^- \rightarrow O_2 + 2\,H_2 \tag{3}$$

A minimum cell voltage is required to start up the process of electrolysis which is given under standard conditions by the following equation:

$$E_{cell}^o = \frac{-\Delta\,G}{n * F} \tag{4}$$

Where ΔG is the change in Gibbs free energy under standard conditions and n is the number of electrons transferred (Zeng & Zhang, 2010). There are several ways of expressing the efficiency of an electrolyser. First, the performance of an electrolyser can be indicated by calculating the voltage efficiency and thermal efficiency (Zeng & Zhang, 2010):

$$\eta_{voltage} = \frac{(E_{anode} - E_{cathode}) * 100}{E_{cell}} \tag{5}$$

$$\eta_{thermal\,(25^oC)} = \frac{1.481\,V}{E_{cell}} \tag{6}$$

The voltage efficiency is the proportion of effective voltage to split water compared to the total applied voltage which is a good approximation of the system's efficiency. The thermal efficiency relates to the additional cell voltage above the reversible voltage, which is required to maintain the thermal balance within the system. The voltage of 1.481 V indicates operation at thermoneutral voltage. The thermal efficiency of an electrolyser may exceed 100% as the system may absorb heat from the environment if it operates endothermic. The endothermic mode of an electrolyser is shown in Figure 4.
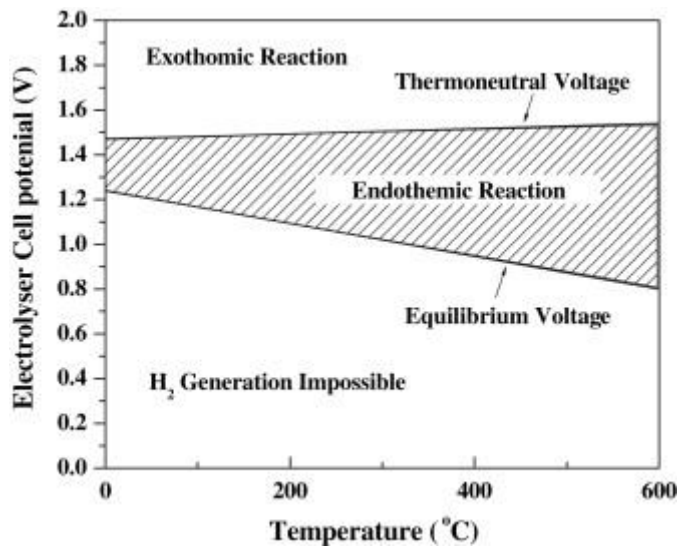
Figure 4 Cell potential for hydrogen production by water electrolysis as a function of temperature (Zeng & Zhang, 2010)

The efficiency mentioned above can be used to compare and evaluate the efficacy of electrolysers. Another way to make a comparison between multiple electrolysers is to calculate the production rate (Zeng & Zhang, 2010):

$$\eta_{H_2,production\,rate} = \frac{V\,(m^3 * m^{-3} * h^{-1})}{u * i * t\,[kJ]} \tag{7}$$

$$\eta_{H_2,yield} = \frac{283.8\,[kJ]}{u * i * t} \tag{8}$$

In the first production rate equation u represents the cell voltage, i represents the current, t represents the time and V is the hydrogen production rate at unit volume electrolyser. This equation expresses the hydrogen production rate per unit of electrical energy input. The second equation t stands for the time needed for the production of one gram of hydrogen. 283.8 kJ is the higher heating value (HHV) of hydrogen.

Methods of water electrolysis
There are several ways of hydrogen production by water electrolysis. Zouilias et al., (2017) reviewed several methods including alkaline electrolysis, proton exchange membrane (PEM) electrolysis, and steam electrolysis which are described briefly below.

Two molecules of water are reduced to one molecule of hydrogen (H_2) and two hydroxyl ions (OH^-) at the cathode during the process of alkaline water electrolysis. Then, the hydrogen exits from the surface of the cathode recombined in a gaseous form and the hydroxyl ions flow through a porous diaphragm to the anode, where they are discharged to ½ molecule of oxygen and one molecule of water. The oxygen escapes at the electrode surface as a gas like hydrogen. The recently developed alkaline electrolysers can withstand temperatures up to 150 °C and variable pressures from 5 to 30 bar. Diaphragms used in this type of electrolyser allow a current density of up to 10 kA/m^2, which is more than three times higher than the conventional low-pressure alkaline electrolyser.

Proton exchange membrane water electrolysis uses a solid electrolyte. A PEM electrolyser is fed with ultrapure water to the porous titanium anode. Hydrated protons are conducted through the membrane from the anode to the cathode. The PEM technology has several advantages over the alkaline such as (1) greater safety and reliability due to the absence of corrosive electrolyte, and (2) the membranes could sustain high differential pressure without being damaged and can efficiently prevent gas mixing (Millet et al., 1995). The operating conditions of a PEM are approximately 10 kA/m^2 with a temperature of 80°C and a cell voltage of 1.75 V.

Conventional electrolysers have a high electricity demand. A method to reduce the electricity demand of electrolysers is steam electrolysis which reaches higher total energy efficiency compared to alkaline and PEM. Steam electrolysis is the process of electrolysing water at high temperatures (800 – 1000 °C) which is more favourable from a thermodynamic point of view. The main advantage is that a substantial part of the required energy is heat which is often cheaper than electricity. The overall increased system efficiency is caused by the high temperatures that accelerate the reaction kinetics, reducing the energy loss due to electrode polarization.

Next to the three methods of electrolysis mentioned above, several other production methods are under development that could become significant in the future hydrogen supply chains, including (Dodds et al., 2015):

- High-temperature electrolysis, using heat from nuclear reactors or concentrating solar power (CSP), which increases the overall process efficiency.
- Thermolysis, which uses extreme heat from nuclear or solar energy to split hydrogen from water.
- Photocatalytic water splitting, which utilizes sunlight to directly produce hydrogen from water.
- Fermentation of biological material, producing hydrogen from direct fermentation.

Water electrolysis is the cleanest way of producing hydrogen (Zoulias et al., 2017). Although, environmental pollution remains unsolved when fossil fuels are the primary source of electricity. Therefore, using renewable energy sources (RES) at times when it is abundant is crucial for the production of emission-free hydrogen.

2.1.2. Hydrogen storage

As described earlier, hydrogen has the lowest energy density per volume among all fuels. Therefore, it's important to reduce its volume to increase the energy density of hydrogen. There are several types of hydrogen storage which increase its density. Two types of hydrogen storage can be distinguished, namely physical storage and chemical storage. Physical storage includes compressed, liquid, and cryo-compressed hydrogen and chemical storage can be distinguished in sorbents (MOF, carbon-based materials), metal hydrides (simple and complex) and chemical hydrides (borohydrides and ammonia borane) (Zhangi et al., 2015). Only the two main physical types of hydrogen storage are described due to the focus of this study.

High-pressure gas storage

Storing hydrogen in high-pressure gas cylinders is the most common way of hydrogen storage (Züttel, 2004). Using this relatively mature method of pressurizing hydrogen gas has several benefits, including low storage energy consumption, relatively low cost (at low to medium pressure), high speed of hydrogen release, releasing at room temperature, and simple to adjust the release of hydrogen by controlling a valve (Zhangi et al., 2015). Compressed hydrogen gaseous storage is mainly used in stationary or vehicle-mounted applications (Zhangi et al., 2015). The maximum amount of pressure depends on the strength of the cylinder material. As the pilot will use cylinders with a pressure of 300 bar (30 MPa), super-compressed hydrogen vessels can withstand pressures up to $70 - 80$ MPa, increasing its volumetric density up to 36 kg/m^3 (Zhangi et al., 2015; Züttel, 2004). Although the volumetric density increases with pressure, the energy density per weight of hydrogen decreases due to the need for increased wall thickness for strength (Züttel, 2004). Besides the relative maturity and benefits of pressurized gaseous hydrogen storage, there is a safety concern, especially in highly populated regions (Züttel, 2004).

Liquid

The other physical way of increasing hydrogens density and storage is by liquefaction. Liquid hydrogen is stored at a cryogenic temperature of 21 Kelvin. The volumetric density of liquid hydrogen is 70.8 kg/m^3, which is roughly twice as high as pressurized hydrogen gas (Züttel, 2004). Liquid hydrogen is an overall good method in terms of mass and volumetric densities, however, there are two major challenges. First, liquefaction of hydrogen is an energy-intense process which can take up to 30% of the total hydrogen energy in practical applications and secondly, it is difficult to achieve the necessary thermal insulation of a liquid hydrogen vessel (Zhangi et al., 2015).

2.1.3. Hydrogen to electricity

Hydrogen can be used in multiple ways to convert it from an energy carrier to useful energy in the form of heat and electricity. It can be used as a fuel for a combustion engine or a fuel cell. Due to the focus of this study, hydrogen combustion is only described briefly.

Hydrogen combustion

Hydrogen can be used as an alternative to natural gas, however, there are several engineering factors which determine the compatibility with different types of gases (Dodds et al., 2015). The Wobbe-index (WI) is often used as a comparison metric for gases. This index indicates the quality of gas by dividing the gross caloric value by the relative density of the gas compared to the air (TU Delft, 2022).

$$W = \frac{Hs}{\sqrt{d}} \tag{9}$$

Where:

W = Wobbe-index [MJ/m^3]

H_s = Gross Caloric Value [MJ/m^3]

d = Relative density of the gas compared to the air [-]

Devices are engineered for gases with a certain Wobbe-index. Using fuel with the wrong Wobbe-index can cause undesired effects such as burner overheating, incomplete combustion (CO-forming) when the WI value is too high or the flame extinguishes when the WI value is too low (Dodds et al., 2015; TU Delft, 2022). The Wobbe-index of pure hydrogen is approximately 48 MJ/m^3 (Zachariah-Wolff et al., 2007), which is within the safety range for burners in some European countries. Although the WI of hydrogen is similar to natural gas, burners that are designed for use with natural gas cannot generally be used directly with hydrogen (Dodds et al., 2015). This is because the combustion velocity, also known as the flame speed, is much higher for hydrogen than for natural gas which leads to a more challenging flame to control and requires a different burner head design (Dodds et al., 2015). In practical terms, it would be necessary to replace all current burner heads in order to burn hydrogen rather than natural gas. However, it should be possible to inject hydrogen to complement the natural gas and lower the carbon content of the supplied gas without changing existing appliances (Dodds et al., 2015).

Fuel cells

Fuel cells are electric cells which – unlike battery cells – can be continuously fed with fuel allowing maintaining electrical power as long as there's fuel (Felseghi et al., 2019). A fuel cell can convert fuel such as hydrogen directly into electricity and heat through an electrochemical reaction of hydrogen with oxygen. This process is the inversed process of water electrolysis:

$$2\,H_2 + O_2 \rightarrow 2\,H_2O + energy \tag{10}$$

Similar to an electrolyser, a fuel cell consists of an anode, a cathode, and an electrolyte. Despite the different types of fuel cells, they all work on the same principle (Felseghi et al., 2019):

1) Hydrogen or a hydrogen-rich fuel is introduced to the anode, where the anode-coated catalyst separates electrons from positive ions (protons).
2) At the cathode, oxygen is combined with electrons and, in some cases, with protons or water, resulting in hydrated water or ions.
3) The electrons that form at the fuel cell anode cannot pass directly through the electrolyte to the cathode, but only through an electrical circuit.

Inside a fuel cell, fuel oxidation takes place at the anode, while molecular oxygen reduction occurs at the cathode (Felseghi et al., 2019). A reaction in which oxidation and reduction find place is also called a redox reaction. Figure 5 shows the working principle and components of a fuel cell. Fuel cells can be classified according to several criteria such as the type of fuel, electrolyte used, or operating temperature. The US department of energy summarized the technical specifications of five fuel cell technologies, which are shown in Table 1. All of the five mentioned fuel cells can use hydrogen, however, only PEM, AFC, and PAFC can use pure H_2 as where SOFC and MCFC can also utilize other fuels like CO and CH_4 (Mekhilef et al., 2012). Looking at the technical specifications of the fuel cells PEM seems interesting for utilisation on construction sites since its low operating temperature, high electrical efficiency, and its advantages of quick start-up and load following. Therefore, the PEM fuel cell is described in more detail.

In a PEM fuel cell (PEMFC), the hydrogen gets activated by a catalyst to form proton ion and eject electrons at the anode. The proton goes through the membrane while the electron is forced to flow

to the external circuit and generate electricity. Then, the electron flows back to the cathode and interact with oxygen and proton ion to form water. The reactions of a PEM fuel cell can be described as:

Anode: $$H_2(g) \rightarrow 2\,H^+ + 2\,e^- \qquad (11)$$

Cathode: $$\left(\frac{1}{2}\right)O_2\,(g) + 2H^+ + 2e^- \rightarrow\ H_2O\,(l) \qquad (12)$$

Overall reaction: $$H_2(g) + \left(\frac{1}{2}\right)O_2\,(g) \rightarrow H_2O\,(l) \qquad (13)$$
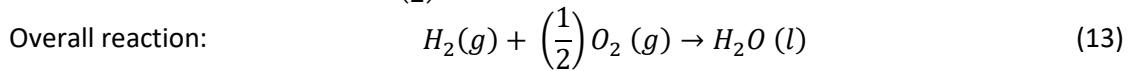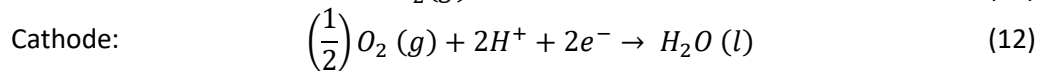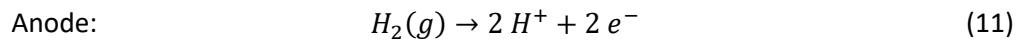
PEM fuel cells operate at low temperatures, are lightweight compact systems and have a rapid start-up process (Crespi et al., 2021; Mekhilef et al., 2012). Lu et al., (2021) performed a study on hot and cold starting characteristics of a PEM fuel cell. The results of this study showed that the start time is very dependent on the temperature. At -30 °C, the starting time was 8 – 16 minutes, 2 minutes for 0 °C and only 0.5 minutes for 20 °C (Lu et al., 2021). As reaction time increases with temperature, it is favourable from an efficiency point of view to operate at higher temperatures. However, an operation temperature above 100 °C will vaporize the water which causes dehydration to the membrane and leads to a reduction in the proton conductivity (Mekhilef et al., 2012). Crespi et al., (2021) used a ramp rate of 2 kW/s which equals 2% of the installed power of the used PEM Fuel cell in the simulations to limit stack degradation while respecting the desired ramp rates. Results of this study suggest that both in ramp-up and ramp-down, a PEM fuel cell can reach the power set point in 40 seconds. The sealing of electrodes in PEMFC is easier than in other types of fuel cells due to the solid electrolyte. In addition, PEMFC requires a minimum amount of maintenance due to the absence of moving parts in the power-generating stacks of the fuel cells (Mekhilef et al., 2012). Due to their high electrical efficiency and power density PEMFC's are very suitable for transportation applications (Mekhilef et al., 2012).
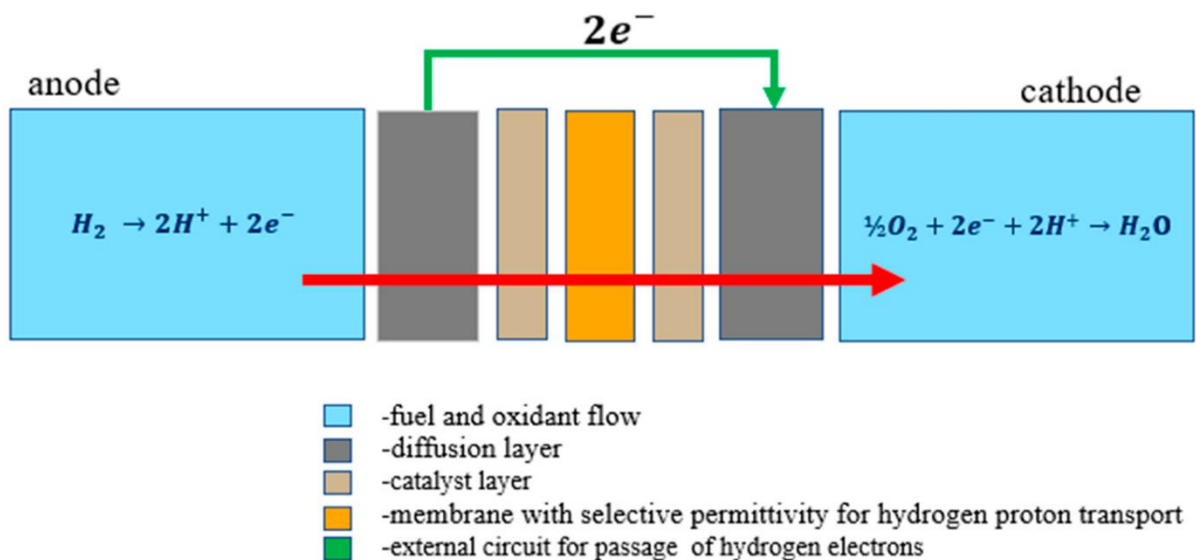
Figure 5 Components of a fuel cell (Felseghi et al., 2019)

Table 1 Different types of fuel cell technologies and their characteristics (US Department of Energy, 2016)

	Common Electrolyte	Operating Temperature	Typical Stack Size	Electrical Efficiency (LHV)	Applications	Advantages	Challenges
Polymer Electrolyte Membrane (PEM)	Perfluoro sulfonic acid	<120	<1 kW - 100 kW	60% direct H2	Backup power, Portable power	Solid electrolyte reduces corrosion, low temperature, quick start-up and load following	Expensive catalysts, sensitive to fuel impurities
Alkaline (AFC)	Aqueous potassium hydroxide soaked in a porous matrix, or alkaline polymer membrane	<100	1 - 100 kW	60%	Military, space, backup power, transportation	Wider range of stable materials allows lower cost components, low temperatures, quick start-up	Sensitive to CO_2 in fuel and air, electrolyte management (aq), electrolyte conductivity (polymer)
Phosphoric Acid (PAFC)	Phosphoric acid soaked in a porous matrix or imbibed in a polymer membrane	150 - 200	5 - 400 kW	40%	Distributed generation	Suitable for CHP, increased tolerance to fuel impurities	Expensive catalysts, long start-up time, sulfuric sensitivity
Molten Carbonate (MCFC)	Molten lithium, sodium, and/or potassium carbonates, soaked in a porous matrix	600 - 700	300 kW - 3 MW	50%	Electric utility, distributed generation	High efficiency, fuel flexibility, suitable for CHP, hybrid/gas turbine cycle	High temperature corrosion and breakdown of cell components, long start-up time, low power density
Solid Oxide (SOFC)	Yttria stabilized zirconia	500 – 1,000	1 kW - 2 MW	60%	Auxiliary power, electric utility, distributed generation	High efficiency, fuel flexibility, solid electrolyte, CHP, hybrid/gas turbine cycle	High temperature corrosion and breakdown of cell components, long start-up time, limited number of shutdowns

2.2. BATTERY TECHNOLOGIES

There is a wide variety of battery technologies each with different characteristics and applications. A battery can be described as a group of electrically connected electrochemical cells based on reversible electrochemical reactions (Fan et al., 2020). During charging, the anode active material is oxidised to generate electrons, while the cathode active material is reduced, consuming the electrons. The charge balance is provided by ion flow between electrodes through an ion-conducting electrolyte. These

processes are reversed during discharging through an ion-conducting electrolyte (Fan et al., 2020). Several batteries can be used for large-scale energy storage such as lead-acid, lithium-ion, nickel-cadmium, and sodium-sulphur (Poullikkas, 2013). The characteristics of these batteries are summarized in Table 2. Only the lithium battery technology is described focusing on LFP batteries due to the focus of this study.

There are several types of lithium-ion batteries including cobalt (LCO), manganese (LMO) and phosphate (LFP). These types of batteries are used in transportation, but can also be used for utility-scale applications such as power regulation and management. The advantages of Lithium-ion batteries are high energy density, cycling performance, high cell voltage, low self-discharge, and excellent rate capabilities. However, these types of batteries are expensive, have a low-temperature tolerance, and need protective circuitry to prevent cell degradation (Poullikkas, 2013; Soloveichik, 2011). The advantages and operation conditions of a lithium-ion-based battery technology make it interesting for zero-emission construction sites. Figure 6 shows the working principle in a schematic overview of a lithium-ion battery.

A battery lifetime can be separated into two processes: calendar life and cycle life. Calendar life refers to the battery degradation caused by storage without cycling and cycle life considers the battery degradation caused by charge and discharge cycles (Han et al., 2019). In general, a battery lifetime is dependent on temperature, charge/discharge rate (C-rate), and SOC windows. (high and low) is one of the most important ageing mechanisms of batteries (Waldmann et al., 2014). The appropriate working temperature of Li-on batteries is around 15 – 35 $^{\circ}$C and when the temperature is higher, the side reaction rate is higher (Han et al., 2019). At even higher temperatures, the battery can trigger self-heating which results in battery thermal runaway. When operating at low temperatures, the polarization will increase due to the increase in internal resistance, which may lead to additional side reactions (Han et al., 2019). Charging at low temperatures may lead to lithium deposition, which may lead to severe degradation and even safety problems (Han et al., 2019). The SOC also can have a significant effect on the battery lifetime. A higher SOC relates to a higher terminal voltage, which suggests a lower anode potential (Han et al., 2019). Lower SOC indicates higher anode potential and lower cathode potential, which generally has a positive effect on the battery lifetime. With a too low SOC, the corrosion of the anode and the cathode active material structure distorts which can severely decrease the battery lifetime (Han et al., 2019). Higher charge rates increase the battery temperature and also influence the battery terminal and internal voltage, which results in side reactions and a decreased battery lifetime (Han et al., 2019). In addition to that, high c-rates can lead to lithium plating and lithium deposition due to limited lithium-ion migration (Han et al., 2019).

The ageing mechanisms of Li-on batteries differ for each chemistry. While the C-rate does affect NMC and LCO batteries, the lifetime of an LFP battery does not seem to be affected (much) by its charge or discharge rate, which makes it interesting for backup power (Lamb & Pollett, 2020). Although many studies suggest that SOC windows do affect the lifetime of an LFP battery, Lamb & Pollet (2020) found that LFP batteries benefit from full cycles instead of decreased SOC windows. All types of Li-on batteries are very sensitive to temperature increases and for all chemistries – except for LCO – temperature has the most significant impact on the ageing behaviour of Li-on batteries (Lamb & Pollett, 2020). Thus, LFP is very sensitive to temperature followed by the variation in SOC windows and shows almost no effect at various charging rates (Lamb & Pollett, 2020).

Table 2 Comparison of battery technologies (Fan et al., 2020; Poullikkas, 2013; Soloveichik, 2011)

|	Specific energy [wh/kg]	Specific power [w/kg]	Round-trip efficiency (RTE) [%]	Cycle life	Operating temperature [°C]	Advantages	Disadvantages
Lead-Acid	30 - 50	75 - 300	70 - 80	500 – 1,000	18 – 45	Low costs, high battery voltage, good high-rate performance	Limited life cycle when deeply discharged, limited energy density
Nickel-cadmium	50 - 75	150 - 300	60 - 70	2,000 – 2,500	40 – 50	Long cycle life, long-term storage, low maintenance	Limited energy density, relatively expensive
Sodium-sulphur	150 - 240	150 - 230	75 - 90	2,500	300 – 350	High power and energy density, high efficiency, long cycle life	Production costs, safety concerns, high operating temperature
Lithium-ion	75 - 200	150 - 315	85 - 98	1,000 – 10,000	26 – 65	High power and energy density, high efficiency, long cycle life, long shelf life, rapid charge capability	High production cost, requires special charging circuit, poor high temperature performance
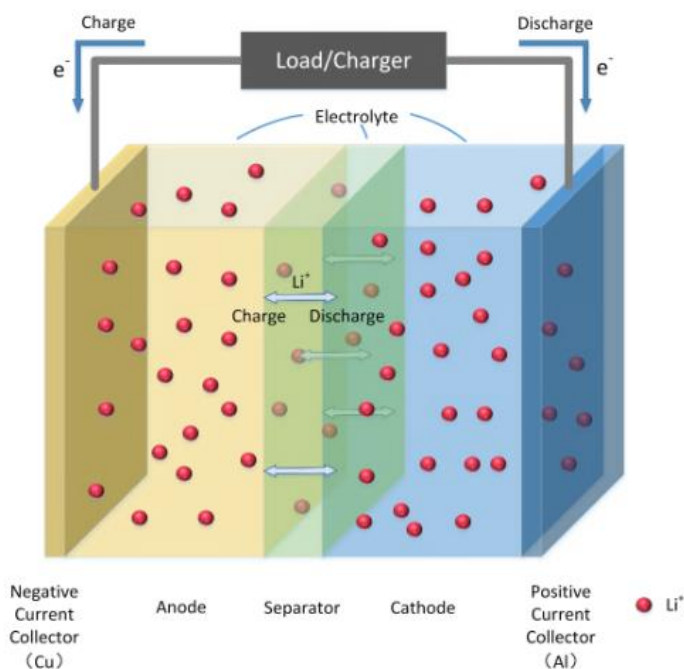
Figure 6 Schematic overview of a lithium-ion battery (Zhang et al., 2018)

3. PROBLEM STATEMENT AND RESEARCH GOAL

The construction sector must make the transition from a large polluter towards a sustainable emission-free sector. However, the construction sector is a traditional sector making slow progress in this transition (Palm & Bryngelson, 2023) and requires specific and extreme conditions. Technologies to improve the sustainability of this sector do exist and are advancing rapidly, although many technologies are still immature (NREL, 2022; Palm & Bryngelson, 2023; Stokke et al., 2023). In the Netherlands, a pilot is set up to work towards a solution for zero-emission construction sites. For this pilot, an energy system is considered including a PEM fuel cell and an LFP battery (FCPB-system: Fuel Cell & Power Bank). The FCPB-system will be designed for a pilot which includes a zero-emission construction site for new residential homes in the Netherlands. Implementing such a relatively new energy system in a harsh working environment with limited experience and knowledge entails several challenges. The current construction sector operates mainly with heavy-duty diesel vehicles, resulting in limited expertise with an entire electrical energy system (Palm & Bryngelson, 2023; Stokke et al., 2023). Next to that, there's often limited grid infrastructure (ANP & Businessinsider, 2021; Netbeheer Nederland, 2023; Stokke et al., 2023) on construction sites. This leads to the main research question:

What are cost-effective and environmental-friendly strategies for deploying a fuel cell and battery system on construction sites?

To address this question, five sub-questions are formulated:

1) What is the power and energy demand of the pilot construction site?
2) What are the possible configurations of the FCPB-system while always meeting the energy and power demand?
3) What are the main economic factors of the FCPB-system and how does it relate to the BAU scenario?
4) What is the environmental impact of the FCPB-system and how does it relate to the BAU scenario?
5) What is the economic and environmental potential for implementing renewable energy on a zero-emission construction site?

The first sub-question (1) is focused on investigating the energy and power demand of electrical construction equipment to create an energy profile. The energy demand profile is then used to size the system (2) together with technical data of LFP batteries and PEM fuel cells. The system is sized for different configurations considering a grid-connected and off-grid scenario and different size combinations of the battery and fuel cell. Then, the FCPB-system is viewed from an economic (3) and environmental perspective (4). The economic factors of the FCPB system include CAPEX, energy costs, LCOS and LCOE; while environmental factors of the system include emissions such as CO_2 and nitrogen. In addition to that, the trend of decreasing CO_2 emission factors is considered to show the FCPB-systems' future CO_2 emissions. The results of the economic and environmental analyses are compared to the BAU scenario where diesel equipment is used. Finally, the potential for utilizing renewable energy on construction sites (5), especially for the FCPB-system is considered. The potential renewable energy utilization is first expressed in the potential for direct charging and battery energy storage. Then, the reduction in energy cost and CO_2 emission are quantified.

The outcome of this research should contribute to the current knowledge regarding system design and implementation strategies of batteries and fuel cells for the construction sector in the Netherlands including technical, economic and environmental aspects.

4. METHODOLOGY

The study aims to identify strategies for deploying an FCPB-system that can reduce energy costs, reduce environmental impact, and meet the energy and power demand of construction sites. Strategies can potentially be influenced by many technical, economic, or environmental factors. Therefore, simulations of the FCPB-system are necessary in order to find cost-effective and environment-friendly strategies for a successful implementation. In addition to that, sensitivity analyses identify sensitive parameters which can support strategy recommendations for the FCPB-system. The methodology consists of three phases which involve a combination of a literature review and data collection, modelling and simulations, a techno-economic-environmental analysis, and a comparison of the FCPB-system versus the BAU scenario. A general overview of the three research phases is shown in Figure 7. Each of these research phases is described in the following sections.
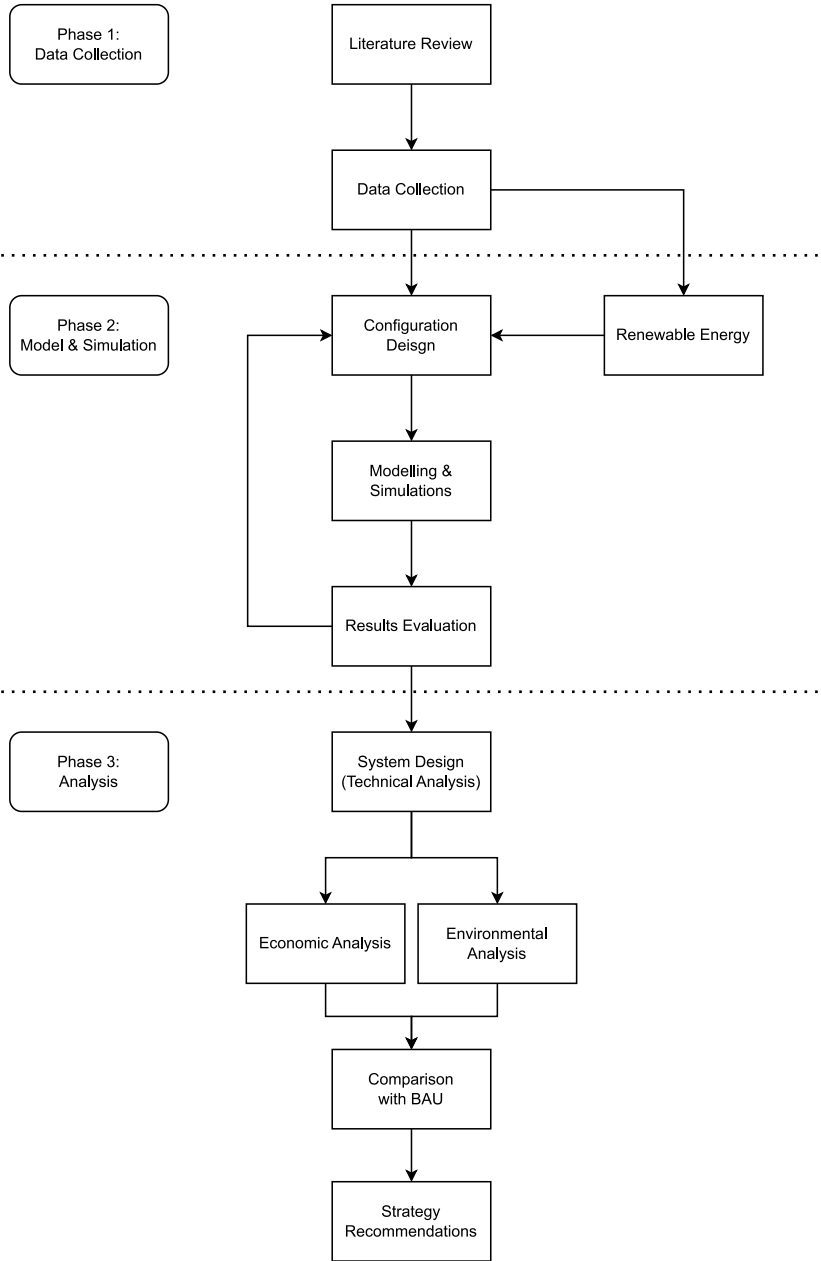

Figure 7 A general overview of the three research phases

4.1. PHASE 1: DATA COLLECTION

During the initial research phase, a literature review and data collection were conducted. The primary objective of the initial research phase was collecting data for identifying the energy profile and input for the energy sizing model. Input for the model includes techno-economic-environmental data of the construction machines and power systems

4.1.1. Energy profile of the pilot construction site

Four battery-electric machines will be used during the pilot, namely a mini-excavator, wheel loader, concrete mixer and a kipper. Data of the machines originate from the manufacturer. Whenever the technical specifications were not available, data of similar type and size machine is used. There was no energy profile nor working schedule in the pilot defined yet. In order to create a realistic scenario, the technical specifications of the four construction machines and the collective agreement order (CAO) of the construction sector are used. Over a period of 13 weeks the working day may not exceed 8 hours and the minimum amount of break is 0.5 hours (FNV, 2023; Rijksoverheid, 2011). Therefore, it's assumed that the machines will be used for a maximum of 8 hours a day. Only one machine can last for 8 hours continuously. Thus, the need for fast charging and the required break of 0.5 hours are combined to interfere as little as possible with the operation schedule of the construction company. The maximum amount of charge capacity is used for normal charging. Data of the construction machinery is summarised in Appendix A (Table A- 1).

4.1.2. Power system data

Electricity grid connection

A commercial grid connection provides more power than a regular household connection, however, a commercial grid connection can only provide a share of the required charge capacity and in some cases, it might not be possible to get an electricity grid connection (yet). In many places in the Netherlands, the grid is congested leading to limited transportation capacity. Netbeheer Nederland created a map with an overview of the electricity transport capacity in the Netherlands for electricity withdrawal. This map is made for companies who are planning projects which require a grid connection above 3x80 ampere (55 kW) and as it shows many regions of the Netherlands have limited (yellow and orange areas) or even no (red) available transport capacity. As the power system is supposed to be mobile which can be used for other projects in different regions of the Netherlands, the grid capacity is limited to 55 kW.

All data including energy cost and emissions from the grid are summarised in Appendix A (Table A- 2). As for all energy sources, the LCA approach is taken into account. Thus, the total CO_2 emission factor of the grid is the emission factor from production and chain supply combined.

LFP battery

In a recent optimization study by Sayfutdinov & Vorobev (2022), the authors focused on optimal utilization strategies for LFP batteries, specifically considering peak shaving for 1 and 2 cycles. The objective of this study was to find the optimal battery capacity considering the lowest daily CAPEX while considering the battery lifetime and capacity degradation (Sayfutdinov & Vorobev, 2022). The results indicated that increasing the battery capacity by 47.7% and 77.3% for 1 and 2 cycles respectively, resulted in the lowest daily CAPEX. The optimal SOC windows were found to be 27% - 95.8% for the one peak scenario and 58.8% - 95.2%; 38% - 95.2% for the two peak scenarios. The increased capacity and SOC windows resulted in a calculated lifetime of 15 and 12 years for the 1 and 2 peak scenarios respectively. It's worth noting that Sayfutdinov & Vorobev (2022) used an End of Life criterion of 75%; while many other studies apply an EoL of 80% which seems to be widely accepted

(Hu et al., 2020; Lamb & Pollett, 2020; Sui et al., 2021). This threshold of 80% is set to ensure the safety and reliability of the battery-powered system (Hu et al., 2020). However, increasing the EoL decreases the lifetime of the battery. Assuming a linear degradation of the battery capacity, the battery lifetime obtained in the study of Sayfutdinov & Vorobev (2022) can be used to determine the lifetime with an 80% EoL. The battery degradation and new lifetime are determined by equations 14 and 15.

Battery degradation in percentage equals to:

$$Battery_{Degradation} = \frac{1 - EoL_{Criterion} \ [\%]}{Lifetime \ [yr]}$$

(14)

The new lifetime in years with an 80% EoL criterion is then calculated by:

$$Lifetime_{EOL@80\%} = \frac{1 - EoL_{Criterion,new} \ [\%]}{BC_{Deg} \ [\%]}$$

(15)

The battery degradation for 1 and 2 cycles are 1.7% and 2.1% respectively which translates to a battery lifetime with an 80% EoL criterion of 12 and 9.6 years. All relevant techno-economic data of the LFP battery which is being used for simulations are summarised in Appendix A (Table A- 3).

PEM Fuel Cell

In order to determine the appropriate size of a PEM fuel cell, a method that takes operating conditions into account is used. This method, which has been applied to predict the lifetime of vehicle fuel cells and is applicable to fuel cells in various applications, is described in studies by Chen et al. (2015) and Pei et al (2008). Four distinct operating conditions were identified and their impact on the lifetime of a PEMFC has been quantified and summarised in (Table A- 4). These degradation rates are used to predict the lifetime according to the operating conditions of different scenarios involving normal charging and/or fast charging. The operating conditions are quantified by using the energy profile from Figure 14. Table A- 4 demonstrates that factors such as the number of start-stop cycles, idling duration, and high power load operation significantly influence the fuel cell's lifetime (Chen et al., 2015; Pei et al., 2008). Pei et al., 2008 introduced a difference factor (k) of 1.72, which is found by comparing the tested and real voltage degradation. This factor is incorporated in equation (19) to predict the lifetime of the fuel cell. Typically, the voltage of a PEMFC cell is designed around 0.70 volts and the technical lifetime of a PEMFC is reached when 10 % of the cell voltage is degraded (Chen et al., 2015; Pei et al., 2008). The lifetime is calculated by:

$$Lifetime_{PEMFC} = \frac{V_{Cell} * 0.10}{k(\sum n_i V_i + \sum t_j U_j)}$$

(16)

Where n_i is the number of cycles per operation condition and V_i is the corresponding voltage degradation per cycle, t_j is the time of operating condition in hours and U_j is the corresponding voltage degradation per hour. Idling is not taken into account for the lifetime prediction of the fuel cell, since there's no need for idling on the construction site. In addition to that, fuel cells can start up fast and respond well to load changes (Lu et al., 2021). The predicted lifetime for three different scenarios based on the identified operating conditions and load scenarios are presented in Table A- 5. The lifetime calculation is performed for three distinct operating conditions as follows (Figure 8):

1) Normal charging without operating at high load. In this scenario, the power demand never exceeds 60% of the installed power of the fuel cell. The lifetime is predicted based on this power requirement. These operating conditions apply to configurations I-FCPB and II-FCPB.

2) Normal charging while operating at a high power load. In this scenario, the installed power of the fuel cell matches the highest power demand during operation. The lifetime is calculated considering this maximum power demand (> 60%).

3) Fast and normal charging. In this scenario, the installed power of the fuel cell is set to meet the highest power demand which is during the fast charging. Thus, the fuel cell only operates for 0.5 hours at a high power load. These operating conditions apply to configuration II-FC.

By considering these three operating conditions, the lifetime of the fuel cell is estimated, providing valuable information for investment decisions. Since the lifetime of the second operating condition is significantly lower, only operating conditions 1 and 3 are considered where normal charging is done < 60% of installed power. In addition to that, the fuel cell efficiency is dependent on the operating power compared to the installed power (Figure 9). The voltage degradation for these three scenarios is summarised in Appendix A (Table A- 5). All techno-economic-environmental data used for simulations are summarised in Table A- 6.
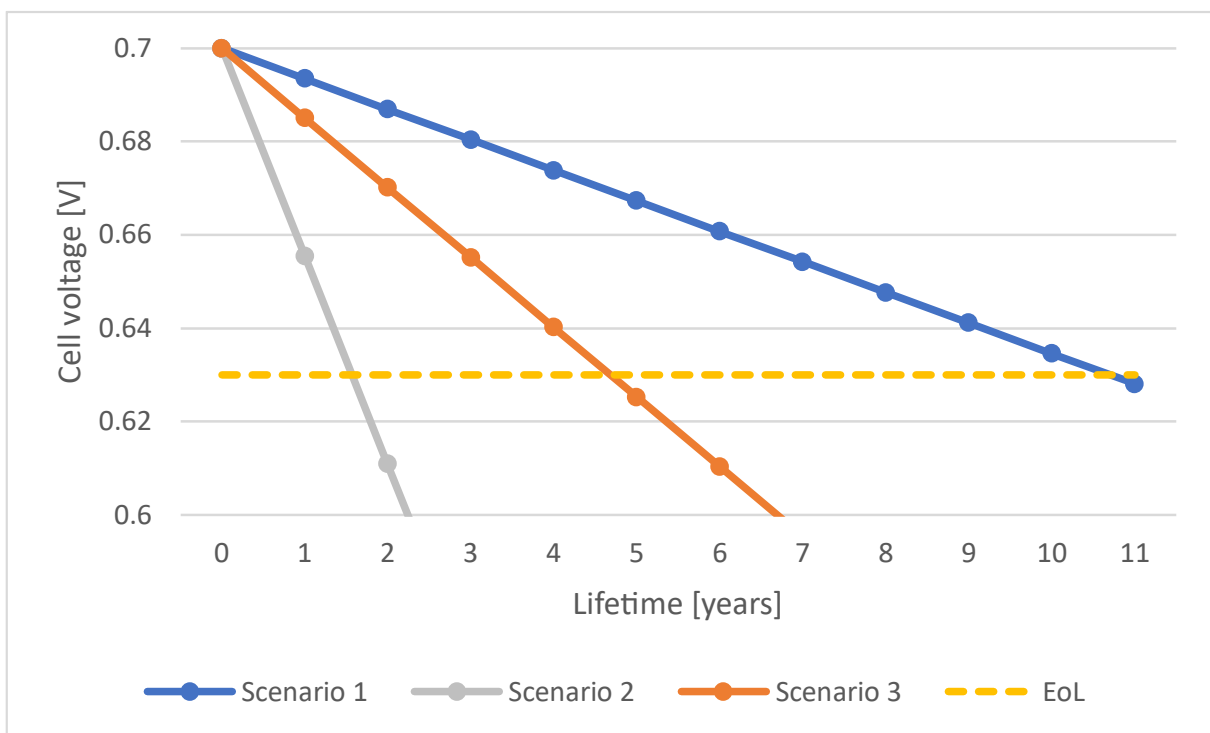
Figure 8 Lifetime of the PEMFC according to operating conditions
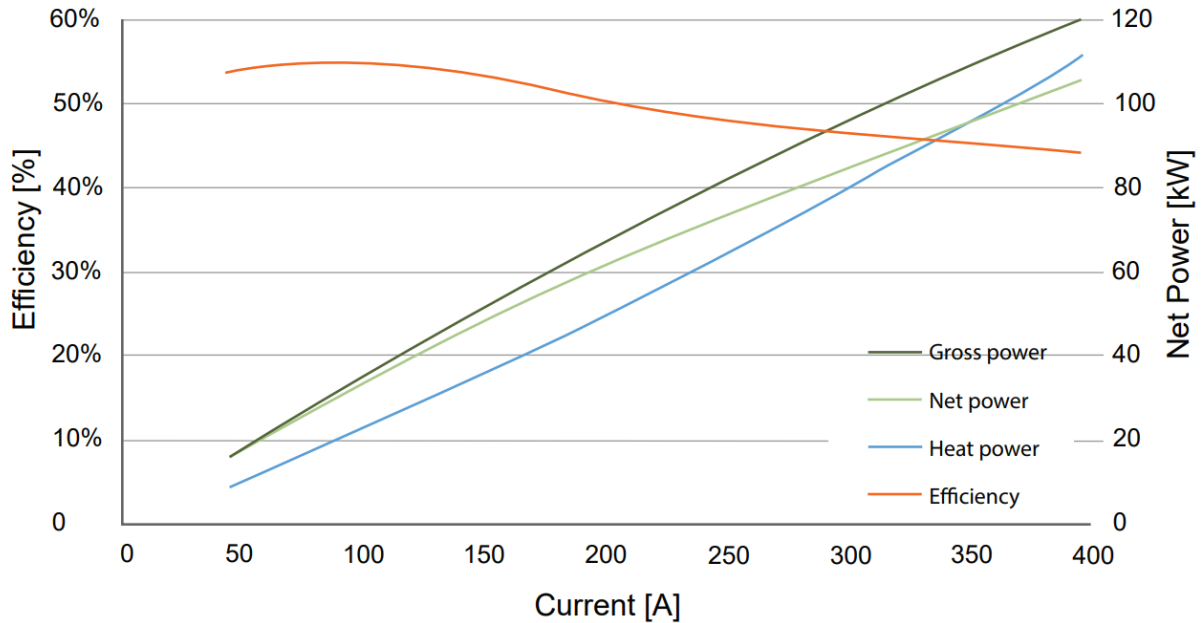
Figure 9 Efficiency curve of the PowerCellution PEM fuel cell (PowerCellution, 2023)

4.1.3. Container

The battery and fuel cell will be built in a container (containerized) for safety and mobility purposes. Besides the power technology (battery/fuel cell), other necessary technologies are built inside the container such as inverters, control systems, transformers and a cooling system (PowerCellution, 2023). Different container sizes are summarised in Table 3.

Costs of the container exclude the fuel cell or battery but include all of the other technologies necessary to make it employable (controlling and cooling system, inverters, etc.). The original price is from PowerCellution for a 20ft containerized PEM fuel cell and the other container prices are calculated using the price of the 20ft container and divided by the container size. To determine the required container size for the battery and fuel cell, current projects are used as an example. The average energy density of these containerized batteries is used to determine the required container size for the configurations with a battery. Multiple containerized batteries are found, while containerized PEM fuel cells are less common. Examples of containerized LFP batteries and PEM fuel cells are summarised in Appendix A (Table A- 7 & Table A- 8).

Table 3 Container size and cost

	6ft	8ft	10ft	20ft	40ft	Reference
Length	1.80	2.27	2.8	5.9	12	(Bdcontainers,
Width	1.86	2.10	2.35	2.35	2.35	2023)
Height	1.71	2.05	2.39	2.39	2.39	
Volume	5.7	9.8	15.7	33.1	67.4	
Cost [€]	90,000	120,000	150,000	300,000	600,000	(PowerCellution, 2023)

4.1.4. Comparison data of diesel construction machinery

To provide a comprehensive understanding of the FCPB-system's results, a comparison is made with the current situation which consists of diesel-fuelled machinery. The comparison includes energy costs and CO_2 emissions. In order to determine fuel costs and CO_2 emissions, diesel consumption is

calculated. Four similar diesel machinery are found to make a comparison. The technical specifications of the diesel machinery are summarised in Appendix A (Table A- 9). Economic and environmental data of diesel machinery used for comparison are shown in Appendix A (Table A- 10).

4.1.5. Implementation of renewable energy

The utilization of battery-electric vehicles and an LFP battery introduces the potential to implement renewable energy on construction sites. Construction projects can have periods of several months up to years. Therefore, renewable energy is implemented in the simulation model to show the technical, economic and sustainability potential benefits of renewable energy. Four different rated powers are chosen to simulate its potential for electric construction sites and the FCPB-system. The rated power of renewable energy equals:

- 1x Normal charging
- 0.5x fast charging
- 1x fast charging
- 2x fast charging

In addition to that, the specifications of wind turbines are taken into account. A power curve belongs to a wind turbine with specific technical specifications like hub height and rotor diameter. Therefore, "regular" sizes of wind turbines are considered for practical reasons including available data such as hub height, available power curve, and minimizing deviation in simulation results by taking the installed power which belongs to a specific power curve. This phenomenon does not apply to solar energy, but to make a fair comparison between the two renewable energy sources, the same amount of installed power is used for solar and wind energy. The location of the simulated renewable energy is chosen by taking a 50 km distance from the hydrogen hub and enough space for the solar panels or wind turbine into account. Power purchase agreement (PPA) prices are used to calculate the energy costs of renewable energy. The data of renewable energy used for simulations are summarised in Appendix A (Table A- 11). The energy profile for solar is used from PVGIS with the provided input and simulation results shown in Table A- 12. The wind energy profiles are used from Renewable.ninja (Pfenninger & Staffell, 2016; Staffell & Pfenninger, 2016).

4.1.6. Future environmental impact of the electricity grid and green hydrogen

The Dutch government has ambitions and targets to decarbonize its electricity grid. The Dutch environmental agency (PBL) calculated the future CO_2 emission factor of the Dutch electricity grid according to the governmental plans of increasing the installed renewable power (PBL, 2022). PBL calculated the grid emission factors for 2025 and 2030. For 2035, the emissions from the electricity grid are calculated by linear interpolating and assuming that the direct emissions are 0 kg CO_2/KWh in 2050. The supply chain emissions for the electricity grid are taken into account for future WTW emission factors. However, no development of supply chain emissions for the Dutch electricity grid was found, thus no change in chain supply emissions is considered. The same principle applies to green hydrogen. Although hydrogen does not emit CO_2 emissions itself, there is some CO_2 emission during the production phase of hydrogen and renewable energy technologies such as PV panels and wind turbines. The Hydrogen Council examined the production of (green) hydrogen and its future CO_2 emissions (Hydrogen Council, 2021). They found that the emissions will decrease significantly in 2030 and 2050. The emission factors for 2025 and 2035 are calculated by linear interpolation. The future CO_2 emission factors (Figure 10) are used to show the future reduction of CO_2 emissions of electric-powered construction sites. The future CO_2 emission factors are summarised in Appendix A (Table A- 14).
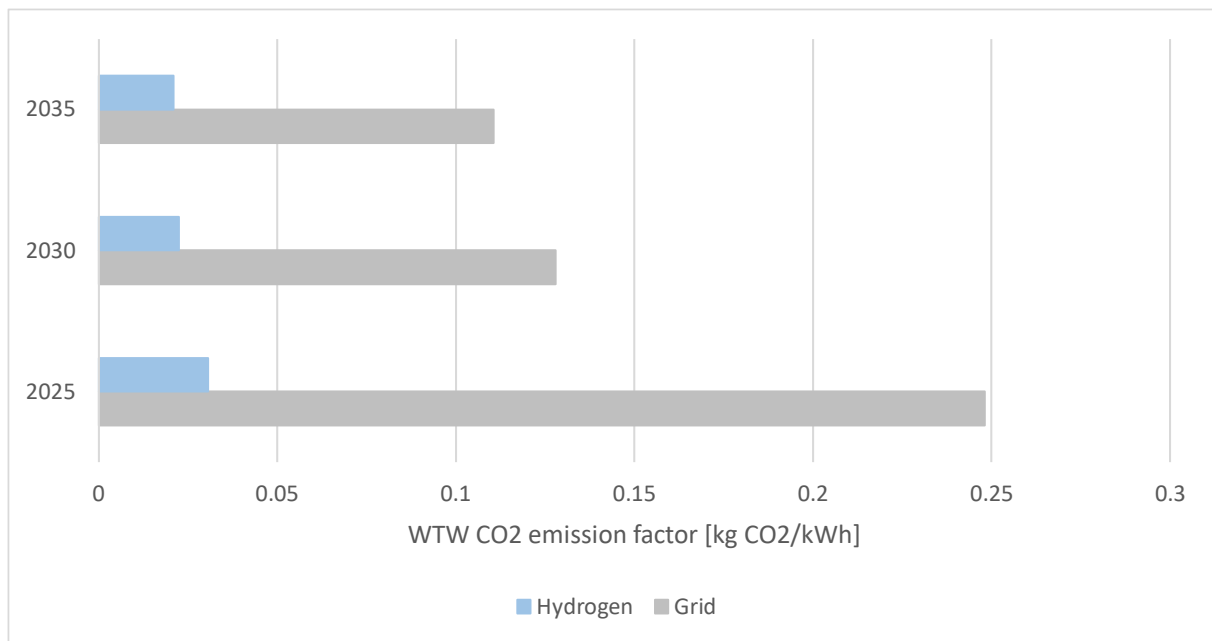
Figure 10 Current and future electricity grid and hydrogen emission factor

4.2. PHASE 2: MODELLING AND SIMULATION

4.2.1. Scenario development

A simulation model is developed based on the data found in the first research phase (4.1). The energy profile is used to identify possible configurations for a zero-emission construction site. Five configurations are considered of which three configurations are grid-connected (indicated with "I") and two configurations are off-grid (indicated with "II"). The considered configurations are:

I-FCPB: A grid-connected construction site with a battery used for fast charging and a small fuel cell to supply energy power and energy for normal charging. The battery can be charged by either the electricity grid or the fuel cell.

I-PB: A grid-connected construction site with one large battery for fast and normal charging. The battery is dependent on the electricity grid for charging.

I-FC: A grid-connected construction site with one large fuel cell for fast and normal charging.

II-FCPB: An off-grid construction site with a battery for fast charging and a fuel cell for normal charging. The battery can only be charged by the fuel cell.

II-FC: An off-grid construction site with one large fuel cell for fast and normal charging.

Sizing constraints are taken into account for sizing the FCPB-system (Table 4). The main sizing constraint (1) is the system's obligation to always have the capability of delivering sufficient power and energy during the day (100% reliable). Considering this constraint, the system cannot rely on external energy sources such as renewable energy. Then, the battery and fuel cell must fit into a small (<20ft) container, because 40 feet containers make transportation of the energy system less smooth and more expensive (2). The grid connection (0) is limited to 55 kW as the possible grid connection is still unknown and the grid capacity is limited in many regions of the Netherlands (3). The pilot is a joint effort between multiple companies and the hydrogen supplier supplies the exchangeable hydrogen tube trailers with 500 kg of hydrogen (4).

Table 4 Sizing constraints for the energy system

	Sizing constraint	Description
1	Always sufficient energy & power	The on-site energy system is always able to deliver enough power and energy. Thus, the construction equipment is 100% reliable on the FCPB-system.
2	< 40ft container	The battery and the fuel cell must fit in a small container, preferably smaller than 20ft container separately. Smaller containers are more mobile and cheaper to move; a 40ft container makes transport less smooth and more expensive
3	Grid connection	There is limited grid capacity in many places in the Netherlands. Netbeheer Nederland made a map which gives an overview of the grid transportation capacity above 3x80a or 55 kW. Therefore, the maximum grid capacity for sizing the energy system is set to 55 kW.
4	Hydrogen tank	The hydrogen and storage tank will be delivered by an external company. For this pilot, the company delivers 500 kg of hydrogen in tube trailers. The price of the hydrogen is 25 €/kg.

4.2.2. Power and energy demand

The energy profile of the construction site is determined by the technical specifications of the machines and the required 0.5-hour break according to the CAO. The energy profile is used to determine the minimum size of the FCPB-system for the grid-connected and off-grid configurations in terms of power and capacity. The power demand and energy demand are calculated for the fast and normal charging cycle by:

$$Power\ Demand\ [kW] = \sum_{Max\ Charge\ Power}^{Machines} \tag{17}$$

$$Energy\ Demand\ [kWh] = \frac{\sum_{Max\ Charge\ Power}^{Machines}}{Charge\ duration\ [h]} \tag{18}$$

4.2.3. Model set-up

An Excel model is developed to design the energy system considering technical, economic and environmental data. In addition to this data, the model incorporates the energy profile (Figure 14), an economic merit order (Figure 12), sizing constraints (4.2.1) and renewable energy profiles from external databases. A schematic overview of the energy sizing model input and output is shown in Figure 11. Output of the energy sizing model including technical results are then used for economic, environmental, and comparison analyses. The main technical results of the model include:

- Required minimal power per power source
- Energy distribution of the configurations
- Required energy for battery charging
- Required size of the container
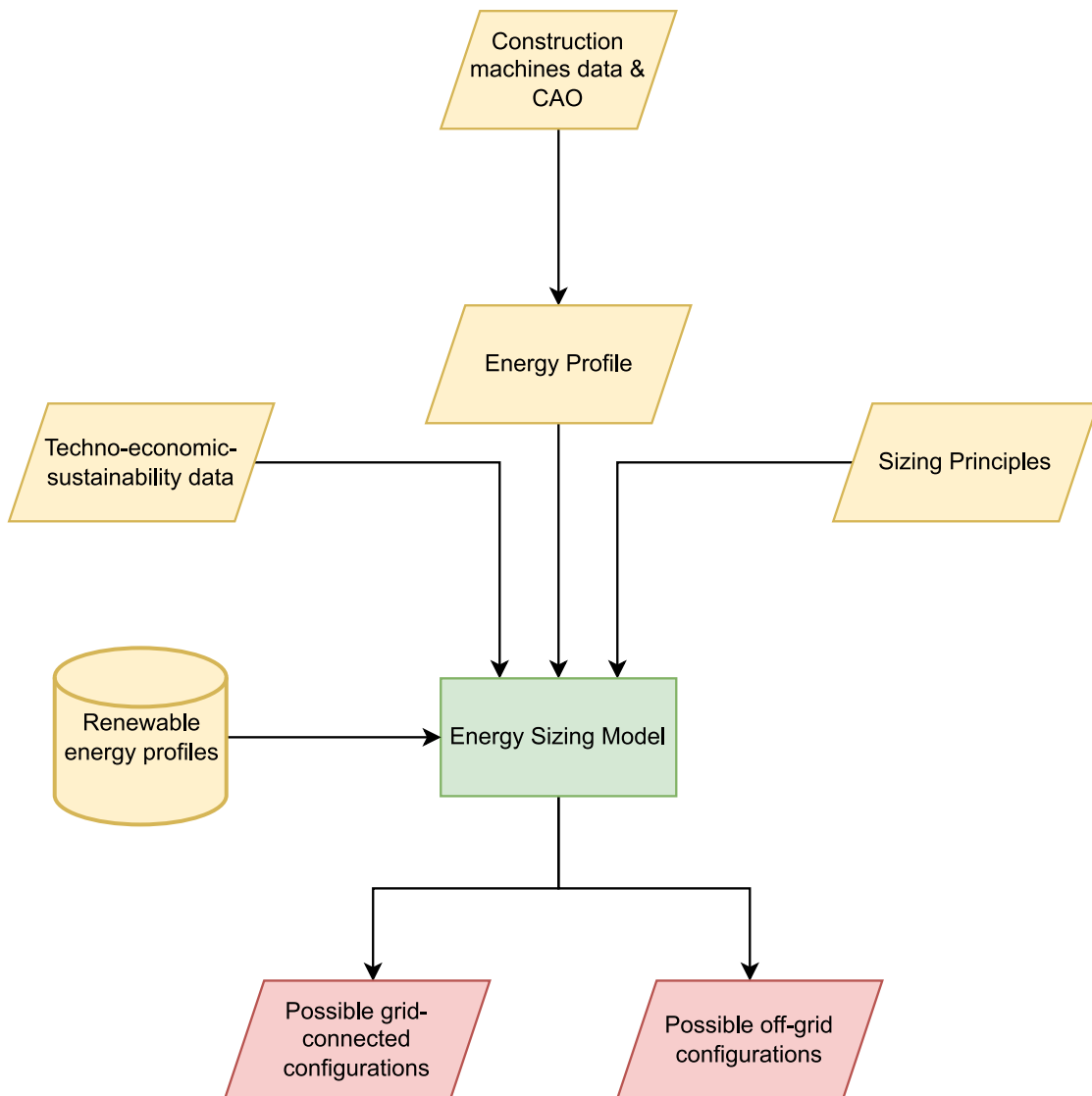
Figure 11 Energy sizing model input and output

4.2.4. Economic merit-order

To provide the construction site with the cheapest energy, an economic merit order is taken into account. As the levelized cost of energy/storage (LCOE/LCOS) is not known beforehand, the base electricity price is considered. The economic merit order looks as follows:

Grid-connected: *Wind energy -> Solar energy -> Electricity Grid -> Battery -> Fuel cell*

Off-grid: *Wind energy -> Solar energy -> Fuel cell -> Battery*

The price of the battery is dependent on the power source and due to the RTE, it is always more expensive than the power source. Figure 12 shows the decision-making tree of the economic merit order which is used in the model. The energy prices used for the merit order can be found in Appendix A.
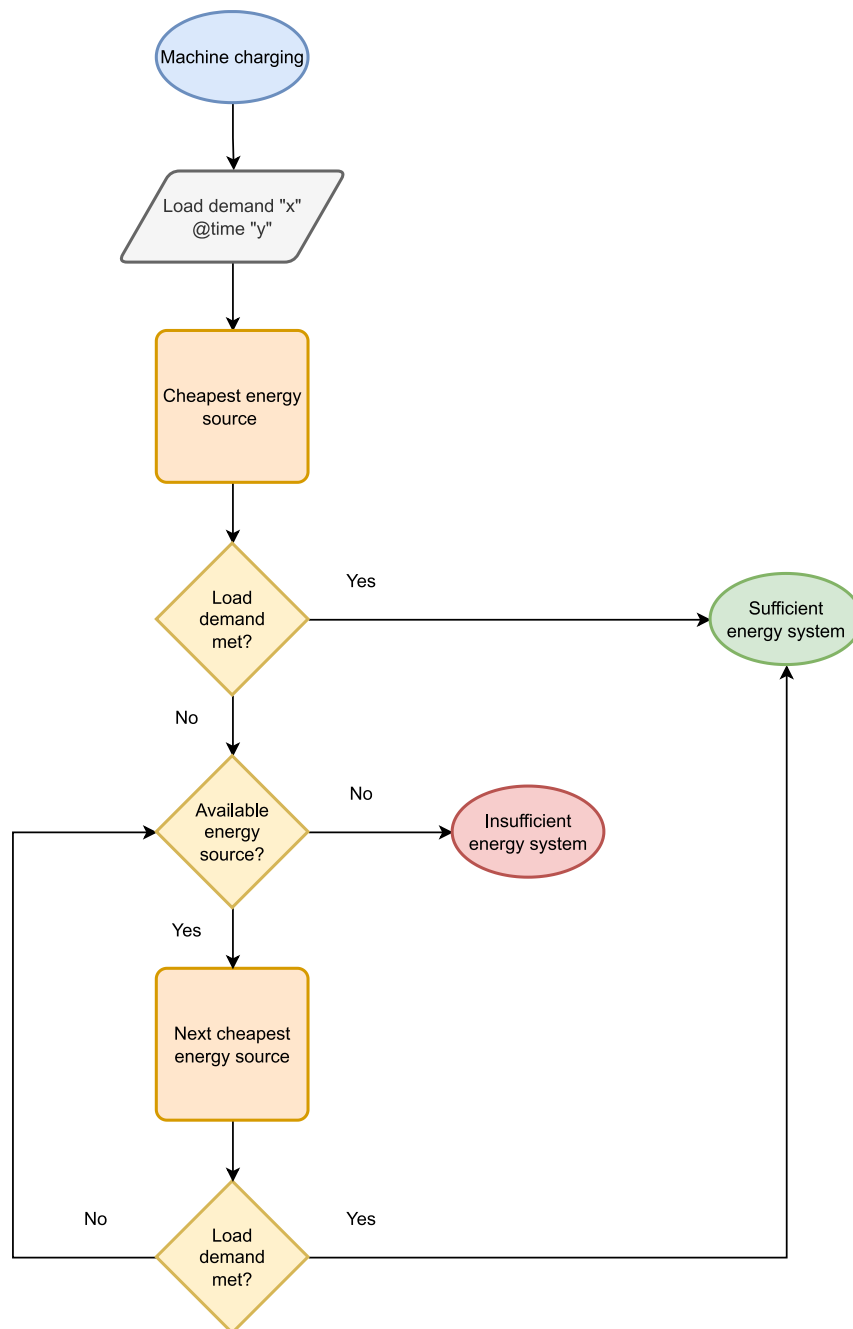
Figure 12 Economic merit-order of the energy sizing model

29

4.3. PHASE 3: SYSTEM DESIGN AND ANALYSES

After simulating the five different configurations, analyses are done from a technical, economic, and environmental perspective. Results of the economic (energy costs [€/year]) and environmental analyses (CO_2 [kg CO_2/year]) are compared to the BAU-scenario.

4.3.1. Sizing the FCPB-system

The technical analysis focuses mainly on the minimum required size in terms of power and energy of the FCPB-system. The minimum required size of the FCPB is determined by the power and energy demand of the construction site and includes the sizing principles of the LFP battery and PEM fuel cell (4.1). Considering the sizing principles from Table 4, the FCPB-system should always be able to provide power:

$$FCPB_{Size}[kW] = Power\ Required\ [kW] \leq = FCPB\ size\ [kW] \tag{19}$$

The battery must be able to provide enough power and energy during the charge cycle(s) it is designed for:

$$Battery\ Capacity\ [kWh] = \frac{\frac{Energy\ Required_{Cycle}\ [kWh]}{RTE\ [\%]}}{Available\ energy\ [kWh]} \tag{20}$$

Where available energy is the amount of energy that can be used taking the SOC windows into account:

$$Available\ Energy\ [kWh] = Battery\ Capacity\ [kWh] * (SOC_{max} - SOC_{min}) \tag{21}$$

Hydrogen is supplied by a tube trailer with a capacity of 500 kg of hydrogen. The required hydrogen is calculated by:

$$H2\ consumption\ [kg] = \frac{\frac{Energy\ Required_{Cycle}\ [kWh]}{\eta\ Fuel\ Cell\ [\%]}}{H2_{LHV}\left[\frac{kWh}{kg}\right]} \tag{22}$$

The hydrogen tank exchanges and replacement rate are then calculated by:

$$H2\ tank\ exchanges\ [n] = \frac{H2\ consumption\ [kg]}{Tube\ trailer\ volume\ [kg]} - 1 \tag{23}$$

$$H2\ tank\ replacement\ rate = \frac{Opertaional\ days\ [days]}{H2\ tank\ exchanges\ [n]} \tag{24}$$

4.3.2. Economic analysis

The economic analysis considers the main economic factors such as investment costs (CAPEX), operational costs (OPEX), energy costs, and the LCOS/LCOE of the FCPB-system. Thereafter, a sensitivity analysis is done for the LCOS/LCOE with several factors including the mentioned economic factors, grid and hydrogen price, and the lifetime of the FCPB-system. The results of a sensitivity analysis tells which parameters are most likely to affect the system costs and assists in validating the results (Smith et al., 2008).

The levelized cost of storage and energy (LCOS/LCOE) is calculated for two reasons: (1) to identify the average cost of electricity storage and (2) to make a comparison between configurations taking discharged energy and lifetime into account. The LCOS/LCOE is calculated using the equation from (Blok & Nieuwlaar, 2017):

$$LCOS \left[\frac{€}{kWh}\right] = \frac{\alpha * CAPEX \, [€] + OPEX \, [€] + Charge_{costs}[€]}{Energy \, Discharged \, [kWh]} \qquad (25)$$

$$LCOE \left[\frac{€}{kWh}\right] = \frac{\alpha * CAPEX \, [€] + OPEX \, [€] + Fuel_{costs}[€]}{Energy \, generated \, [kWh]} \qquad (26)$$

Where α is the capital recovery factor which includes a discount rate (r) and the lifetime (n):

$$\alpha = \frac{r}{1 - 1(+r)^{-n}} \qquad (27)$$

The discharged energy is equal to the energy demand. The battery charge costs are equal to:

$$Battery \, charge \, costs \, [€] = \frac{Energy \, Discharged \, [kWh]}{RTE \, [\%]} * Charge_{Price}\left[\frac{€}{kWh}\right] \qquad (28)$$

4.3.3. Environmental analysis

The environmental analysis is mainly focused on the CO_2 emissions of the FCPB-system, as there are no nitrogen emissions expected from this system. The CO_2 emission factors include emissions from operational and production phase. Future emission factors for both hydrogen and the electricity grid in 2025, 2030 and 2035 are considered to show the future environmental impact of grid electricity and hydrogen. CO_2 emissions from battery electricity are dependent on the power source and due to the RTE, it is slightly higher. The CO_2 emission of the LFP battery equals:

$$CO2 \, Battery \, [kg \, CO2] = \frac{Energy \, delivered \, [kWh]}{RTE \, [\%]} * CO2_{EF}[kg \, CO2/kWh] \qquad (29)$$

4.3.4. Comparison analysis

The maximum power of the machines is used to calculate the diesel consumption. However, it is important to note that these machines do not operate at their maximum power, similar to electric machinery (where continuous power is used). Therefore, a load factor (LF) is introduced to determine diesel consumption. In a study by Klanfar et al., (2016), diesel consumption was calculated for different types of machinery using load factors. The average load factors derived from this study are used and the diesel consumption is calculated by (20):

$$Diesel \, consumption \, [L] = \frac{Power \, [kW] * Runtime \, [hr] * LF}{\eta_{Diesel}} \qquad (30)$$

The fuel costs and CO_2 emissions are calculated by multiplying the diesel consumption by the diesel price and CO_2 emission factor. However, the nitrogen emission from diesel is twofold since it originated from NO_x and NH_3. The NO_x and NH_3 emissions from diesel are calculated by:

$$NOx\ [kg] = Diesel_{Consumption}[\frac{L}{year}] * EF_{NOx}[\frac{kg}{L}] \qquad (31)$$

$$NH3\ [kg] = Runtime\ \left[\frac{hours}{year}\right] * EF_{NH3}\ \left[\frac{kg}{L}\right] \qquad (32)$$

An average molar mass of NO and NO_2 is used to calculate the nitrogen emissions from NO_x. The total nitrogen emission from NO_x and NH_3 is calculated by:

$$Total\ nitrogen\ [kg] = NO_{x,Total} * \frac{MM_N}{\frac{MM_{NO}+MM_{NO2}}{2}} + NH_{3,Total} \frac{MM_N}{MM_{NH3}} \qquad (33)$$

4.3.5. Renewable energy implementation

A solar and wind energy profile is used for investigating the reduction potential of energy costs and CO_2 emissions. Renewable energy is used in two ways, namely for direct charging the machines and charging the battery. Renewable energy can only be used for direct charging (fast and normal charging); while for battery charging (energy storage) it can be used at all times whenever there's renewable energy left after direct charging, the battery is not discharging, and its capacity is below the maximum state of charge. The full potential of renewable energy for charging the battery is calculated by using the maximum amount of time the battery has to charge during the day until it reaches its maximum SOC. Therefore, the amount of renewable energy (R.E.) that is stored equals:

$$Total\ R.E.storage\ [kWh] = \sum_{S,Energy}^{T,off} <= Battery\_energy\_required\ [kWh] \qquad (34)$$

Where $T_{,off}$ = the time the battery is not discharging.

5. RESULTS

5.1. ENERGY PROFILE CONSTRUCTION SITE

The working day starts at 07:00 in the morning and when the break starts at 12:00 the machines are fast-charged to supply enough energy to the machines' batteries for the rest of the day. Start of the break at 12:00 the machines' battery state of charge (SOC) is 49%, 44%, 34% and 34% respectively. The required charge capacity during the 0.5-hour break is 516 kW. After fast charging, the machines' batteries are charged up to 69%, 50%, 51%, and 51% respectively. The eight hours of work are reached at 15:30 and normal charging of the construction machinery begins. The required charge capacity is 93 kW and decreases slightly to 89 kW and 86 kW until the mini excavator and the wheel loader are fully charged. The total energy demand from charging the machines is 990 kWh/day of which 258 kWh during fast charging and 732 kWh during normal charging. Figure 13 shows the state of charge of the vehicles' batteries and Figure 14 shows the required charge power.
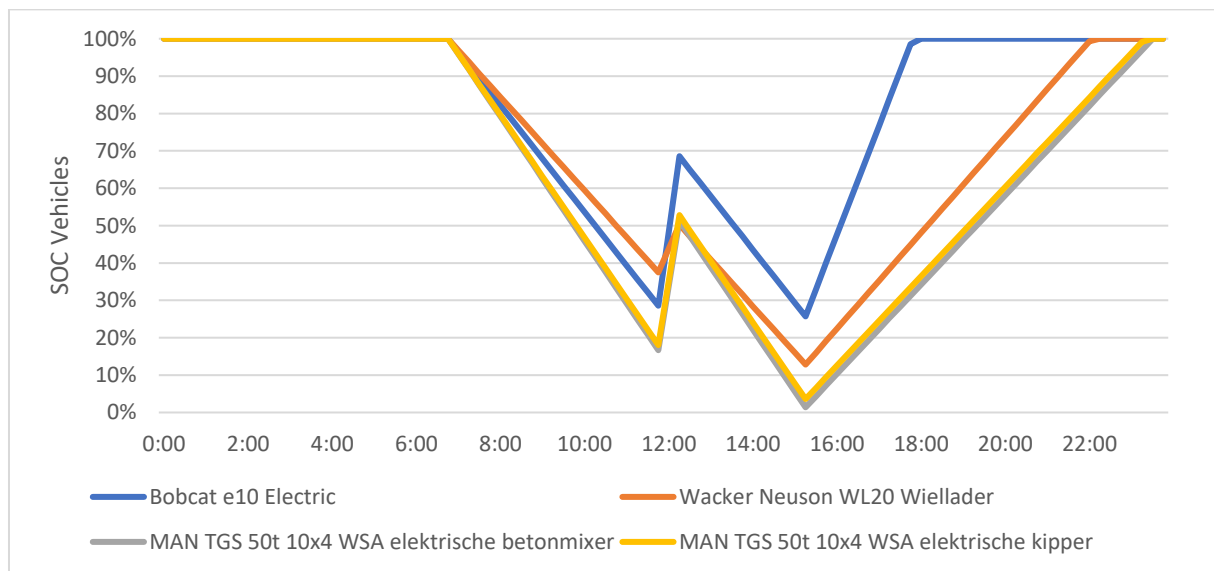

Figure 13 State of Charge (SOC) of the vehicles' batteries during the day
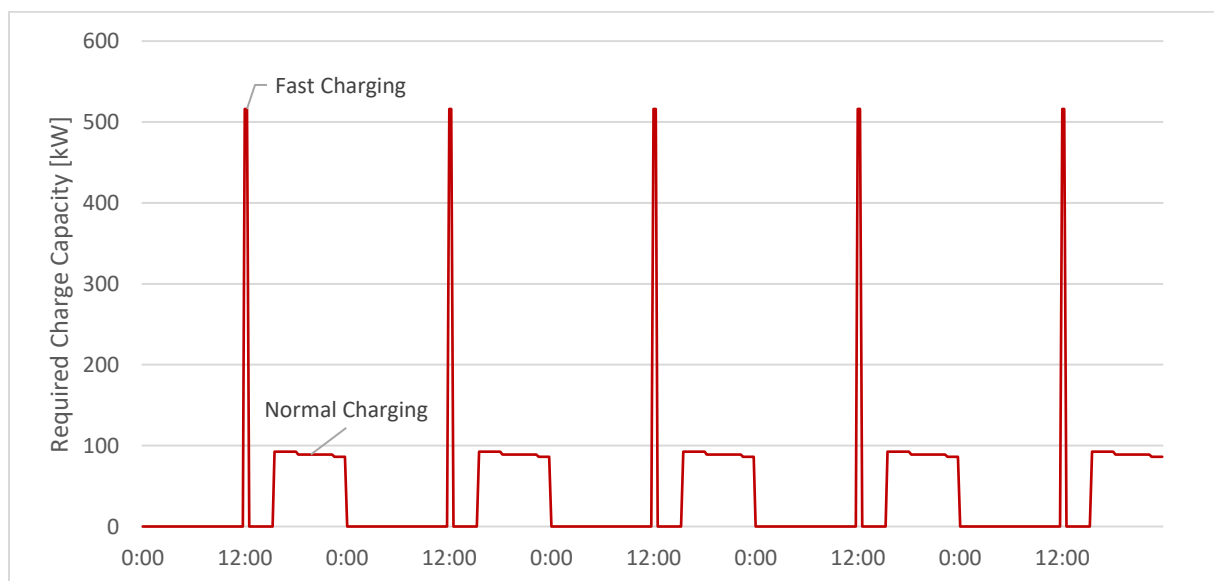
Figure 14 Energy profile of the pilot construction site

5.2. DESIGN OF THE FCPB-SYSTEM

Five possible configurations are identified based on the energy profile and the chosen mix of technologies. For the grid-connected scenario, three configurations are possible; while for the off-grid scenario, only two configurations are possible, as the battery cannot be employed solely without a power source for charging it. The configurations are based on the energy profile (Figure 14) which shows the requirement for fast charging during the day and normal charging at the end of the working day. The required power and amount of daily cycles per technology are summarised in (Table 5). Both scenarios are described in the following sections.

Table 5 Possible configurations for grid-connected and off-grid construction sites based on the energy profile

Configuration	Electricity Grid [kW]	Battery [kW]	Fuel Cell [kW]
I-FCPB	55	461 – 1 cycle, fast charging	38 – 1 cycle, normal charging
I-PB	55	461 – 2 cycles	-
I-FC	55	-	461 – 2 cycles
II-FCPB	-	516 – 1 cycle, fast charging	93 – 1 cycle, normal charging
II-FC	-	-	516 – 2 cycles

5.2.1. Possible configurations for grid-connected construction sites

For the grid-connected scenario, three configurations are possible, namely (I-FCPB) a battery and a fuel cell, (I-PB) a stand-alone battery or (I-FC) a stand-alone fuel cell. The first configuration uses the battery for fast charging and the fuel cell supports the electricity grid for normal charging. The second configuration uses a large battery for fast and normal charging which leads to an increased amount of required battery capacity and daily cycles. The third configuration is similar to configuration II, but a fuel cell is used instead of a battery.

In every configuration, the electricity grid delivers its maximum power of 55 kW since it's the cheapest available power source. Therefore, the amount of energy supplied to the construction machines by the electricity grid to the construction site (125,190 kWh; 49%) remains unchanged in every configuration. Next, to direct charging of the construction machinery, the grid is used for charging the battery in configuration I-FCPB and I-PB. The grid delivers 66,984 kWh and 147,734 kWh to the battery in configuration I-FCPB and I-PB respectively. Thus, the grid delivers a total amount of energy of 192,174 kWh and 272,924 kWh in configuration I-FCPB and I-PB respectively.

The first configuration has the most diverse energy distribution due to the implementation of three technologies. The battery delivers 23% of the total energy during fast charging and the fuel cell delivers 28% of the total energy during normal charging. Configuration I-PB only utilizes a large battery for fast and normal charging. Hence, the battery is used for 2 cycles per day and requires a larger capacity

(+89%) than the battery in configuration I-FCPB. Due to the lack of a fuel cell in configuration I-PB and using the battery for both charging moments, the battery delivers 51% of the total energy demand. Besides the electricity grid, configuration III (Figure 18) only includes a large fuel cell for fast and normal charging. Therefore, hydrogen consumption in configuration I-FC is 78% more than in the first configuration, resulting in almost the double amount of hydrogen tank exchanges (Table 6). The hydrogen tube trailer must be replaced every 33 and 19 working days in configuration I-FCPB and I-FC respectively.

The lower SOC windows of the LFP battery in configuration I-FCPB and I-PB (Figure 16 & Figure 17) corresponds to the optimal limits found by Sayfutdinov & Vorobev (2022). Only in configuration II the upper SOC window of 95.2% is not reached due to limited time for recharging the battery between the fast and normal charging events. To supply enough energy between these SOC windows, the ratio of optimal capacity vs. energy demand is higher than the study of Sayfutdinov & Vorobev (2022) suggested. The ratio in configuration I-FCPB is only slightly higher (1.453 vs 1.447), however the ratio in configuration I-PB is significantly higher (2.747 vs 1.779). This can be explained by the difference in the E/P ratio of the LFP battery and the limited time for the battery to recharge in configuration I-PB.
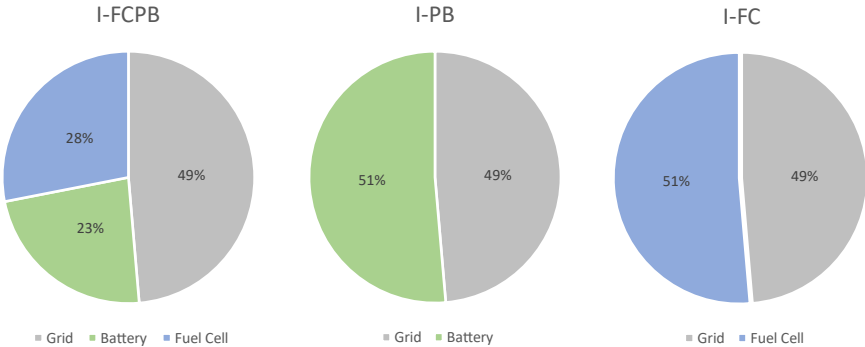
Figure 15 Energy distribution of the grid-connected configurations

Table 6 Required hydrogen and yearly tank exchanges of the grid-connected scenario

	Configuration I-FCPB	Configuration I-FC
Required hydrogen [kg]	4,251	7,548
H2 Tank Exchanges [n/year]	8	15
Hydrogen tank replacement rate [days/n]	33	17
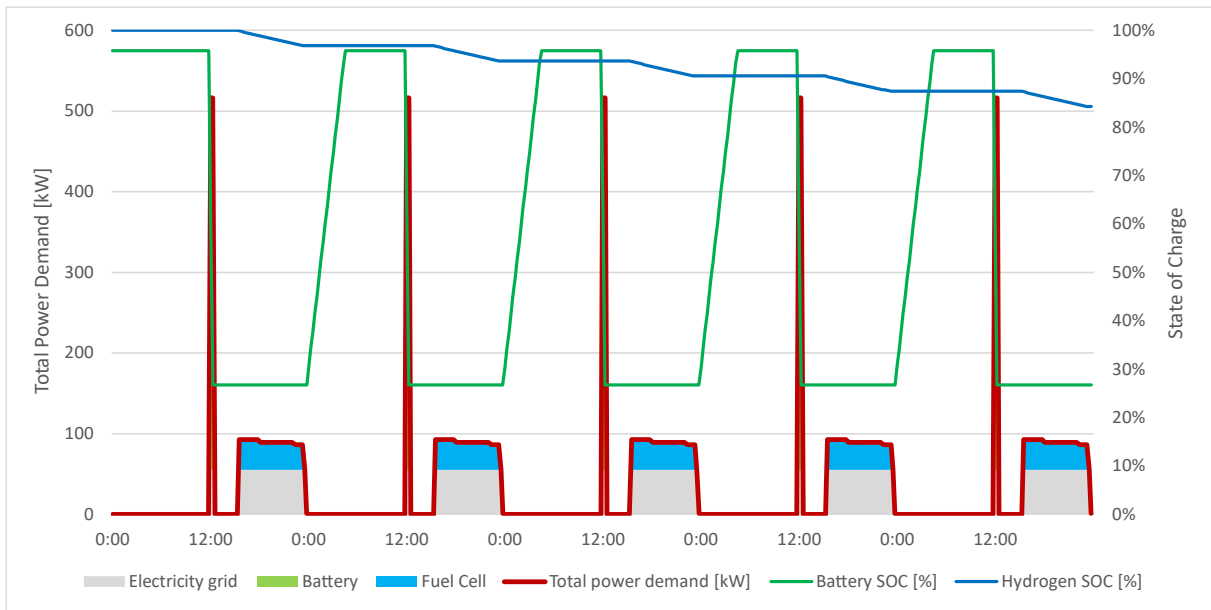
Figure 16 Energy profile configuration I-FCPB
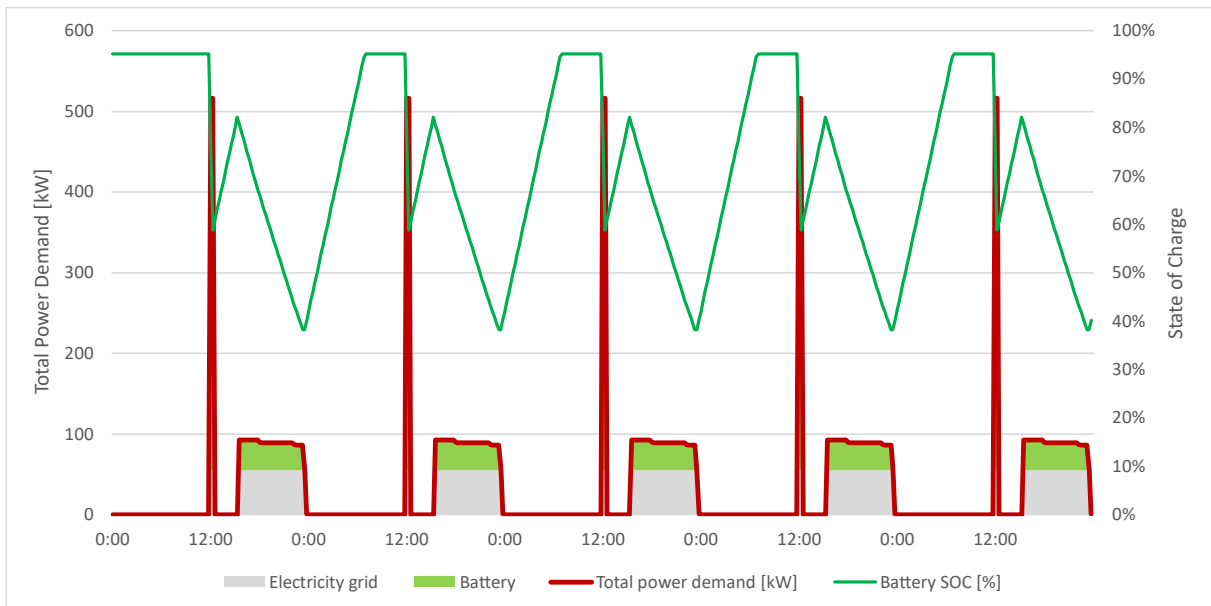
Figure 17 Energy profile configuration I-PB
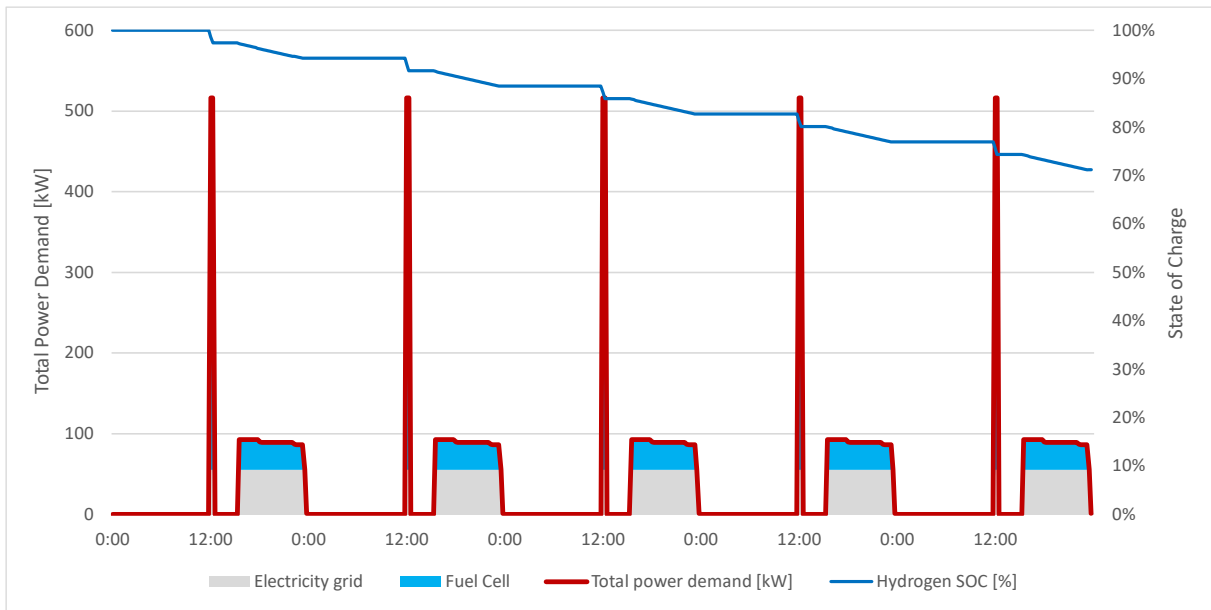
Figure 18 Energy profile configuration I-FC

5.2.2. Possible configurations for off-grid construction sites

For the off-grid scenario, only two configurations are possible, namely (II-FCPB) a battery and a fuel cell or (II-FC) a stand-alone fuel cell. Configuration II-FCPB is similar to the first configuration of the grid-connected scenario apart from the grid. The fuel cell delivers power for normal charging of the vehicles and charges the battery; while the battery is used for fast charging. Configuration II-FC utilises the fuel cell for normal and fast charging; therefore its rated power must be adequate to deliver the required power during fast and normal charging.

In configuration II-FCPB, the battery delivers 516 kW during fast charging, while the fuel cell delivers 93 kW during normal charging and charging of the battery (Figure 20). The optimal battery capacity is found using the optimal SOC windows (27% – 95%), which results in 397 kWh. For the fuel cell to deliver power up to 60% of the installed power (for a longer lifetime), the minimum installed power is 155 kW in configuration II-FCPB. The battery delivers 26% of the energy during the day, while the fuel cell delivers 74% (Figure 19). The fuel cell in configuration II-FCPB delivers 100% of the required power and energy (Figure 21). Technically, the fuel cell delivers 100% of the energy in both configurations since the battery is charged by the fuel cell. Nevertheless, the total required hydrogen in configuration II-FCPB is slightly higher due to the battery round-trip-efficiency leading to an increased amount of hydrogen tank exchanges from 29 to 31 (Table 7).
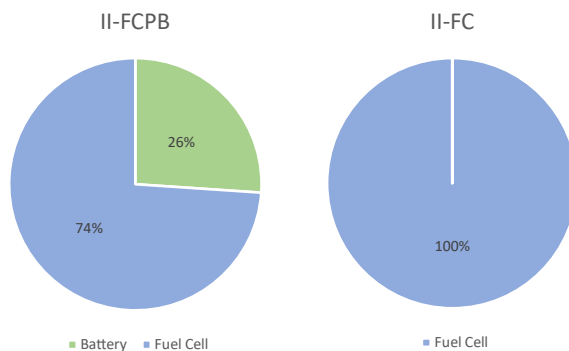
Figure 19 Energy distribution off-grid configurations

Table 7 Required hydrogen and yearly tank exchanges of the off-grid scenario

	Configuration II-FCPB	Configuration II-FC
Required hydrogen [kg]	15,605	14,694
H2 Tank Exchanges [n]	31	29
Hydrogen tank replacement rate [days/n]	8.4	9.0
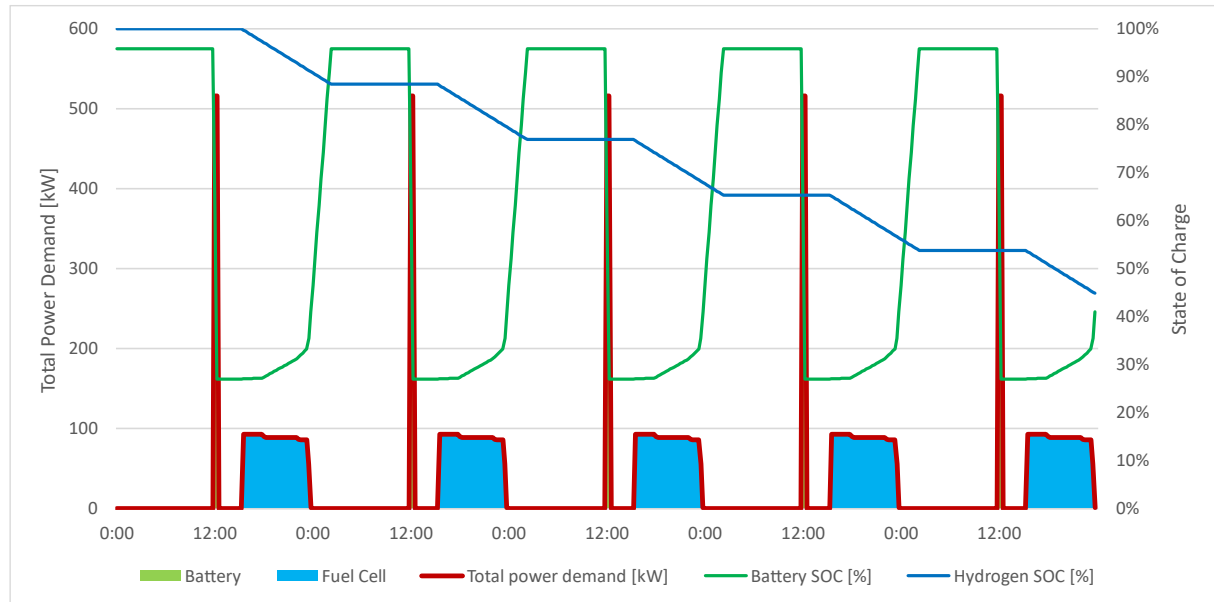
Figure 20 Energy profile configuration II-FCPB
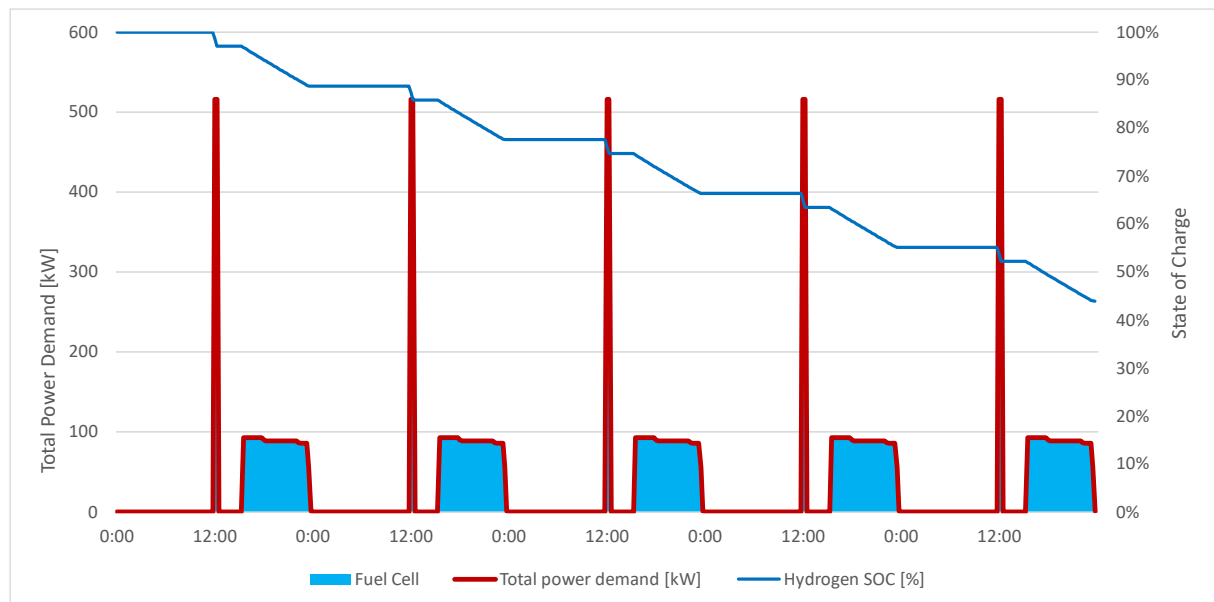
Figure 21 Energy profile configuration II-FC

5.3. MAIN ECONOMIC FACTORS OF THE FCPB-SYSTEM

In a grid-connected scenario, the total and yearly CAPEX of configuration I-PB is found to be the lowest among the three configurations (Table 8 & Figure 23). Considering just the technologies, configuration I-FCPB would have the lowest CAPEX, but configuration I require two containers instead of one, becoming more expensive than configuration II. As one container per technology is considered for

modular, safety, and practical reasons. Compared to the first configuration, the difference in total CAPEX is -10.2% for configuration II, however, the difference is 102% for configuration I-FC. For the yearly CAPEX, the difference is 0.6% and 290% for configurations I-PB and I-FC respectively. The large difference can be explained by the high investment [€/kW] of fuel cells and the reduced lifetime of the PEMFC when it is used for two cycles. Looking at the off-grid configurations, configuration II-FCPB is significantly cheaper in CAPEX and total yearly costs than configuration II-FC. The significant difference is caused by the increased size of the fuel cell and the operating conditions (similar effect as configuration I-FCPB and I-FC). The large fuel cell requires a large investment and the operation conditions impact the lifetime negatively; increasing the yearly CAPEX. Although the need for two technologies and a slight increase in energy costs, configuration II-FCPB is technically and economically favourable when taking (yearly) CAPEX, OPEX and lifetime into account.

The yearly energy cost of configuration I-PB is found to be the lowest among all configurations, due to the use of solely electricity and no hydrogen. The off-grid configurations have a significantly higher yearly energy cost since all of the energy comes from hydrogen. Due to the absence of the electricity grid in the off-grid scenario, the yearly energy cost is 85% and 44% higher for configurations II-FCPB and II-FC respectively (compared to their grid-connected equivalent configuration I-FCPB and I-FC). The high energy cost of configuration I-FC is due to the high consumption of hydrogen compared to configuration I (Table 6).

Looking further at the total yearly costs, configuration II is found to be the cheapest option. This is mainly due to the relatively low energy costs and the requirement of only one container. Configurations become significantly more expensive along with the increase in hydrogen use, installed fuel cell power, or number of containers. In all aspects (CAPEX, yearly CAPEX, Energy cost, and O&M), configurations I-FC and II-FC are by far the most expensive configurations. These results show that – economically – large fuel cells are not (yet) interesting compared to batteries. Thus, economically and logistically, configurations I-FC and II-FC are the least favourable of configurations

The LCOS of the LFP battery in configuration I-FCPB is €1.35 and €1.19 €/kWh for configuration I-PB. The lower LCOS in configuration I-PB is due to the fact of two daily cycles and therefore delivers relatively more energy. However, the effect of this on the LCOS is dampened by the lower lifetime (Table A- 3). The LCOS in configuration II-FCPB is significantly higher compared to I and II due to the use of hydrogen for charging instead of the electricity grid. The same principle applies to the LCOE of the PEM fuel cell, which delivers more energy in the configurations without a battery (I-FC & II-FC), but the lifetime is decreased significantly. The economic results are summarised in Appendix D including a breakdown in CAPEX for the battery and fuel cell (Table D- 1 & Table D- 2).

Table 8 Economic results of the five configurations

	I-FCPB	I-PB	I-FC	II-FCPB	II-FC
CAPEX FCPB [€]	€ 328,804	€ 337,066	€ 876,204	€ 528,145	€ 980,704
CAPEX Container [€]	€ 180,000	€ 120,000	€ 150,000	€ 210,000	€ 150,000
OPEX [€/yr]	€ 9,414	€ 8,427	€ 30,667	€ 16,139	€ 34,325
Energy Cost [€/yr]	€ 209,188	€ 146,148	€ 255,727	€ 385,963	€ 367,342
Yearly CAPEX [€/yr]	€ 44,811	€ 51,625	€ 231,611	€ 71,442	€ 259,234
Total costs [€/yr]	€ 288,188	€ 224,579	€ 557,655	€ 501,827	€ 700,551
LCOS [€/kWh]	€ 1.35	€ 1.19		€ 2.43	
LCOE [€/kWh]	€ 1.94		€ 3.71	€ 1.81	€ 2.72
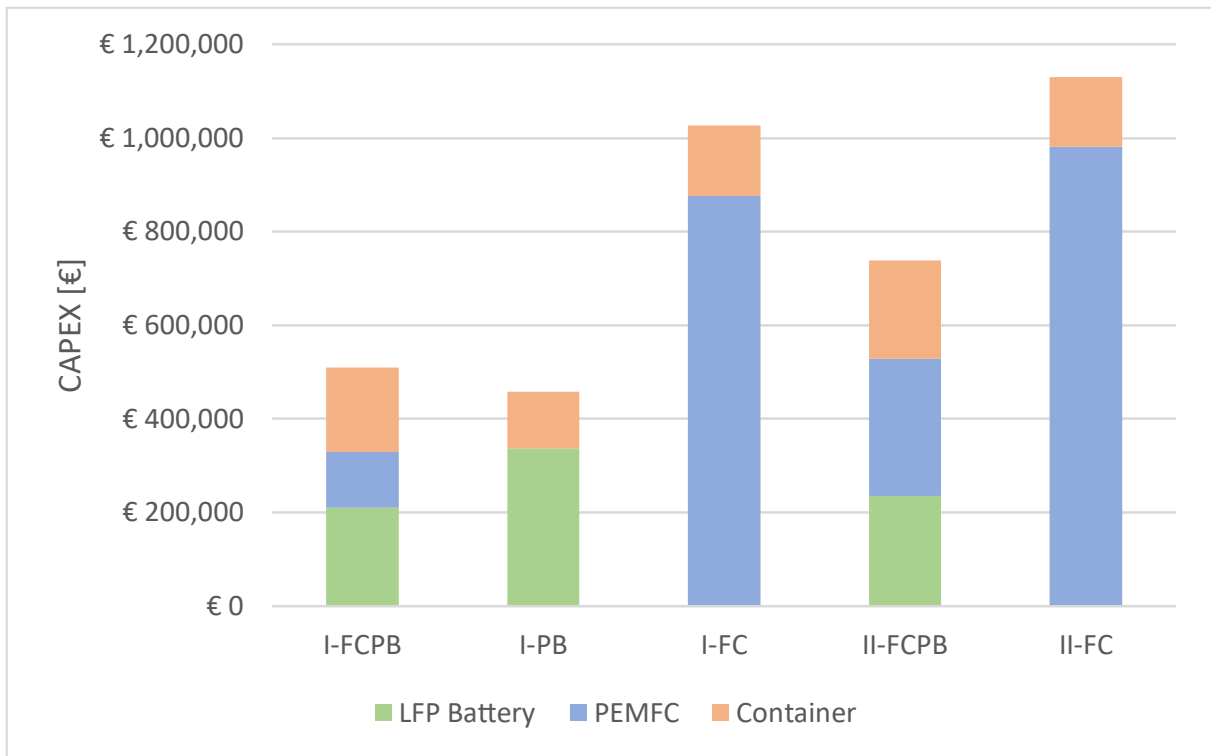
Figure 22 CAPEX of the five configurations
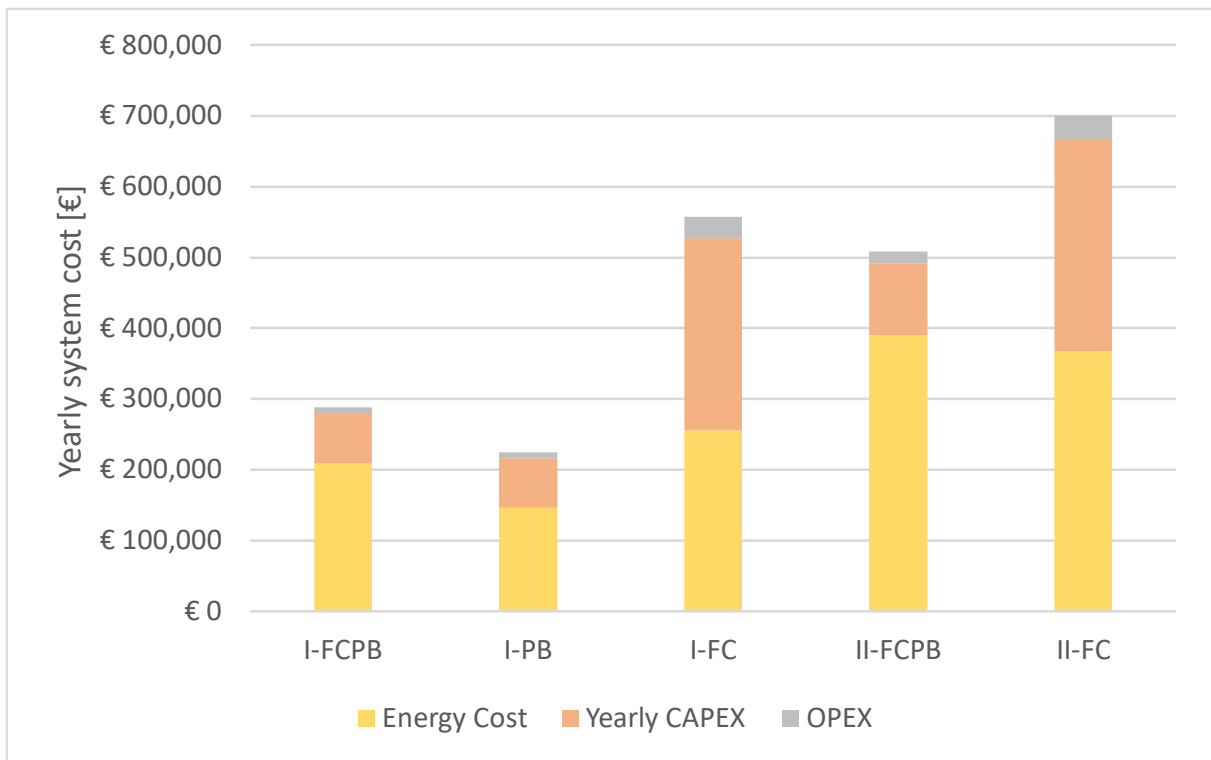
Figure 23 Yearly costs of the five configurations
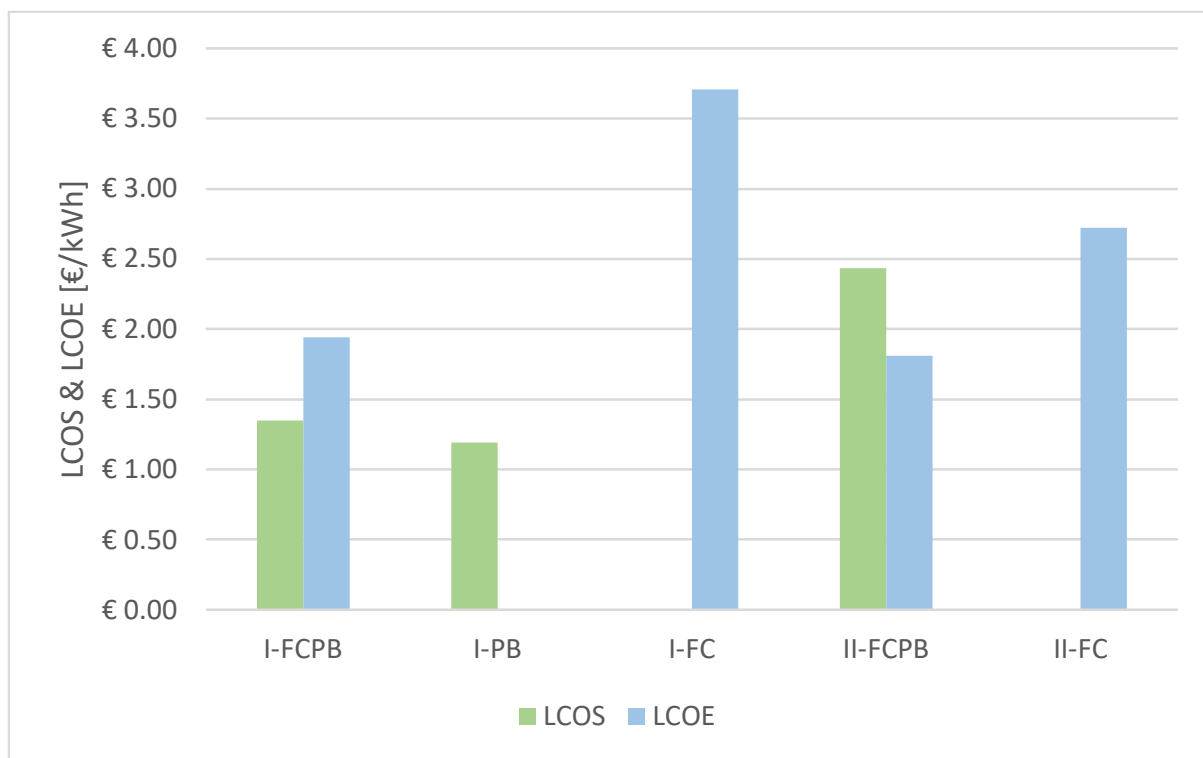
Figure 24 LCOS of the LFP battery and LCOE of the PEMFC of the five configurations

5.3.1. Economic sensitivity analyses

Figure 25 shows the results of the sensitivity analyses on the LCOS and LCOE of every configuration. The results of the sensitivity analyses show that three important parameters can be distinguished for the LFP battery, namely: Round-Trip-Efficiency (RTE), lifetime, and grid/hydrogen price. The RTE is the most sensitive parameter of the battery in every configuration followed up by the grid/hydrogen price as the second most sensitive parameter and lifetime as third parameter. Although RTE is the most sensitive parameter, its effect is limited due to its limited range, since the RTE is set to 89.5% which cannot surpass 100%. The grid and hydrogen price has a major effect on the LCOS due to its sensitivity and large range. Similar effects of grid and hydrogen price is seen for the battery in every configuration. Although the figure shows a maximum of 30% change, the grid and hydrogen price can change unlimited theoretically. Lifetime is an important parameter, but its positive effect is dampened due to the capital recovery factor. Its negative impact increases significantly when the lifetime decreases. Somewhat similar to RTE, the range of lifetime is limited due to technical limitations.

Similar parameters are found to be important for PEM fuel cells: efficiency, lifetime, and hydrogen price. The most sensitive parameter for fuel cells is the efficiency followed by hydrogen price and lifetime as third most sensitive parameter. Only configuration I-FC has a different order of sensitive parameters, namely: CAPEX power (FC), lifetime, efficiency, and hydrogen price. Similar to the RTE of a battery, the efficiency has a limited range due to technical limitations and therefore its potential effect on the LCOE is limited. The CAPEX power of fuel cells is a more sensitive parameter for larger fuel cells (Configuration I-FC & II-FC) than for smaller fuel cells. The results of the sensitivity analysis are presented in a table in Appendix D (Table D- 3)
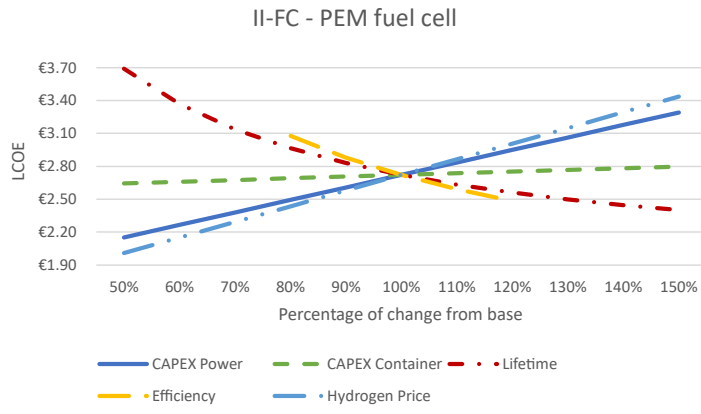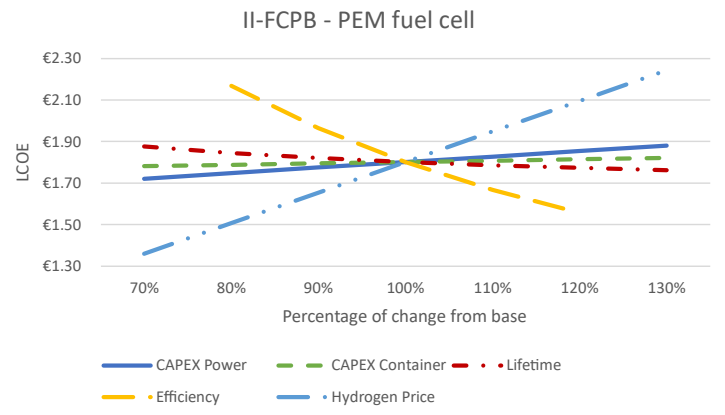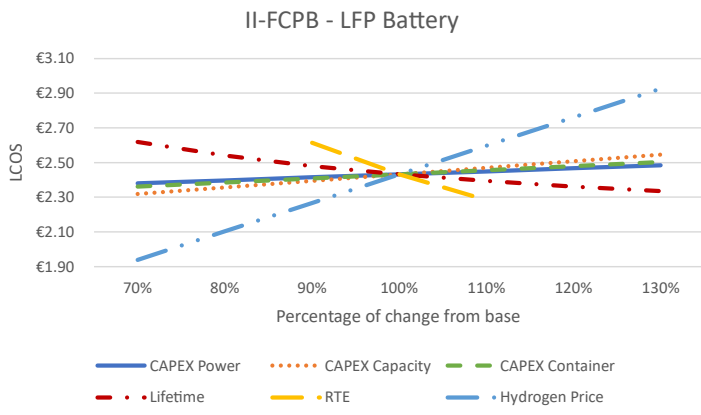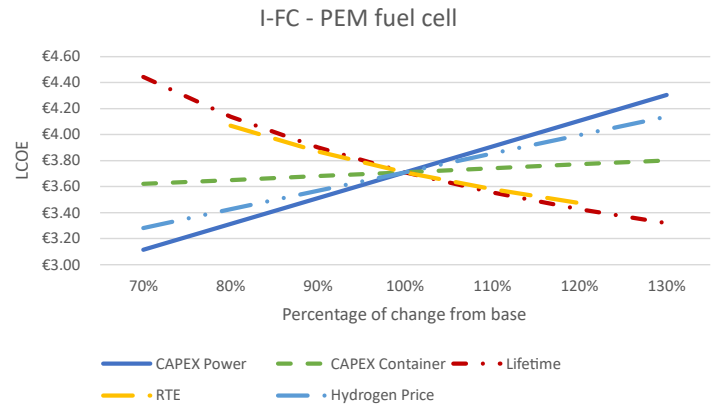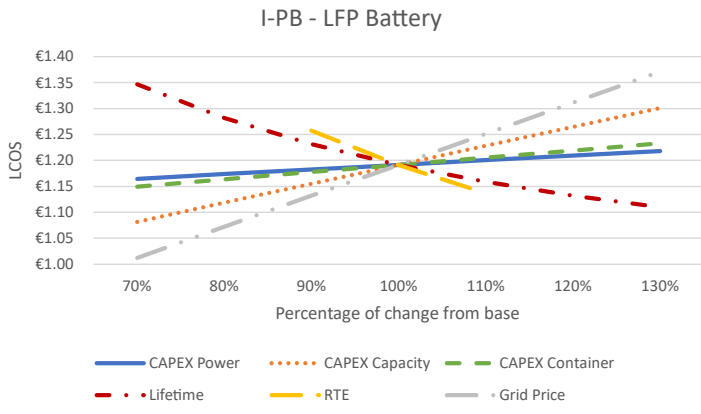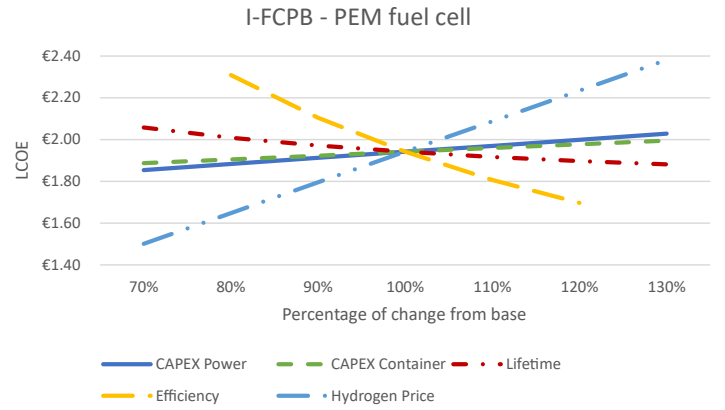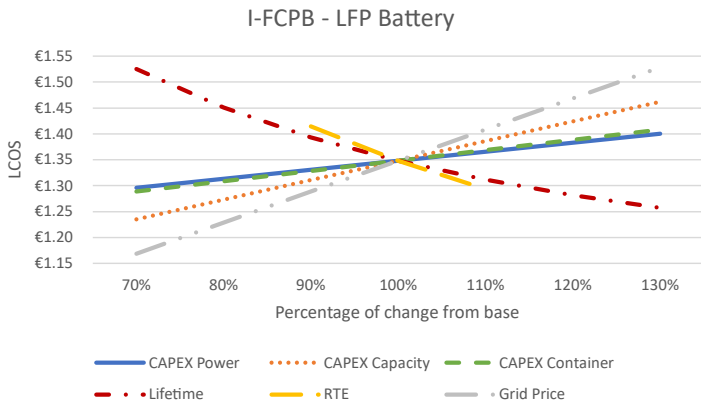
Figure 25 Sensitivity analysis LCOS & LCOE for every configuration

5.3.2. FCPB energy cost compared to BAU

Looking at the difference in energy costs of the FCPB-system and diesel, it is evident that the current use of diesel is significantly cheaper than electricity and hydrogen. Table 9 summarises the yearly energy costs of the current situation using diesel and the FCPB-system. Again, this table shows that a grid connection (configurations I-FCPB & I-FC) limits the increase of energy costs compared to the off-grid configurations (Configuration II-FCPB & II-FC). As the yearly energy costs increase by an increasing use of hydrogen.

Table 9 Comparison in yearly energy cost of BAU (diesel) and the FCPB-system (electricity/hydrogen)

Scenario / Configuration	Energy Cost [€/year]	Difference in energy cost [%]
BAU	€ 89,323	
I-FCPB	€ 209,188	+134%
I-PB	€ 146,148	+64%
I-FC	€ 255,727	+186%
II-FCPB	€ 385,963	+332%
II-FC	€ 367,342	+311%

5.4. ENVIRONMENTAL IMPACT OF THE FCPB-SYSTEM

5.4.1. FCPB emissions compared to BAU

To put the environmental impact of the FCPB-system into perspective, a comparison is made with a business-as-usual (BAU) construction site where diesel equipment is used (Figure 26). The machines are the diesel equivalent of the electric vehicles used to determine the energy profile of the zero-emission construction site. The CO_2 emissions of the FCPB-system are calculated for the configurations as described in 5.1. The environmental results used for comparison are summarised in Appendix E (Table E- 1 & Table E- 2).

The yearly CO_2 emissions from the FCPB-system are significantly lower than the emissions from the BAU scenario (Figure 26). As the Well-to-Wheel (operational + production phase) CO_2 emissions from diesel in the BAU scenario are 214,480 kg CO_2; while the emissions from the FCPB range from 51,216 – 65,118 kg CO_2 for the grid-connected configurations and 26,816 – 28,479 kg CO_2 for the off-grid configurations in 2025. The Tank-to-Wheel emissions (operational phase) from diesel is 162,573 kg CO_2 and the emissions from the FCPB range from 23,786 – 51,856 kg CO_2, while the off-grid configurations have zero emissions. The reduction in CO_2 emissions is relatively similar for both approaches, as the reduction in CO_2 emissions considering WTW are 76% – 82% for the grid-connected configurations and 93% for the off-grid configurations; while considering TTW the reduction in emissions is 68% – 85% for the grid-connected configurations and 100% for the off-grid configurations. The off-grid scenarios have the lowest CO_2 emissions due to the absence of the electricity grid which has a relatively high emission factor compared to hydrogen. In configurations where the battery delivers a considerable amount of energy, have an increased amount of emissions due to the RTE of the battery.

Besides GHG emissions, the emission of nitrogen is currently an important topic in the Netherlands. The current legislation around nitrogen emissions can determine whether a construction project can be started, continued, or not. In the BAU scenario, 46 kg of nitrogen is emitted as a result of diesel combustion. Due to the absence of high temperatures and combustion, there are no nitrogen emissions from the FCPB-system (Lewis, 2021). This fact can be of great importance for continuing construction projects and the national targets for building residential homes, despite the increase in costs.
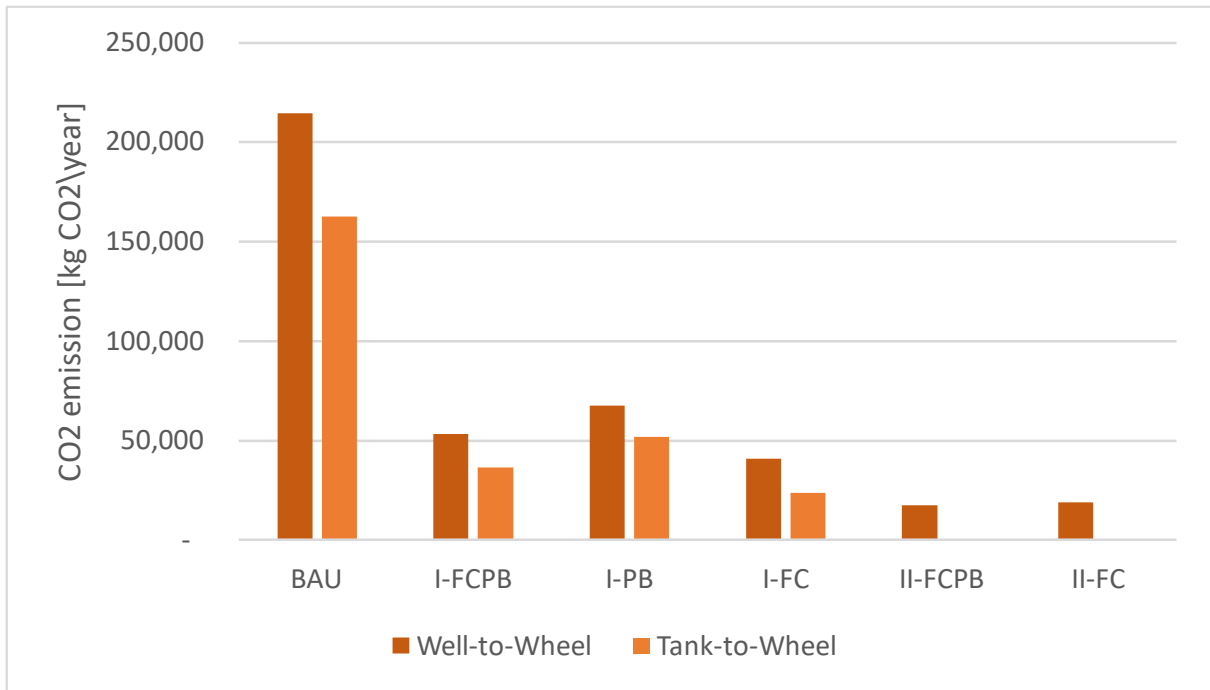
Figure 26 CO2 emission comparison BAU (diesel) vs FCPB-system (electric) in 2025

5.4.2. Future CO2 emissions of the FCPB-system

The CO_2 emissions from the electricity grid and (green) hydrogen are expected to decrease in the future (Figure 10) due to the implementation of more renewables in the Netherlands and renewables combined with nuclear energy worldwide (de Kleijne et al., 2022). The yearly CO_2 emission decreases significantly in all configurations, especially in the grid-connected configurations (Figure 27). The CO_2 emission of the grid-connected configurations can decrease by 44% – 48% in 2030 and 51% – 55% in 2035. The off-grid configuration – where the CO_2 emission is already significantly lower compared to the BAU scenario – can decrease 26% of its CO_2 emission in 2030 and 31% in 2035. The future CO_2 emissions of the FCPB-system is summarised in Appendix E (Table E- 4).
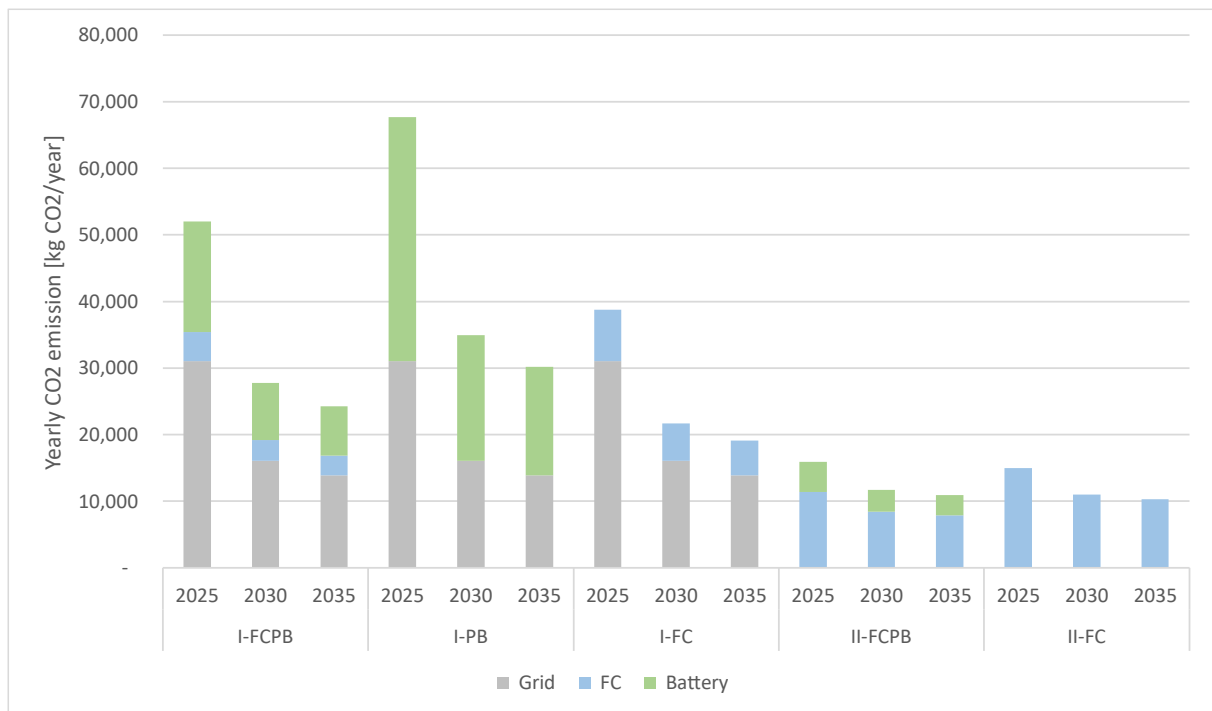
Figure 27 Future CO2 emission of the FCPB-system in 2030 and 2035

5.5. IMPLEMENTATION OF RENEWABLE ENERGY ON A ZERO-EMISSION CONSTRUCTION SITE

The potential use of renewable energy is simulated considering the power demand of the machinery and technical specifications of wind turbines (4.1.5). The corresponding installed power of renewable energy for simulations is found to be 100 kW, 250 kW, 500 kW, and 1000 kW.

5.5.1. Utilizing renewable energy

The potential production and utilization of solar and wind energy is simulated for every configuration and the new energy distribution is shown in Figure 28 and Figure 29. Looking at the implementation of renewable energy for charging the machines directly, solar energy can deliver 11,358 – 72,790 kWh and wind energy can deliver 105,681 – 229,449 kWh considering the installed powers. This means that solar energy can deliver 4.4%, 10.8%, 18.9%, and 28.2% of the total required amount of yearly energy for the installed solar power of 100, 250, 500, and 1000 kW respectively. Wind energy can deliver 41.1%, 62.0%, 77.6%, and 89.1% of the total required yearly energy for the installed wind power of 100, 250, 500, and 1000 kW respectively.

As configurations I-FC and II-FC can only utilize energy for direct charging the construction machinery, the other configurations can store a share of the renewable energy within the battery. Configurations with a battery (I-FCPB, I-PB, and II-FCPB) have a significantly higher self-consumption rate (SCR). The SCR of solar energy seems to be higher among configurations with a battery; while configurations without a battery show higher SCRs of wind energy (Figure 30). This can be explained by the fact that wind turbines have a higher capacity factor (CF) and produce more energy. As the battery's share in the energy distribution declines significantly more with the implementation of wind energy compared to solar energy.

Where the SCR is the rate of used renewable energy considering direct charging and energy for battery charging compared to the total production of solar energy. The highest SCR is found in configuration I-PB due to the large capacity of the battery and the two daily cycles instead of one. In configurations I-FCPB and II-FCPB – where the battery is only used for one cycle per day – the amount of solar energy

45

for battery charging increases with an increase of installed power first but then declines in the scenarios of 500 and 1000 kW installed solar power. This can be explained by the fact that the battery is used less often during fast charging and thus requires less energy to be recharged again. However, the percentage of batteries charged by renewable energy is increased in all of the configurations. This phenomenon is not seen for wind energy, as wind energy can be used significantly more for direct charging than solar energy. The utilization of renewable energy and the new energy distribution including solar or wind energy is summarised in Appendix F (Table F- 1, Table F- 3, Table F- 3, Table F-4).
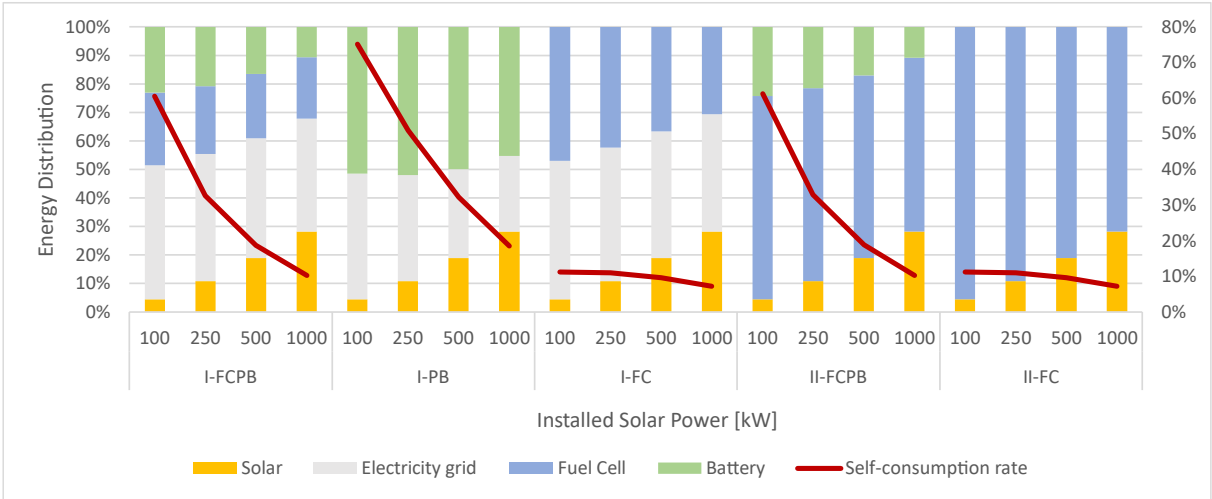
Figure 28 Energy distribution FCPB-system including solar energy
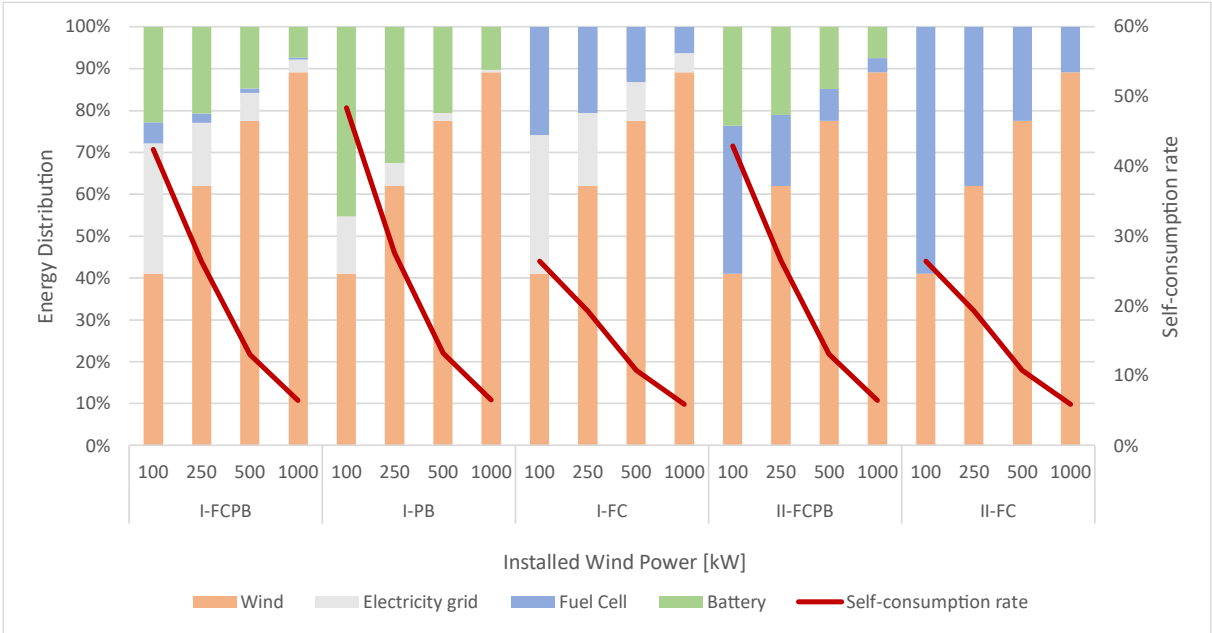
Figure 29 Energy distribution FCPB-system including wind energy
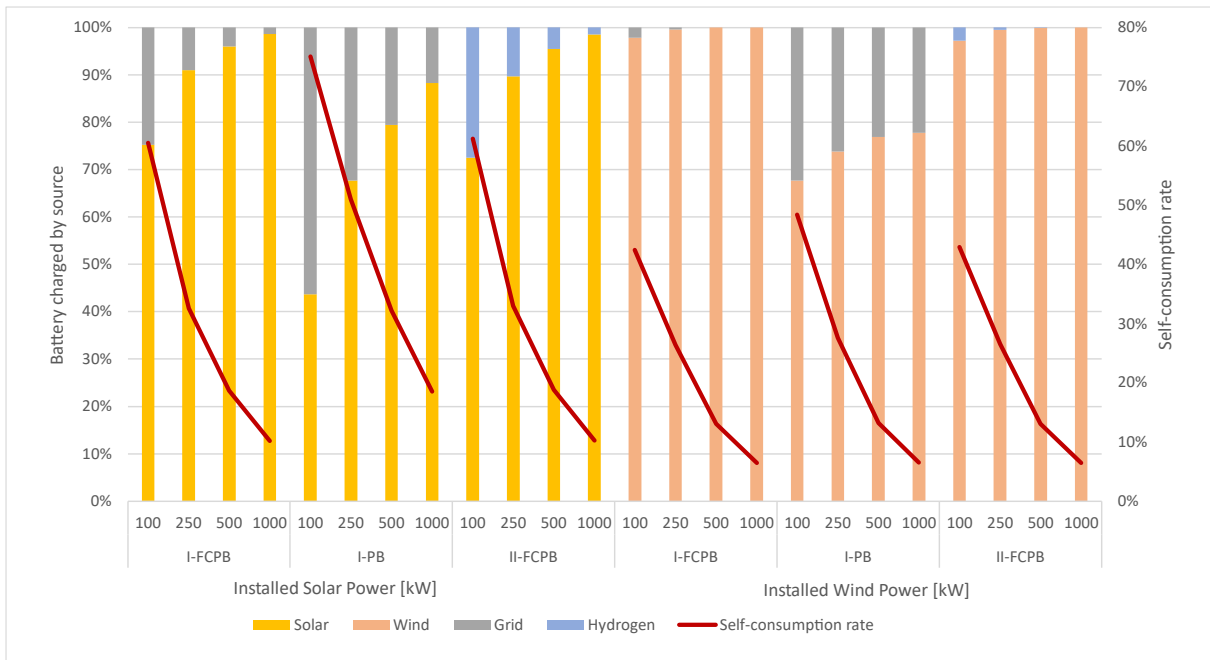
Figure 30 Battery charging by source and the self-consumption rate of solar energy

5.5.2. Effect of renewable energy on the yearly energy cost

The potential of renewable energy use on the construction site are used to show its effect on energy costs (Figure 31 & Figure 32). All configurations benefit economically from renewable energy due to the low energy price of solar and wind energy (PPA). The off-grid configurations seem to benefit the most from renewable energy compared to the grid-connected scenario. In addition to that, configurations with a battery or high hydrogen consumption have the most potential to implement renewable energy for energy cost reduction. Configuration II-FCPB has the highest absolute energy cost reduction followed by configuration II-FC. The high potential for cost reduction in configuration II-FCPB is because the battery is normally charged by hydrogen. Yet, configuration I-PB has the highest relative cost reduction (percentage-wise) when renewable energy is utilized. This is because the energy costs in the base scenario (no renewable energy) are already low compared to the other configurations and configuration II has the potential to utilize the most amount of renewable energy due to two daily battery cycles (Figure 17 & Figure 30). The highest relative cost reduction when wind energy is utilized is seen in configuration II-FCPB. The cost reduction by solar and wind energy is summarised in Appendix F (Table F- 5 & Table F- 6).
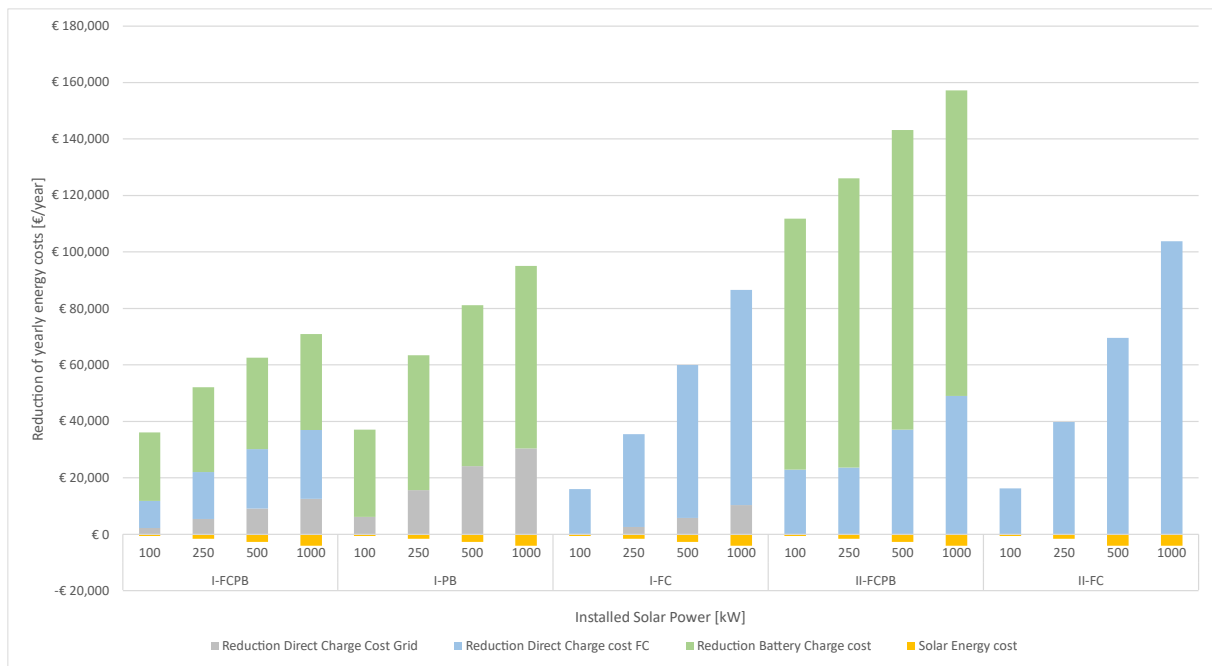
Figure 31 Reduction of yearly energy costs by implementing solar energy
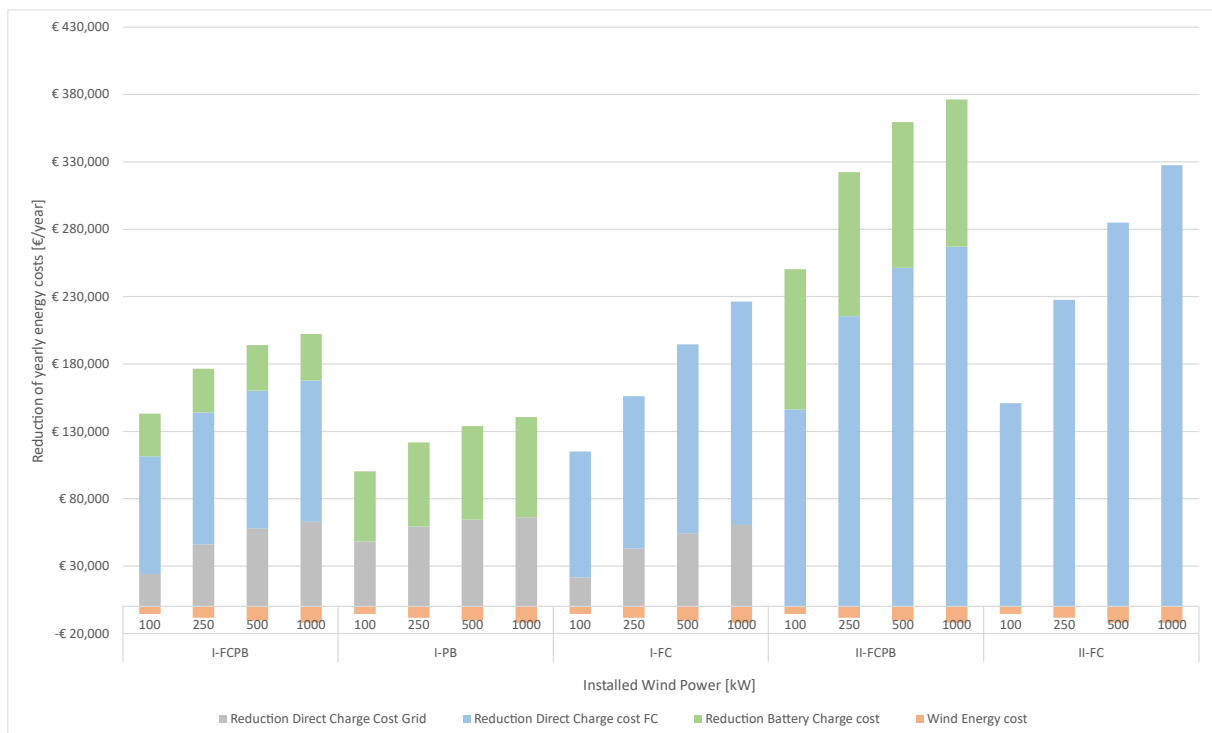
Figure 32 Reduction of yearly energy costs by implementing wind energy

5.5.3. Effect of renewable energy on CO2 emissions

Even though the CO_2 emission of the base scenario is already significantly lower than the BAU scenario with diesel, renewable energy can reduce these emissions even further (Figure 33 & Figure 34). The most potential for CO_2 emission reduction is in the grid-connected configurations as grid electricity has the highest CO_2 emission factor. Configuration I-FC has the highest CO_2 emission reduction (26% – 66%) followed by configuration I-FCPB (25% – 42%) with the implementation of solar energy. Utilization of wind energy even shows larger CO_2 emission reduction of 54% – 74% in configuration I-PB and 41% – 67% in configuration I-FCPB. The relatively low CO_2 emission reduction in configuration I-FC compared

to configuration I-FCPB & I-PB is due to the absence of a battery and the high consumption of green hydrogen. The configurations where hydrogen has a significant share of the energy distribution show a lower reduction in emissions due to its already (assumed) low emission factor. It seems that wind energy has a larger potential to reduce CO_2 emissions in the grid-connected configurations compared to solar energy due to its larger potential for direct charging and reducing grid energy. For the off-grid configurations, solar energy has more potential for CO_2 emission reduction due to a lower emission factor compared to wind. The CO_2 emission reduction by solar and wind is summarised in Appendix F (Table F- 7 & Table F- 8).
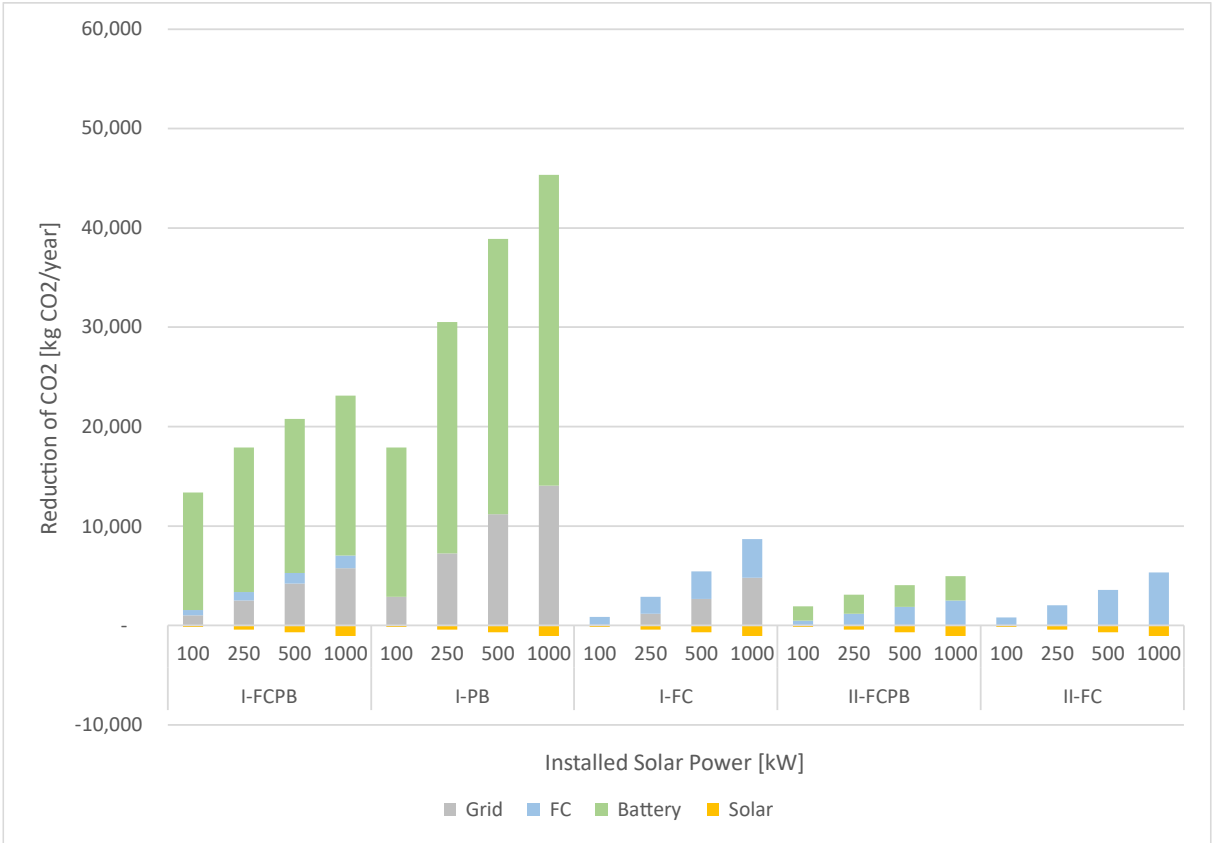
Figure 33 Reduction of CO2 emission by implementing solar energy
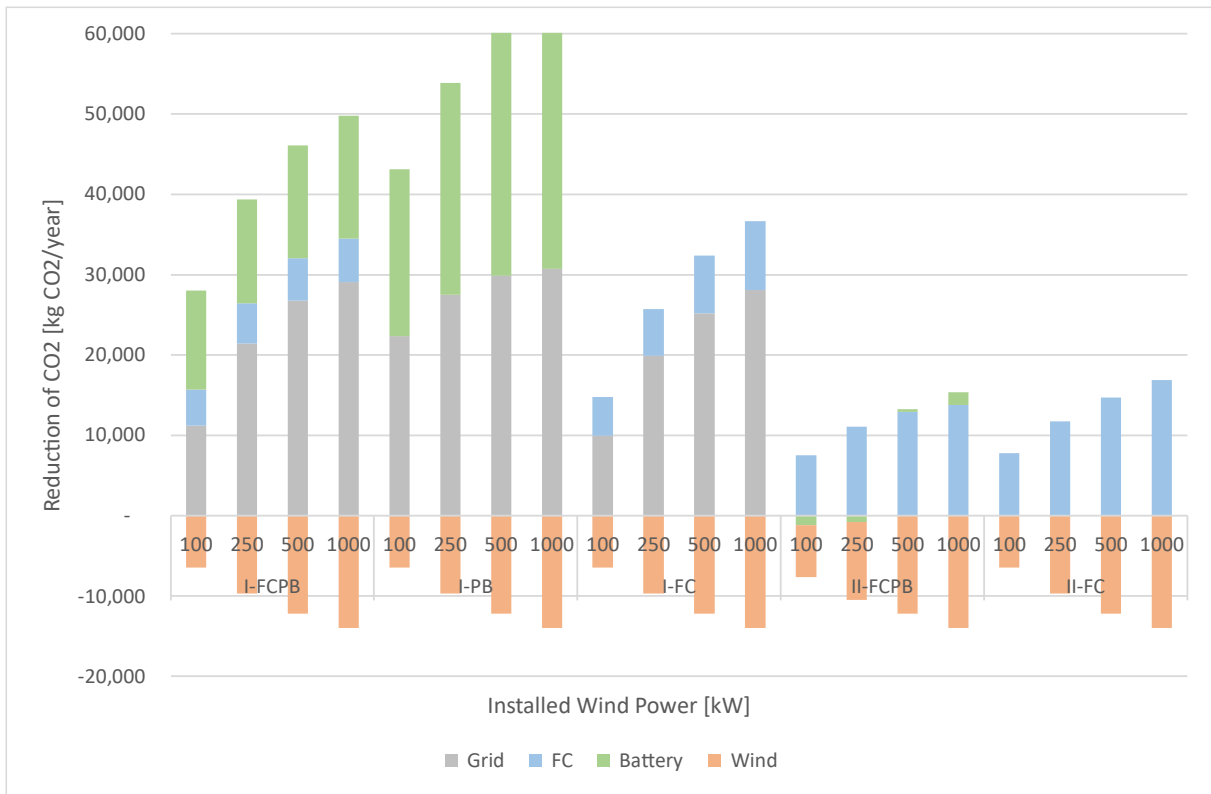
Figure 34 Reduction of CO2 emission by implementing wind energy

6. DISCUSSION

Possible configurations for an electric zero-emission construction site have been examined taking technical, economic and sustainability parameters into account. Results of this study show that an LFP battery and PEM fuel cell have potential for employment on construction sites. Especially an LFP battery is interesting due to its lifetime, relatively low CAPEX, low total yearly costs and its potential to utilize renewable energy. PEM fuel cells are likely more interesting as backup power, normal charging where the power demand is relatively low and consistent, and off-grid construction sites due to high CAPEX and hydrogen price. Despite the high energy costs, the FCPB-system has a great advantage over the current business-as-usual construction sites using diesel, namely the fact that this system does not emit nitrogen (NO_x, NH_3) and the possibility to implement renewable energy for the reduction of energy costs and CO_2 emissions. The outcome of this study is further discussed in the following sections.

6.1. INTERPRETATION OF RESULTS

The results of this study are validated in two ways: (1) the sensitivity analysis of the LCOS/LCOE and (2) comparing results with the literature and other studies. First, the results of a sensitivity analysis helps in validation by detecting unrealistic model behaviour, identify important assumptions, and suggest the accuracy for calculating parameters (Smith et al., 2008). Furthermore, input data and results from this study is compared to the literature and results from other studies in this section.

According to the literature, it is very difficult to generalize the ageing behaviour of lithium batteries with respect to operational conditions (Vermeer et al., 2022). In addition to that, the literature around LFP batteries can be contradicting sometimes as some found that SOC windows or DOD do not have (much) effect on the lifetime; while others suggest that SOC windows or DOD is, next to temperature, a large or even the main ageing component. However, many studies use SOC windows or DOD to model or predict the lifetime of LFP batteries (Beltran et al., 2019; Sayfutdinov & Vorobev, 2022; Vermeer et al., 2022). The used lifetime of the battery of 9,6 years (2 cycles/day) and 12 years (1 cycle/day) are found by using an EoL criterion of 80% instead of 75% from Sayfutdinov and Vorobev (2022). An EoL criterion of 80% is used since the majority of the literature uses this threshold. Sayfutdinov and Vorobev (2022) found these lifetimes for daily cycles, thus 365 days a year; this would translate to 4380 cycles (1 cycle/day) and 7008 (2 cycles/day) cycles. In this pilot study, the lifetime is not adjusted for the number of days, as with 260 working days per year, the number of cycles would be 3,120 and 4,992 which corresponds more to the current literature that suggests cycle lifetimes of 2,400 – 4,550 cycles (Lamb & Pollett, 2020; Viswanathan et al., 2022). In addition to that, the operating conditions on construction sites are expected to be harsher which can have a negative effect on the lifetime. Therefore, a more conservative approach towards cycle lifetime is chosen.

A lifetime prediction method is used to calculate the lifetime of the PEM fuel cell according to its operating conditions. Although this method includes four different operating conditions, it does not include normal or low power load (<60% of installed power). Where the fuel cell degrades severely when it is used for high power load (>60%), degradation from normal or low power load cannot be calculated. Thus, purely theoretically, the fuel cell would not degrade when it starts up for one time and continues to operate at normal to low load according to this approach. The predicted lifetimes of 4.7 – 10.4 years or 10,998 – 34,384 hours do correspond to the literature and market. The lifetime is calculated by multiplying the lifetime in days with the operating conditions where fast charging takes 0,5 hours, normal charging takes 8,5 hours, and battery charging in configuration II-FCPB takes 3,1 hours. Whenever the PEMFC operates at high power during the entire normal charging cycle (8,5

hours), the lifetime decreases severely to 1.6 years or 3,472 hours. The range in lifetime is quite large and depends highly on the operating conditions. The predicted lifetime of a fuel cell vehicle was 1,000 hours in the study of Pei et al., (2008) and 20,000 hours according to the manufacturer PowerCellution. Stayers found that fuel cell components (membranes and hardware) can last for 10,000 hours up to 23,000 hours and when extrapolated, lifetimes beyond 40,000 hours might be possible (Stayers, 2014). Then, there is the longest-running PEM power plant of more than 65,000 hours developed by NEDSTACK (NEDSTACK, n.d.). Hence, the predicted lifetimes at the upper range of this research are relatively high when compared to the manufacturer data and Stayers, but they are not unusually. The lifetime prediction method of Pei et al., (2008) and Chen et al., (2015) was used for a fuel cell vehicle and was only 10% off compared to a real fuel cell vehicle with a lifetime of 1,100 hours. Which shows that the prediction method can estimate the lifetime quite accurate. Although Pei et al., (2008) and Chen et al., (2015) mention that this method can be used for predicting the lifetime of fuel cells in every operating mode, it is unknown how well the prediction method works for stationary fuel cells considering the operating conditions and the absence of voltage degradation of normal load in the calculation approach.

Whenever possible, data from the most recent years is used. Therefore, the study was conducted using the grid electricity price from 2022, which was exceptionally high. According to data from CBS, the yearly mean electricity prices from 2018 – 2022 range from 0.214 – 0.256 €/kWh while the electricity price in 2022 was 0.54 €/kWh (CBS, 2022). Electricity costs directly influence yearly energy costs, LCOS of the battery, and cost reduction by renewable energy. The effect of the grid price is shown in the sensitivity analyses (Figure 25 and Table D- 3). The used hydrogen price is 25 €/kg H_2 or 0.75 €/kWh, which is also exceptionally high compared to the literature or market. EEX is the first market-based hydrogen index and their published hydrogen price for Germany is ranging from 0.2177 €/kWh up to 0.2598 €/kWh (EEX Group, 2023). A study performed by CE Delft (2018) investigating different routes for hydrogen, found a maximum LCOH of 5.5 €/kg H_2 (CE Delft, 2018). Tromp et al., (2022) found in a cost minimisation study a LCOH of 6.24 – 11.29 €/kg H_2 (Tromp et al., 2022). The LCOH of both studies is found for green hydrogen. Thus, the used hydrogen price is several times higher than the literature suggests. This can partly be explained by the fact that the hydrogen price includes transportation and storage. It is expected that the (green) hydrogen price will decrease due to the increase in demand, installed renewable power, and technological innovations which leads to lower energy costs and LCOE of the PEM fuel cell. Similarly to the grid price, the hydrogen price influences the results of the economic analyses immediately (Figure 25 and Table D- 3).

The LCOS of the LFP battery (1.19 – 2.43 €/kWh) is relatively high compared to the literature. In an energy storage comparison study, Viswanathan et al., (2022) found that the LCOS of LFP batteries ranges between 0.300 – 0.500 €/kWh (Viswanathan et al., 2022). The used battery size for calculating the LCOS in the comparison study was significantly higher than the required size for the construction site in this study. Jülch et al., (2015) found a range of LCOS of LFP batteries using PV electricity of 0.75 – 0.83 €/kWh for 2013 and expected it to drop towards 0.17 – 0.25 €/kWh in 2020. The difference in LCOS can be explained by four factors. First, the significantly higher electricity price used in this study of 0.54 €/kWh in 2022, as Jülch used an energy price of 0.9 – 0.14 €/kWh and Viswanathan et al., (2015) used 0.03 €/kWh. Secondly, Viswanathan assumed 365 cycles of 100% DOD compared to 260 cycles and a DOD of 36.4 – 68.8 % which is used for this study. As third, the energy to power (E/P) ratio used in this study is unusual, as most batteries' E/P ratios are 1.0 or above like in the studies where Jülch used an E/P ratio of 1.0 and Viswanathan used E/P ratios of 1.0 – 10. An increase in E/P ratio increases the total CAPEX but usually decreases the installed price per unit of energy (€/kWh) due to the scale of economy. In addition to that, a higher E/P means that the battery also can discharge more energy, decreasing the LCOS. Lastly, the container costs are included in the LCOS which increases the total

CAPEX. Similar to the LCOS of the LFP battery, the LCOE of the PEMFC (1.81 – 3.71 €/kWh) is relatively high as well. As the NREL suggest that the LCOE of a stationary PEM fuel cell is 0.368 €/kWh, however, the NREL used a cheap storage method of salt caverns and large installed powers (NREL, 2021). It is expected that the LCOE and LCOS of battery and fuel cell technologies will remain higher on construction sites compared to the large-scale stationary equivalents due to the mentioned factors (lack of economy of scale, containerized, harsh working environment) for the LFP battery and PEMFC.

As the results from the sensitivity analysis indicate, the LFP battery is the most sensitive to changes in Round-Trip-Efficiency, grid/hydrogen price, and lifetime. The LCOE of PEM fuel cells is most sensitive to a change in efficiency, hydrogen price and lifetime. This applies to all configurations except for configuration I-FC (grid-connected with one large fuel cell) where CAPEX power is the most sensitive parameter. This result can be explained by the fact that the total CAPEX is relatively high in configuration I-FC compared to configuration I-FCPB and II-FCPB and its energy delivery is relatively low compared to configuration V due to the grid connection. However, the impact of RTE/efficiency and lifetime is only limited due to technical limitations whereas the grid and hydrogen prices can change more than 100%. The positive change in RTE/efficiency is technically limited due to the maturity of the technologies and the theoretical maximum values. For that reason, the range of RTE and efficiency are adjusted by 10% and 20% respectively. Even with the adjusted range of the RTE, it is more likely that the increase of RTE is even below 10%, as 96% seems to be the upper limit (Choi et al., 2016). For PEM fuel cells the maximum efficiency in theory is 83% (Bharti & Natarajan, 2022); while in practice this would be around 60% (US Department of Energy, 2016). Considering the maximum efficiency in practice, this is an increase of 14 – 18% from the base values of 51% – 52.6%.

For simulating the potential of renewable energy for the battery, it is assumed that the battery can be charged at all times whenever it is not discharging. Therefore, the battery charge time is very extended and dependent on renewable energy. In practice, risks of insufficient battery energy would be avoided and therefore it is expected that the grid would be used more often to ensure that the battery's SOC is at its desirable state; leading to a lower self-consumption rate, and a lower reduction in costs and CO_2 emissions. However, forecasting of renewable energy generation is improving (Lima et al., 2020; Sweeney et al., 2020) which can help utilise as much renewable energy as possible for battery charging, by postponing and minimizing charging from the grid and fuel cell.

For calculating the CO_2 emissions, an LCA approach is used for the energy use on the construction site, considering CO_2 emissions from the operational and production phase. The WTW approach includes emissions from the production phase and the use phase. As for hydrogen and renewables, only emissions from the production phase can be considered, as there are no emissions during the use phase from these energy sources. This is done to make a fair comparison of the environmental impact of different configurations and energy sources (Dutch electricity grid, hydrogen, and renewables). Due to this approach, the emissions from diesel and electricity grid (Figure 26) are approximately 32% and 31% (in 2025) higher compared to the emissions from the operational phase or the Tank-to-Wheel (TTW) approach. However, the CO_2 emission reduction by the FCPB-system compared to the BAU scenario considering the WTW and TTW approach, are relatively similar in 2025. Usually, emissions from renewables and green hydrogen are set to zero, as often only the emissions from the operational phase are accounted to the end-user. Emissions from producing the battery, fuel cell, and container are not taken into account due to the scope and time limitations.

6.2. LIMITATIONS
The focus of this study was identifying potential configurations of fuel cells and battery for the electrification of construction sites. The model was used for a pilot construction site, and therefore the

results cannot be generalized directly. However, the results and the model provides a framework for future projects. Further research can be done to make the FCPB-system a more general and modular system so it can be utilized effectively on multiple sorts of construction sites (6.2).

As the main focus of this study was towards the FCPB-system, capacity fade and SOC windows of the construction machines' batteries are not taken into account. The simulated results are for the initial year of the construction site and the batteries' state of health (SOH) of the construction machinery is expected to be 100%. The charging schedule would presumably look somewhat different when capacity fade and SOC windows for optimal battery life of the construction equipment are taken into consideration. When the SOH decreases over time, the required fast charging moment (currently at 12:00) might be scheduled earlier in the day and/or take longer. Perhaps, as the batteries' SOH decreased significantly, two fast-charging cycles are necessary during the working day as the SOC of the larger machines is near zero at the end of the working day.

Power fade of batteries and PEM fuel cells depends on several factors and no general method of calculating the power loss was found in the literature (Roshandel & Parhizgar, 2013; Sayfutdinov & Vorobev, 2022). Therefore, power fade of the LFP battery and PEM fuel cell is not taken into consideration. Power fade is expected to be an important aspect for fast charging the machines during the working day, as time is an important factor in the construction sector. In addition to that, power is also an important factor for the PEMFC's lifetime, as high power load (>60%) increases its voltage degradation severely.

The hydrogen tank replacements in the model are done whenever the tank reaches 0% and is then replaced immediately. However, in practice, whenever the hydrogen tank would reach 0% during a charge cycle, it is expected that the tank would be replaced before reaching 0%, or the charging process must be taken over by another power source (electricity grid/battery). The hydrogen tank isn't replaced before 0% in the model, so the right amount of hydrogen tank replacements can be counted.

For calculating the required container size, market examples are used. Within a container, necessary technologies such as transformers, inverters, control systems, and a cooling system can be found. The energy density (including all earlier mentioned technologies) of the containerized LFP batteries ranges from 45.3 to 90.5 kWh/m^3 and the PEM fuel cell from PowerCellution has a power density of 36.2 kWh/m^3. However, it is unknown how much space is required for the other technologies (transformers, cooling system, etc.) and thus the required container size could be on the short side. However, the container cost does not have a large effect on the LCOS/LCOE but is convenient to know the required size for practical reasons such as transportation and placing of the container on the construction site. Costs for containerizing the PEM fuel cell are used for calculating containerizing the LFP battery since there was no data about containerizing costs for (LFP) batteries. Therefore, the containerized costs for the LFP battery can be different, however similar technologies for a containerized battery are necessary. Thus similar costs are to be expected.

6.3. FUTURE RESEARCH

As the FCPB-system is solely designed for this particular pilot, the system is less versatile compared to a system that is designed for the average project. In order to have a versatile FCPB-system that can be used for different types of construction sites, market research can be done to determine the general needs for small, medium or large construction sites.

The results of this study indicate that the energy costs and the LCOS/LCOE of the FCPB-system are not yet competitive with the current diesel system. Also, other studies (Palm & Bryngelson, 2023; Stokke et al., 2023) point out that economic factors are barriers to adopting electric or zero-emission

construction sites. Even though technologies for electrification and decarbonisation of the construction sector are available, economic factors are serious barriers. More research is necessary for decreasing the overall investment cost and energy cost for lowering the LCOS of batteries and LCOE of fuel cells. Improvements in efficiency and lifetime and a decrease in PEMFC CAPEX and hydrogen price will assist in decreasing the overall system costs as the sensitivity analyses indicate.

For systems such as the FCPB-system, an EMS is necessary to operate and control it correctly. Although the model in this study is made in Excel, data/results can still be implemented in an EMS. In addition to that, the prediction of solar and wind energy would be a useful addition to enhance the implementation of renewable energy for reducing energy costs and CO_2 emissions. Next to operating and controlling the FCPB-system, an EMS could also be used for predicting the hydrogen tank replacements.

Many sectors, including the construction sector, are facing challenges around nitrogen emissions since this factor can determine whether a project can get a building permit or not. The model can calculate nitrogen emissions from the current situation or BAU scenario where diesel equipment is used. Nitrogen emission legislation is dependent on the location, as it is important to reduce emissions around the so-called "Nature 2000 areas". All of the 162 Dutch nature 2000 areas are listed by the Ministry of Agriculture, Nature, and Food Quality at https://www.natura2000.nl/gebieden. Whenever the project location and the required machinery are known, it is possible to investigate the amount of nitrogen emissions from diesel equipment. In some cases, this might mean that a combination of diesel equipment up to the allowable threshold and electric equipment will be employed, as BAU is still cheaper. However, the model does not consider the nitrogen emission threshold yet, due to its location dependency.

7. CONCLUSION

This thesis aimed to identify possible configurations for electrifying construction sites including technical, economic and sustainability aspects. Based on the power and energy demand of construction equipment, a moment of fast charging during the day is necessary for the large machines while all machines can be charged up to 100% before the start of the next day. Various combinations of fuel cells and batteries were considered, subjected to a 100% reliability principle. Three different configurations are possible for the grid-connected scenario; while only two configurations are possible for off-grid situations as a battery cannot be utilized solely without another power source to charge it.

The LFP battery seems to be a robust power source with a lifetime of 9.6 – 12 years, considering the required operating conditions. On the contrary, the lifetime of a PEM fuel cell is very dependent on the operating conditions, as voltage degradation increases significantly with the increase of start-stop cycles, load changes, and high power load. For the considered operating conditions, the lifetime of the PEM fuel cell was predicted to be 4.7 – 10.4 years.

The economic analysis shows that large PEM fuel cells are not (yet) competitive compared to LFP batteries. The same principle counts for hydrogen, as large consumption of hydrogen is not (yet) competitive with the electricity price in the Dutch power system. For the grid-connected scenario, utilizing just one large LFP battery (configuration I-PB) for both charging cycles is the best economic option, while for the off-grid situation, an LFP battery for fast charging and a small PEM fuel cell for normal charging (configuration II-FCPB) is economically favoured. The LCOS of the LFP ranges from 1.19 – 2.43 €/kWh and the LCOE of the PEMFC from 1.81 – 3.71 €/kWh. According to the sensitivity analysis, it seems that efficiencies of the LFP battery and PEMFC are the most sensitive parameters (except for configuration I-FC) followed by the grid/hydrogen price and lifetime. The order of sensitivity depends on the size and amount of energy generated by the technology. Although RTE, efficiency, and lifetime are very sensitive parameters, they can only be expected to increase by a limited amount due to technical limitations. As the maximum efficiency seems to be around 96% for an LFP battery (Choi et al., 2016) and for a PEM fuel cell 60% in practice and 83% theoretically (Bharti & Natarajan, 2022; US Department of Energy, 2016). Grid price on the other hand can change by more than 100% as the grid price increased from 0.254 €/kWh in 2021 up to 0.54 €/kWh in 2022. The same principle counts for the hydrogen price.

From an environmental perspective, green hydrogen is favoured over grid electricity, both now and in the future. Although both CO_2 emission factors drop in the future, green hydrogens' CO_2 emission factor remains significantly lower. Renewable energy is very interesting when looking at its potential for cost and CO_2 reduction. From an economic perspective, renewable energy is mainly interesting for configurations with a battery (I-FCPB, I-PB, II-FCPB) as this allows storing renewable energy next to direct utilization of it and for configurations with a high hydrogen consumption (I-FC, II-FCPB, II-FC). Configurations without a battery can only use renewable energy for direct charging during the day. From an environmental perspective, renewable energy is mainly interesting for grid-connected configurations. Since a large portion of normal charging is done at the end of the day, solar energy only has limited potential for direct charging; while wind energy can still generate at these hours.

Finally, a comparison is made between the BAU scenario with diesel and the FCPB-system. It seems that the energy costs are significantly higher compared to diesel (+64% – +332%). On the other hand, the FCPB-system has a much lower CO_2 emission, zero nitrogen emissions, and the advantage to implement renewable energy for the reduction in energy costs and CO_2.

REFERENCES

Ahn, C. R., & Lee, S. (2013). Importance of Operational Efficiency to Achieve Energy Efficiency and Exhaust Emission Reduction of Construction Operations. *Journal of Construction Engineering and Management*, *139*(4), 404–413. https://doi.org/10.1061/(ASCE)CO.1943-7862.0000609

ANP, & Businessinsider. (2021, June 1). *Bouwbedrijven elektrische machines stikstof en CO2*. https://www.businessinsider.nl/bouwbedrijven-elektrische-machines-stikstof-co2/

Barati, K., & Shen, X. (2017). Optimal Driving Pattern of On-Road Construction Equipment for Emissions Reduction. *Procedia Engineering*, *180*, 1221–1228. https://doi.org/10.1016/j.proeng.2017.04.283

Bauer, L., & Matysik, S. (n.d.). *Wind Turbine Models - Windturbines database*. Retrieved July 11, 2023, from https://en.wind-turbine-models.com/turbines

Bdcontainers. (2023). *Afmetingen zeecontainer*. https://bdcontainers.com/afmetingen-zeecontainer/

Beltran, H., Tomas Garcia, I., Alfonso-Gil, J. C., & Perez, E. (2019). Levelized Cost of Storage for Li-Ion Batteries Used in PV Power Plants for Ramp-Rate Control. *IEEE Transactions on Energy Conversion*, *34*(1), 554–561. https://doi.org/10.1109/TEC.2019.2891851

Bharti, A., & Natarajan, R. (2022). Proton exchange membrane testing and diagnostics. In *PEM Fuel Cells* (pp. 137–171). Elsevier. https://doi.org/10.1016/B978-0-12-823708-3.00007-9

Blok, K., & Nieuwlaar, E. (2017). *Introduction to Energy Analysis*.

BNEF. (2022). *Wind and Solar Corporate PPA Prices Rise Up To 16.7% Across Europe*. https://about.bnef.com/blog/wind-and-solar-corporate-ppa-prices-rise-up-to-16-7-across-europe/

Bobcat. (2019). *E10*. https://www.123machineverhuur.nl/

Bouwmachines.nl. (2023). *Van der Zanden brengt eigen stroom naar de bouwplaats*. https://www.bouwmachines.nl/57929/mega-batterij-brengt-eigen-stroom-naar-de-bouw

CBS. (2020). *Rendementen en CO2-emissie van elektriciteitsproductie in Nederland, update 2020*. https://www.cbs.nl/nl-nl/achtergrond/2022/05/rendementen-en-co2-emissie-van-elektriciteitsproductie-in-nederland-update-2020

CBS. (2022). *Gemiddelde energietarieven voor consumenten*. https://opendata.cbs.nl/#/CBS/nl/dataset/84672NED/table

CBS. (2023). *Hoogste aantal nieuwbouwwoningen in afgelopen decennium.* . Centraal Bureau Voor de Statistiek. https://www.cbs.nl/nl-nl/nieuws/2023/05/hoogste-aantal-nieuwbouwwoningen-in-afgelopen-decennium#:~:text=Door%20registraties%20conform%20BAG%202.0,blijft%20in%20beide%20gevallen%20hetzelfde.

CE Delft. (2018). *Waterstofroutes Nederland Blauw, groen en import*. www.ce.nl

CE Delft. (2022). *Ketenemissies elektriciteit Actualisatie elektriciteitsmix 2019*.

Chen, H., Pei, P., & Song, M. (2015). Lifetime prediction and the economic lifetime of proton exchange membrane fuel cells. *Applied Energy*, *142*, 154–163. https://doi.org/10.1016/j.apenergy.2014.12.062

Choi, D., Crawford, A., Huang, Q., Viswanathan, V. V, Cw Kintner-Meyer, M., & Sprenkle, V. L. (2016). *Lifecycle Evaluation of Li-ion Battery Chemistries under Grid Duty Cycles Pacific Northwest National Laboratory*.

Cigolotti, V., Genovese, M., & Fragiacomo, P. (2021). Comprehensive review on fuel cell technology for stationary applications as sustainable and efficient poly-generation energy systems. In *Energies* (Vol. 14, Issue 16). MDPI AG. https://doi.org/10.3390/en14164963

CNBC. (2020). *Off-grid construction site taps into hydrogen fuel cell tech to power operations*. https://www.cnbc.com/2020/09/03/construction-site-uses-hydrogen-fuel-cell-tech-to-power-operations.html

Cole, W., Frazier, A. W., & Augustine, C. (2021). *Cost Projections for Utility-Scale Battery Storage: 2021 Update*. www.nrel.gov/publications.

Crespi, E., Guandalini, G., & Campanari, S. (2021). Simulations of a flexible 100 kWelPEM Fuel Cell power plant for the provision of grid balancing services. *E3S Web of Conferences*, *238*. https://doi.org/10.1051/e3sconf/202123804003

de Kleijne, K., de Coninck, H., van Zelm, R., Huijbregts, M. A. J., & Hanssen, S. V. (2022). The many greenhouse gas footprints of green hydrogen. *Sustainable Energy and Fuels*, *6*(19), 4383–4387. https://doi.org/10.1039/d2se00444e

Dodds, P. E., Staffell, I., Hawkes, A. D., Li, F., Grünewald, P., McDowall, W., & Ekins, P. (2015). Hydrogen and fuel cell technologies for heating: A review. In *International Journal of Hydrogen Energy* (Vol. 40, Issue 5, pp. 2065–2083). Elsevier Ltd. https://doi.org/10.1016/j.ijhydene.2014.11.059

EEX Group. (2023). *Hydrix - Hydrogen Germany*.

EIB. (2023, February 9). *Stikstofbesluit zet rem op woningbouw*.

Engineering Toolbox. (2003). *Fuels - Higher and Lower Calorific Values*. https://www.engineeringtoolbox.com/fuels-higher-calorific-values-d_169.html

EST-Floattech. (n.d.). *Containerized battery solutions*. Retrieved June 19, 2023, from https://www.est-floattech.com/

Fan, X., Liu, B., Liu, J., Ding, J., Han, X., Deng, Y., Lv, X., Xie, Y., Chen, B., Hu, W., & Zhong, C. (2020). Battery Technologies for Grid-Level Large-Scale Electrical Energy Storage. In *Transactions of Tianjin University* (Vol. 26, Issue 2, pp. 92–103). Tianjin University. https://doi.org/10.1007/s12209-019-00231-w

Felseghi, R. A., Carcadea, E., Raboaca, M. S., Trufin, C. N., & Filote, C. (2019). Hydrogen fuel cell technology for the sustainable future of stationary applications. In *Energies* (Vol. 12, Issue 23). MDPI AG. https://doi.org/10.3390/en12234593

FNV. (2023). *BOUW INFRA 2023 CAO*. https://www.fnv.nl/cao-sector/bouwen-wonen/bouw-infra/cao-bouw-infra

Global Alliance for Buildings and Construction. (2019). *2019 global status report for buildings and construction*. International Energy Agency.

Greenplanet. (n.d.). *Zero emission bouwlocatie*. Retrieved February 22, 2023, from https://greenplanet-energy.nl/green-planet/projecten/zero-emission-bouwlocatie/

Han, X., Lu, L., Zheng, Y., Feng, X., Li, Z., Li, J., & Ouyang, M. (2019). A review on the key issues of the lithium ion battery degradation among the whole life cycle. In *eTransportation* (Vol. 1). Elsevier B.V. https://doi.org/10.1016/j.etran.2019.100005

Hu, X., Xu, L., Lin, X., & Pecht, M. (2020). Battery Lifetime Prognostics. In *Joule* (Vol. 4, Issue 2, pp. 310–346). Cell Press. https://doi.org/10.1016/j.joule.2019.11.018

Huld, T., Müller, R., & Gambardella, A. (2012). A new solar radiation database for estimating PV performance in Europe and Africa. *Solar Energy*, *86*(6), 1803–1815. https://doi.org/10.1016/j.solener.2012.03.006

Hydrogen Council. (2021). *Hydrogen decarbonization pathways A life-cycle assessment*. www.hydrogencouncil.com.

IEA. (2022). *Buildings, IEA, Paris*. https://www.iea.org/reports/buildings

IPCC. (2021). Summary for Policymakers. In: Climate Change 2021: The Physical Science Basis. Contribution of Working Group I to the Sixth Assessment Report of the Intergovernmental Panel on Climate Change. *Cambridge University Press, Cambridge, United Kingdom and New York, NY, USA, Pp. 3–32.* . https://doi.org/10.1017/9781009157896.001

Jain, I. P. (2009). Hydrogen the fuel for 21st century. *International Journal of Hydrogen Energy*, *34*(17), 7368–7378. https://doi.org/10.1016/j.ijhydene.2009.05.093

Klanfar, M., Korman, T., & Kujundžić, T. (2016). Potrošnja goriva i koeficijenti opterećenja pogonskih motora mehanizacije pri eksploataciji tehničko-građevnog kamena. *Tehnicki Vjesnik*, *23*(1), 163–169. https://doi.org/10.17559/TV-20141027115647

Lamb, J. J., & Pollett, B. (2020). *Micro-Optics and Energy Sensors forrEnergy Devices*.

Lewis, A. C. (2021). Optimising air quality co-benefits in a hydrogen economy: A case for hydrogen-specific standards for NOx emissions. *Environmental Science: Atmospheres*, *1*(5), 201–207. https://doi.org/10.1039/d1ea00037c

Ligterink, N., Dellaert, S., & Mensch, P. van. (2021). *AUB (AdBlue verbruik, Uren, en Brandstofverbruik): een robuuste schatting van NOx en NH3 uitstoot van mobiele werktuigen*.

Lima, M. A. F. B., Carvalho, P. C. M., Fernández-Ramírez, L. M., & Braga, A. P. S. (2020). Improving solar forecasting using Deep Learning and Portfolio Theory integration. *Energy*, *195*. https://doi.org/10.1016/j.energy.2020.117016

Lin, T., Lin, Y., Ren, H., Chen, H., Chen, Q., & Li, Z. (2020). Development and key technologies of pure electric construction machinery. In *Renewable and Sustainable Energy Reviews* (Vol. 132). Elsevier Ltd. https://doi.org/10.1016/j.rser.2020.110080

Lu, Z., Gu, P., Wang, J., & Jiang, C. (2021). Study on hot and cold starting characteristics of fuel cell system. *E3S Web of Conferences*, *257*. https://doi.org/10.1051/e3sconf/202125701088

Mekhilef, S., Saidur, R., & Safari, A. (2012). Comparative study of different fuel cell technologies. In *Renewable and Sustainable Energy Reviews* (Vol. 16, Issue 1, pp. 981–989). Elsevier Ltd. https://doi.org/10.1016/j.rser.2011.09.020

Milieucentraal. (n.d.). *Stikstof - alles wat je moet weten*. Retrieved February 9, 2023, from https://www.milieucentraal.nl/klimaat-en-aarde/milieuproblemen/stikstof-in-de-lucht-en-bodem/#:~:text=Stikstofoxiden%20(NOx)%20en%20ammoniak%20(,ook%20insecten%2C%20vlinders%20en%20vogels

Millet, P., ANDOLFATTOt, F., & Durand, R. (1995). DESIGN AND PERFORMANCE OF A SOLID POLYMER ELECTROLYTE WATER ELECTROLYZER. In *I Il~~'llYJ&wl Flwrg~~* (Vol. 2, Issue 2).

Mpinarada. (n.d.). *Energy Storage - NESP (LFP) Container Solutions*. Retrieved June 19, 2023, from https://mpinarada.com/container-rack-solutions/

Neagu, C., Jansen, H., Gardeniers, H., & Elwenspoek, M. (2000). *The electrolysis of water: an actuation principle for MEMS with a big opportunity*.

NEDSTACK. (n.d.). *Stationary Fuel Cell Power Systems*. Retrieved June 26, 2023, from https://nedstack.com/en/pemgen-solutions/stationary-fuel-cell-power-systems

Netbeheer Nederland. (2023). *Capaciteitskaart - Netbeheer Nederland*. https://capaciteitskaart.netbeheernederland.nl/

NREL. (2020). *DOE Hydrogen and Fuel Cells Program Record Title: Reversible Fuel Cell Targets Table 1a: Technical Targets for High-Temperature Unitized Reversible Fuel Cells (Cell/Stack level) for Electric Energ Storage Applications 1*. https://www.energy.gov/sites/prod/files/2016/07/f33/fcto_battelle_

NREL. (2021). *Today's Topic: Long Duration Energy Storage Using Hydrogen and Fuel Cells*.

NREL. (2022). *Off-Road Vehicle Decarbonization and Energy Systems Integration: R&D Gaps and Opportunities*. https://doi.org/10.2172/1891267

Nylund, N.-O., Rosenblatt, D., Stokes, J., Lama, N., Cádiz, A., Takada, Y., & Kobayashi, M. (2021). *Annex 57 A Report from the Advanced Motor Fuels Technology Collaboration Programme Heavy-Duty Vehicles Performance Evaluation Petri Söderena (project coordination)*.

Palm, J., & Bryngelson, E. (2023). Energy efficiency at building sites: barriers and drivers. *Energy Efficiency*, *16*(2). https://doi.org/10.1007/s12053-023-10088-7

PBL. (2022). *Klimaat- en Energieverkenning 2022*. www.pbl.nl/kev

Pei, P., Chang, Q., & Tang, T. (2008). A quick evaluating method for automotive fuel cell lifetime. *International Journal of Hydrogen Energy*, *33*(14), 3829–3836. https://doi.org/10.1016/j.ijhydene.2008.04.048

Pfenninger, S., & Staffell, I. (2016). Long-term patterns of European PV output using 30 years of validated hourly reanalysis and satellite data. *Energy*, *114*, 1251–1265. https://doi.org/10.1016/j.energy.2016.08.060

Poullikkas, A. (2013). A comparative overview of large-scale battery systems for electricity storage. In *Renewable and Sustainable Energy Reviews* (Vol. 27, pp. 778–788). Elsevier Ltd. https://doi.org/10.1016/j.rser.2013.07.017

PowerCellution. (2023). *Power Container 100*.

Provincie Noord-Holland. (2020). *Stappenplan vergunning stikstof*. https://www.noord-holland.nl/Onderwerpen/Natuur/Natuurversterking_Stikstof/Rol_provincie/Documenten/Stappenplan_vergunning_stikstof

PVGIS. (2022). *PHOTOVOLTAIC GEOGRAPHICAL INFORMATION SYSTEM*. https://re.jrc.ec.europa.eu/pvg_tools/en/

RECO. (2023). *BATTERIJCONTAINER Direct bouwstroom bij netkrapte*.

Rijksoverheid. (2011). *Pauzes tijdens werk*. https://www.rijksoverheid.nl/onderwerpen/werktijden/vraag-en-antwoord/wettelijke-regels-pauzes-tijdens-werk

Rijksoverheid. (2020, July 9). *Vaste afstandsgrens van 25 kilometer voor alle emissiebronnen*. https://www.rijksoverheid.nl/actueel/nieuws/2021/07/09/vaste-afstandsgrens-van-25-kilometer-voor-alle-emissiebronnen

Rijksoverheid, M. van B. Z. (2021, June 9). *Woningbouwkaart toont bouwlocaties tot 2030 - Nieuwsbericht*. https://www.rijksoverheid.nl/actueel/nieuws/2021/06/09/woningbouwkaart-toont-bouwlocaties-tot-2030

Roshandel, R., & Parhizgar, T. (2013). A new approach to optimize the operating conditions of a polymer electrolyte membrane fuel cell based on degradation mechanisms. *Energy Systems*, *4*(3), 219–237. https://doi.org/10.1007/s12667-012-0075-8

RVO. (2022). *Subsidieregeling Schoon en Emissieloos Bouwmaterieel (SSEB)*. https://www.rvo.nl/subsidies-financiering/sseb

SAFT. (n.d.). *Products-solutions Intensium Shift*. Retrieved June 19, 2023, from https://www.saft.com/products-solutions/products/intensium-shift?text=&tech=76&market=&brand=&sort=newest&submit=Search

Sayfutdinov, T., & Vorobev, P. (2022). Optimal utilization strategy of the LiFePO4 battery storage. *Applied Energy*, *316*. https://doi.org/10.1016/j.apenergy.2022.119080

Shadidi, B., Najafi, G., & Yusaf, T. (2021). A review of hydrogen as a fuel in internal combustion engines. In *Energies* (Vol. 14, Issue 19). MDPI. https://doi.org/10.3390/en14196209

Smith, E. D., Szidarovszky, F., Karnavas, W. J., & Bahill, A. T. (2008). Sensitivity Analysis, a Powerful System Validation Technique. In *The Open Cybernetics and Systemics Journal* (Vol. 2).

Soloveichik, G. L. (2011). Battery technologies for large-scale stationary energy storage. In *Annual Review of Chemical and Biomolecular Engineering* (Vol. 2, pp. 503–527). https://doi.org/10.1146/annurev-chembioeng-061010-114116

Soons, M. B., Hefting, M. M., Dorland, E., Lamers, L. P. M., Versteeg, C., & Bobbink, R. (2017). Nitrogen effects on plant species richness in herbaceous communities are more widespread and stronger than those of phosphorus. *Biological Conservation*, *212*, 390–397. https://doi.org/10.1016/j.biocon.2016.12.006

Staffell, I., & Pfenninger, S. (2016). Using bias-corrected reanalysis to simulate current and future wind power output. *Energy*, *114*, 1224–1239. https://doi.org/10.1016/j.energy.2016.08.068

Stayers. (2014). *PROJECT FINAL REPORT*. www.stayers.eu

Stokke, R., Qiu, X., Sparrevik, M., Truloff, S., Borge, I., & de Boer, L. (2023). Procurement for zero-emission construction sites: a comparative study of four European cities. *Environment Systems and Decisions*, *43*(1), 72–86. https://doi.org/10.1007/s10669-022-09879-7

Sui, X., Świerczyński, M., Teodorescu, R., & Stroe, D. I. (2021). The degradation behavior of lifepo4/c batteries during long-term calendar aging. *Energies*, *14*(6). https://doi.org/10.3390/en14061732

Sunpalpower. (n.d.). *Sunpal 1MW 2 MW LFP Battery 20ft 40ft*. Retrieved June 19, 2023, from https://sunpalpower.en.made-in-china.com/product/oFBfTcmOnVhp/China-Sunpal-1Mw-2Mw-Long-Deep-Cycle-Solar-Power-LFP-Battery-20-Ft-40-Ft-Large-Storage-Capacity-Energy-Container-System-Solution.html

Sweeney, C., Bessa, R. J., Browell, J., & Pinson, P. (2020). The future of forecasting for renewable energy. *WIREs Energy and Environment*, *9*(2). https://doi.org/10.1002/wene.365

Tromp, E., Bekkering, J., Hengeveld, E. J., Bellekom, S., & Aué, J. jaap. (2022). Cost minimisation of renewable hydrogen in a Dutch neighbourhood while meeting European Union sustainability targets. *Energy Conversion and Management*, *267*. https://doi.org/10.1016/j.enconman.2022.115903

TU Delft. (2022). *Aardgasconversie - Kwaliteit van aardgas: de Wobbe-index*. https://eduweb.eeni.tbm.tudelft.nl/TB141E/?aardgas-conversie

Un-Noor, F., Scora, G., Wu, G., Boriboonsomsin, K., Perugu, H., Collier, S., & Yoon, S. (2021). Operational feasibility assessment of battery electric construction equipment based on in-use activity data. In *Transportation Research Record* (Vol. 2675, Issue 9, pp. 809–820). SAGE Publications Ltd. https://doi.org/10.1177/03611981211004581

US Department of Energy. (2016). *comparison-fuel-cell-technologies-fact-sheet*.

van den Berg, R. (2022). *STREAM Personenvervoer Emissiekentallen modaliteiten 2022*. www.ce.nl

Vermeer, W., Chandra Mouli, G. R., & Bauer, P. (2022). A Comprehensive Review on the Characteristics and Modeling of Lithium-Ion Battery Aging. *IEEE Transactions on Transportation Electrification*, *8*(2), 2205–2232. https://doi.org/10.1109/TTE.2021.3138357

Viswanathan, V., Mongird, K., Franks, R., Li, X., Sprenkle, V., & Baxter, R. (2022). *2022 Grid Energy Storage Technology Cost and Performance Assessment*.

Volta Energy. (n.d.). *Duurzame energie voor bouwplaats Arnhem*. Retrieved June 28, 2023, from https://volta-energy.com/klanten/duurzame-energie-voor-bouwplaats-arnhem/

Volvo Trucks. (n.d.). *Volvo-FMX specfications*. Retrieved June 1, 2023, from https://www.volvotrucks.nl/nl-nl/trucks/trucks/volvo-fmx/specifications/powertrain.html#engines

Wacker Neuson. (n.d.). *Productinformatieblad*. Retrieved June 1, 2023, from https://www.wackerneuson.nl/produkten/wielladers/wiellader-wl20/medier-og-downloads/fanen

Waldmann, T., Wilka, M., Kasper, M., Fleischhammer, M., & Wohlfahrt-Mehrens, M. (2014). Temperature dependent ageing mechanisms in Lithium-ion batteries - A Post-Mortem study. *Journal of Power Sources*, *262*, 129–135. https://doi.org/10.1016/j.jpowsour.2014.03.112

Zachariah-Wolff, J. L., Egyedi, T. M., & Hemmes, K. (2007). From natural gas to hydrogen via the Wobbe index: The role of standardized gateways in sustainable infrastructure transitions. *International Journal of Hydrogen Energy*, *32*(9), 1235–1245. https://doi.org/10.1016/j.ijhydene.2006.07.024

Zeng, K., & Zhang, D. (2010). Recent progress in alkaline water electrolysis for hydrogen production and applications. In *Progress in Energy and Combustion Science* (Vol. 36, Issue 3, pp. 307–326). https://doi.org/10.1016/j.pecs.2009.11.002

Zhang, J., Zhang, L., Sun, F., & Wang, Z. (2018). An Overview on Thermal Safety Issues of Lithium-ion Batteries for Electric Vehicle Application. *IEEE Access*, *6*, 23848–23863. https://doi.org/10.1109/ACCESS.2018.2824838

Zhangi, Y., -chao JIN, Z., Yuan, Z., & Yang, T. (2015). *Development and Application of Hydrogen Storage Dong-liang ZHA0 2 0. Key La bora tor y of Integ rat ed Inner Mongolia Exploit ation of Baiyu n abo Multi-met al Resources*. www.sciencedirect.com

Zoulias, E., Varkaraki, E., Lymberopoulos, N., Christodoulou, C. N., & Karagiorgis, G. N. (2017). *A REVIEW ON WATER ELECTROLYSIS*.

Züttel, A. (2004). Hydrogen storage methods. In *Naturwissenschaften* (Vol. 91, Issue 4, pp. 157–172). https://doi.org/10.1007/s00114-004-0516-x

Appendices

APPENDIX A. COLLECTED DATA FOR SIMULATIONS

Table A- 1 Vehicles used for the zero-emission construction site pilot

Machine number	Machine type & name	Power [kW]	Battery [kWh]	Battery Runtime [h]	Discharge Rate [kWh/hr]	Normal Charging [kW]	Fast Charging [kW]
1.	Bobcat e10 Electric (Small excavator)	7.5	12.7	7	1.8	3.7	10.2
2.	Wacker Neuson WL20e wiellader (Wheel loader)	-	23.4	8	2.9	3	6
3.	MAN TGS 50t 10x4 WSA elektrische betonmixer (Concrete mixer)	330/60	360	6	60	43	250
4.	MAN TGS 50t 10x4 WSA elektrische kipper (kipper)	330/59	360	6.1	59	43	250

Table A- 2 Electricity grid data used for simulations

Data	Quantity	Reference
Power [kW]	55	(Netbeheer Nederland, 2023)
Energy cost [€/kWh]	0.54	(CBS, 2022)
CO_2 emission from production [kg CO_2/kWh]	0.29	(CBS, 2020)
CO_2 emission from chain supply [kg CO_2/kWh]	0.058	(CE Delft, 2022)

Table A- 3 Techno-economic data of LFP battery used for simulations

Data	Quantity	Reference
Round-trip-Efficiency [%]	89.5	(Viswanathan et al., 2022)
Discharge efficiency [%]	94.6	
Charge efficiency [%]	94.6	
1 Cycle		
Minimum SOC [%]	27.0	(Sayfutdinov & Vorobev, 2022)
Maximum SOC [%]	95.8	
Lifetime [yr]	12	
Optimal Capacity Ratio [%]	144.7	
2 Cycle		
Minimum SOC [%]	38 – 58.8	(Sayfutdinov & Vorobev, 2022)
Maximum SOC [%]	95.2	
Lifetime [yr]	9.6	
Optimal Capacity Ratio [%]	1.779	
CAPEX Power [€/kW]	143	(Viswanathan et al., 2022)
CAPEX Capacity [€/kWh]	405	(Viswanathan et al., 2022)
OPEX [%]	2.5	(Cole et al., 2021)
Discount rate [%]	8%	(NREL, 2020)

Table A- 4 Degradation rate of a PEMFC operating conditions

Operating condition	Degradation [μV] (Chen et al., 2015)
Start-stop [μV/cycle]	13.79
Idling [μV/h]	8.662
load change [μV/cycle]	0.42
High power load [μV/h]	10

Table A- 5 Voltage degradation of a PEMFC considering operating conditions of the construction site

	Normal charging				Fast + normal charging	
	Scenario 1 (I-FCPB, I-FC, II-FCPB)		Scenario 2		Scenario 3 (II-FC)	
Operating condition	Quantity	Degradation [μV/day]	Quantity	Degradation [μV/day]	Quantity	Degradation [μV/day]
Start-stop [cycles]	1	13.79	1	13.79	2	27.58
load change [n/cycles]	3	0.84	2	0.84	2	0.84
High power load [hr]	0	0	8.5	85.00	0.5	5
Total degradation [μV/day]*		26.2		171.4		57.5

Including the difference factor "k"

Table A- 6 Techno-economic-environmental data of PEMFC used for simulations

Data	Quantity	Reference
Electric efficiency [%]	45 - 55%	(PowerCellution, 2023)
Average efficiency [%]	51 / 52.6%	
Cell voltage [Volt]	0.7	(Chen et al., 2015; Pei et al., 2008)
Lifetime reached at degradation [%]	10%	
Peak Power [%]	>60%	
Hydrogen Tank [kg]	500	
Hydrogen LHV [MJ/kg]	120	
Hydrogen LHV [kWh/kg]	33.3	
CO2 emission [kg CO2/kWh H_2]	0.055	(de Kleijne et al., 2022)
CAPEX [€/kW]	1900	(Cigolotti et al., 2021; PowerCellution, 2023)
OPEX [%]	3.5	(NREL, 2020)
Hydrogen cost [€/kg]	25	
Discount rate [%]	8%	(NREL, 2020)

Table A- 7 Examples of containerized LFP batteries

	Energy		Energy density		Power		Power density		Reference
EST-Floattech battery container 20ft	2000	kWh	60.4	kWh/m³					(EST-Floattech, n.d.)
Saft Battery container 20ft	2300	kWh	69.4	kWh/m³	2200	kW	66	kW/m³	(SAFT, n.d.)
	3000	kWh	90.5	kWh/m³	1500	kW	45	kW/m³	
Sunpalpower battery container 20ft	2500	kWh	75.4	kWh/m³	1000	kW	30	kW/m³	(Sunpalpower, n.d.)
Mpinarada 20ft	2880	kWh	86.9	kWh/m³	1440	kW	43	kW/m³	(Mpinarada, n.d.)
	2300	kWh	69.4	kWh/m³	2300	kW	69	kW/m³	
	1840	kWh	55.5	kWh/m³	3690	kW	111	kW/m³	
Reco 10ft	1500	kWh	45.3	kWh/m³	340	kW	22	kW/m³	(RECO, 2023)
Min			45.3	kWh/m³			21.6	kW/m³	
Max			90.5	kWh/m³			111.4	kW/m³	
Average			69.1	kWh/m³			55.4	kW/m³	

Table A- 8 Example of containerized PEM fuel cell

Power		Power density		Reference
1200	MW	36.2	kW/m³	(PowerCellution, 2023)

Table A- 9 Technical specifications and fuel consumption of comparable diesel vehicles

	Bobcat e10	Wacker Neuson	VOLVO FMX	VOLVO FMX
Power [kW] (Bobcat, 2019; Volvo Trucks, n.d.; Wacker Neuson, n.d.)	7.4	18.4	290	290
Runtime [hr/day]	8	8	8	8
Load factor (Klanfar et al., 2016)	0.56	0.27	0.23	0.23
Diesel efficiency (Nylund et al., 2021)	0.45	0.45	0.45	0.45
Diesel consumption [kWh/day]	74	88	1.186	1.186
Diesel consumption [L/day]	7	9	119	119

Table A- 10 Economic and emission data of diesel

Data	Quantity	Reference
Diesel price [€/L]	1.356	(CE Delft, 2022)
CO_2 emission factor [kg CO_2/L]	3.256	(van den Berg, 2022)
NOx emission factor [kg NO_x/L]	0.0014	(van den Berg, 2022)
NH3 emission factor [kg NH_3/L]	0.00088	(Ligterink et al., 2021)
Molar mass N [g/mol]	14	
Molar Mass NO [g/mol]	30	
Molar Mass NO_2 [g/mol]	46	
Molar Mass NH_3 [g/mol]	17	

Table A- 11 Data of renewable energy used for simulations

Data	Quantity	Reference
CO_2 emission solar [kg CO_2/kWh]	0.014	(CE Delft, 2022)
CO_2 emission wind [kg CO_2/kWh]	0.061	
Price solar energy [€/kWh]	0.055	(BNEF, 2022)
Price wind energy [€/kWh]	0.052	

Table A- 12 Provided inputs and simulation results from PVGIS

Provided inputs (Huld et al., 2012; PVGIS, 2022)	
Location [Lat/Lon]	53.271/6.394
Horizon	Calculated
Database used	PVGIS-SARAH2
PV technology	Crystalline silicon
PV installed [kWp]	100
System loss [%]	14
Simulation outputs	
Slope angle [°]	40 (opt)
Azimuth angle [°]	-1 (opt)
Yearly PV energy production [kWh]	1001.78
Yearly in-plane irradiation [kWh/m2]	1232.56
Year-to-year variability [kWh]	41.97
Changes in output due to:	
Angle of incidence [%]	-3.08
Spectral effects [%]	1.83
Temperature and low irradiance [%]	-4.24
Total loss [%]	-18.72

Table A- 13 Used wind turbines for simulations on Renewable.ninja

Turbine type	Installed Power	Average Hub Height	Reference
Xant M21 100	100	30.5	(Bauer & Matysik, n.d.; Pfenninger & Staffell, 2016; Staffell & Pfenninger, 2016)
Nordex N29 250	250	43	
Enercon E40 500	500	53.5	
NEG Micon NM60 1000	1000	75	

Table A- 14 Future emission factors kg CO_2/kWh

		2020	2025	2030	2035	2050
Dutch electricity grid	Tank-to-Wheel	0.29	0.19	0.07	0.053	0
	Well-to-Tank	0.058	0.058	0.058	0.058	
	Grid total (WTW)	0.348	0.248	0.128	0.111	
Hydrogen	Well-to-Tank	0.039	0.031	0.0225	0.021	0.0165
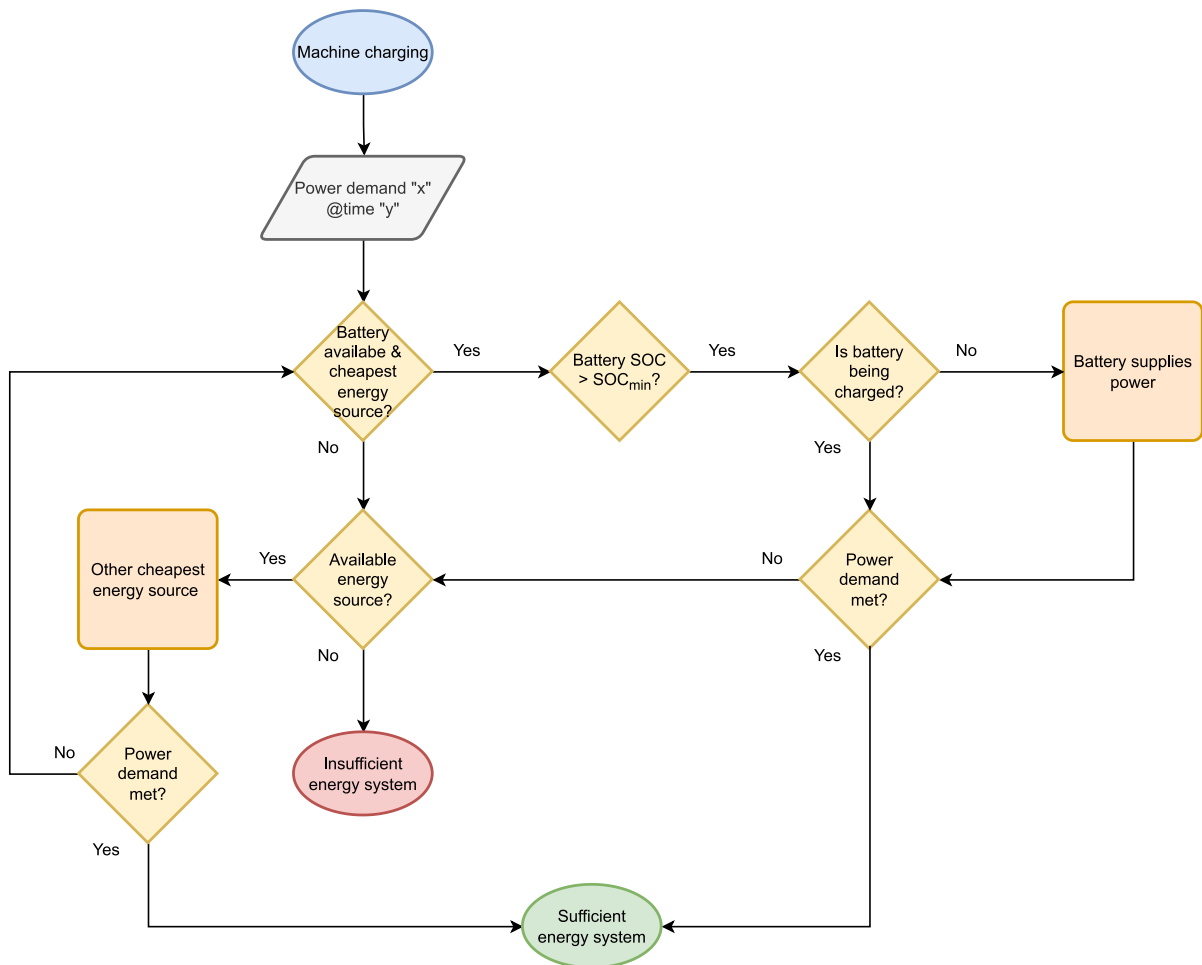
Figure B- 1 Battery decision flowchart
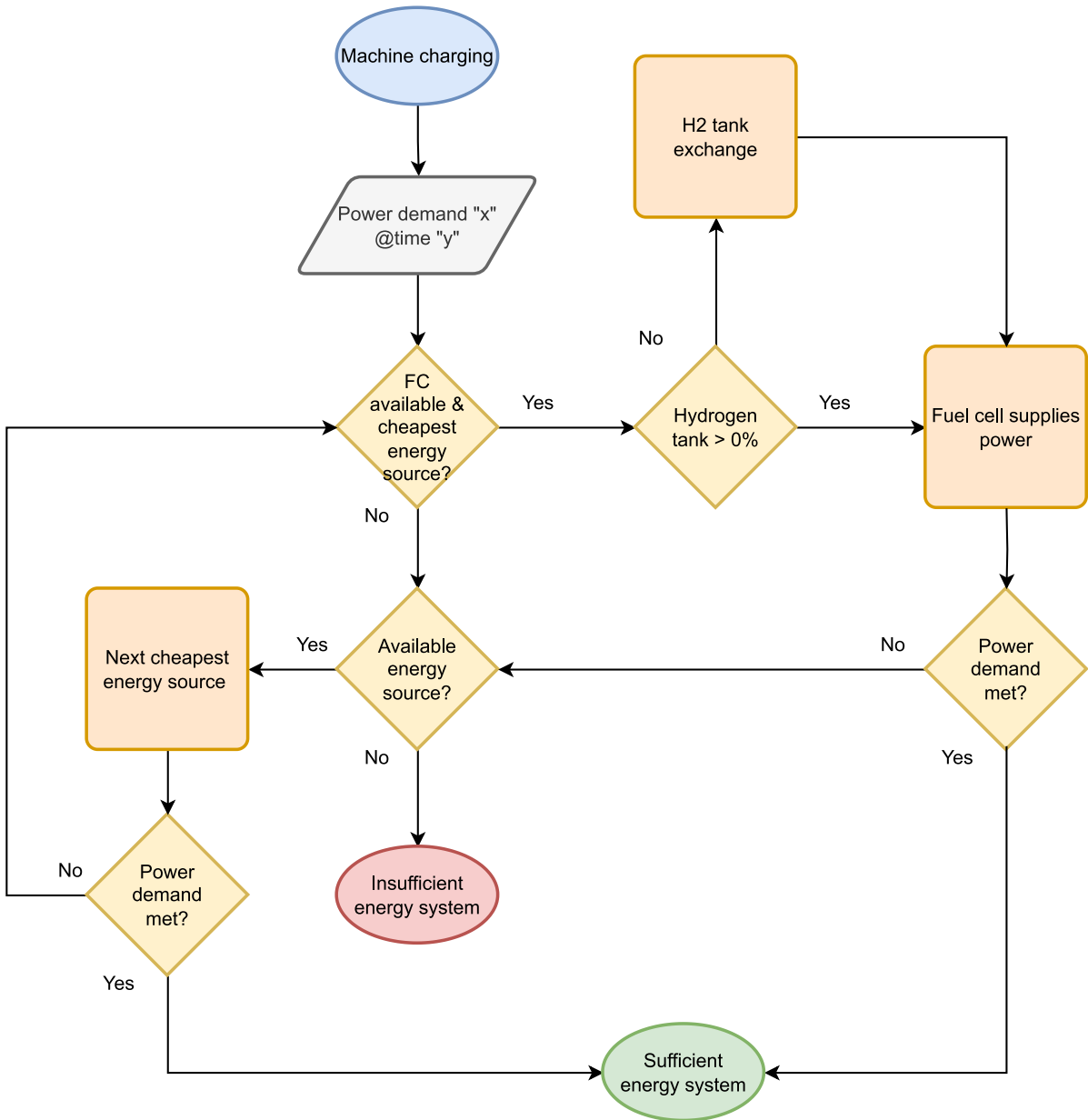
Figure B- 2 Fuel cell model decision flowchart

APPENDIX C. SYSTEM DESIGN AND YEARLY ENERGY PROFILE

Table C- 1 System design and yearly energy distribution of the grid-connected configurations

		I-FCPB		I-PB	I-FC
	Grid*	Battery	Fuel Cell	Battery	Fuel Cell
Maximum Delivered Power [kW]	55	461	38	461	461
Installed Power [kW]	55	461	63	461	461
Optimal Capacity [kWh]		354		670	
Energy Delivered [kWh/year]	125,190	59,951	72,271	132,222	132,222
	49%	23%	28%	51%	51%
Energy to Battery [kWh/year]**		66,984		147,734	
Required Container size [ft]		6	6	8	10

*Results of the grid applies to all configurations **The energy to battery is supplied by the electricity grid*

Table C- 2 System design and yearly energy distribution of the off-grid configurations

	II-FCPB		II-FC
	Battery	Fuel Cell	Fuel Cell
Maximum Delivered Power [kW]	516	93	516
Installed Power [kW]	516	155	516
Optimal Capacity [kWh]	397		
Energy Delivered [kWh]	67,101	190,311	257,412
	26%	74%	100%
Energy to Battery [kWh]*	74,973		
Required Container Size [ft]	8	6	10

Energy to Battery is supplied by the fuel cell using hydrogen

APPENDIX D. ECONOMIC RESULTS FCPB

Table D- 1 Economic results of the grid-connected configurations

		I-FCPB		I-PB	I-FC
	Grid*	Battery	Fuel Cell	Battery	Fuel Cell
CAPEX [€]		€ 209,420	Fuel Cell	€ 337,066	€ 876,204
Container [€]		€ 90,000	€ 119,383	€ 120,000	€ 150,000
OPEX [€]		€ 5,236	€ 90,000	€ 8,427	€ 30,667
Energy Cost [€]	€ 67,038	€ 35,869	€ 4,178	€ 79,110	€ 188,689
Lifetime [years]		12	10.7	9.6	4.7
Yearly CAPEX [€/year]		€ 39,732	€ 106,281	€ 70,005	€ 271,261
LCOS/LCOE [€/kWh]		€ 1.35	€ 1.94	€ 1.19	€ 3.71

*Results of the grid applies to all configurations

Table D- 2 Economic results of the off-grid configurations

	II-FCPB		II-FC
	Battery	Fuel Cell	Fuel Cell
CAPEX [€]	€ 234,595	€ 293,550	€ 980,704
Container [€]	€ 120,000	€ 90,000	€ 150,000
OPEX [€]	€ 5,865	€ 10,274	€ 34,325
Energy Cost [€]	€ 106,094	€ 279,869	€ 367,342
Lifetime [years]	12	10.4	4.7
Yearly CAPEX [€/year]	€ 47,053	€ 54,685	€ 298,884
LCOS/LCOE [€/kWh]	€ 2.43	€ 1.81	€ 2.72

Table D- 3 Results sensitivity analysis

		I-FCPB		I-PB	I-FC	II-FCPB		II-FC
Parameter	Percentage of change from base	Battery	Fuel Cell	Battery	Fuel Cell	Battery	Fuel Cell	Fuel Cell
CAPEX Power	50%	-6.4%	-7.6%	-3.7%	-26.7%	-3.6%	-7.4%	-21.0%
	60%	-5.2%	-6.0%	-3.0%	-21.4%	-2.9%	-5.9%	-16.8%
	70%	-3.9%	-4.5%	-2.2%	-16.0%	-2.1%	-4.4%	-12.6%
	80%	-2.6%	-3.0%	-1.5%	-10.7%	-1.4%	-3.0%	-8.4%
	90%	-1.3%	-1.5%	-0.7%	-5.3%	-0.7%	-1.5%	-4.2%
	100%	0.0%	0.0%	0.0%	0.0%	0.0%	0.0%	0.0%
	110%	1.3%	1.5%	0.7%	5.3%	0.7%	1.5%	4.2%
	120%	2.6%	3.0%	1.5%	10.7%	1.4%	3.0%	8.4%
	130%	3.9%	4.5%	2.2%	16.0%	2.1%	4.4%	12.6%
	140%	5.2%	6.0%	3.0%	21.4%	2.9%	5.9%	16.8%
	150%	6.4%	7.6%	3.7%	26.7%	3.6%	7.4%	21.0%
CAPEX Capacity (battery)	50%	-14.0%				-7.8%		
	60%	-11.2%				-6.2%		
	70%	-8.4%				-4.7%		
	80%	-5.6%				-3.1%		
	90%	-2.8%				-1.6%		
	100%	0.0%				0.0%		
	110%	2.8%				1.6%		
	120%	5.6%				3.1%		
	130%	8.4%				4.7%		
	140%	11.2%				6.2%		
	150%	14.0%				7.8%		
CAPEX Container	50%	-7.4%	-4.6%	-5.8%	-4.0%	-4.9%	-1.8%	-2.8%
	60%	-5.9%	-3.7%	-4.7%	-3.2%	-3.9%	-1.4%	-2.3%
	70%	-4.4%	-2.7%	-3.5%	-2.4%	-2.9%	-1.1%	-1.7%
	80%	-3.0%	-1.8%	-2.3%	-1.6%	-2.0%	-0.7%	-1.1%
	90%	-1.5%	-0.9%	-1.2%	-0.8%	-1.0%	-0.4%	-0.6%
	100%	0.0%	0.0%	0.0%	0.0%	0.0%	0.0%	0.0%
	110%	1.5%	0.9%	1.2%	0.8%	1.0%	0.4%	0.6%
	120%	3.0%	1.8%	2.3%	1.6%	2.0%	0.7%	1.1%
	130%	4.4%	2.7%	3.5%	2.4%	2.9%	1.1%	1.7%
	140%	5.9%	3.7%	4.7%	3.2%	3.9%	1.4%	2.3%
	150%	7.4%	4.6%	5.8%	4.0%	4.9%	1.8%	2.8%

Lifetime	**50%**	**31.0%**	**14.1%**	**30.7%**	**46.2%**	**18.2%**	**9.9%**	**35.6%**
	60%	20.5%	9.3%	20.4%	30.7%	12.0%	6.6%	23.7%
	70%	13.1%	6.0%	13.0%	19.7%	7.7%	4.2%	15.2%
	80%	7.6%	3.5%	7.6%	11.5%	4.4%	2.4%	8.9%
	90%	3.3%	1.5%	3.4%	5.1%	2.0%	1.1%	3.9%
	100%	0.0%	0.0%	0.0%	0.0%	0.0%	0.0%	0.0%
	110%	-2.7%	-1.2%	-2.7%	-4.2%	-1.6%	-0.9%	-3.2%
	120%	-4.9%	-2.3%	-5.0%	-7.6%	-2.9%	-1.6%	-5.9%
	130%	-6.8%	-3.1%	-6.8%	-10.6%	-4.0%	-2.2%	-8.2%
	140%	-8.3%	-3.8%	-8.4%	-13.1%	-4.9%	-2.7%	-10.1%
	150%	-9.6%	-4.4%	-9.8%	-15.2%	-5.6%	-3.1%	-11.7%
RTE/Efficiency	80%		18.9%		9.6%		20.4%	13.1%
	90%	4.9%	8.4%	5.6%	4.3%	7.5%	9.1%	5.8%
	100%	0.0%	0.0%	0.0%	0.0%	0.0%	0.0%	0.0%
	110%	-4.0%	-6.9%	-4.6%	-3.5%	-6.1%	-7.4%	-4.8%
	120%		-12.6%		-6.4%		-13.6%	-8.7%
Grid Price	50%	-22.2%		-25.1%				
	60%	-17.7%		-20.1%				
	70%	-13.3%		-15.1%				
	80%	-8.9%		-10.0%				
	90%	-4.4%		-5.0%				
	100%	0.0%		0.0%				
	110%	4.4%		5.0%				
	120%	8.9%		10.0%				
	130%	13.3%		15.1%				
	140%	17.7%		20.1%				
	150%	22.2%		25.1%				
Hydrogen Price	50%		-37.9%		-19.2%	-33.8%	-40.8%	-26.2%
	60%		-30.3%		-15.4%	-27.0%	-32.7%	-21.0%
	70%		-22.7%		-11.5%	-20.3%	-24.5%	-15.7%
	80%		-15.1%		-7.7%	-13.5%	-16.3%	-10.5%
	90%		-7.6%		-3.8%	-6.8%	-8.2%	-5.2%
	100%		0.0%		0.0%	0.0%	0.0%	0.0%
	110%		7.6%		3.8%	6.8%	8.2%	5.2%
	120%		15.1%		7.7%	13.5%	16.3%	10.5%
	130%		22.7%		11.5%	20.3%	24.5%	15.7%
	140%		30.3%		15.4%	27.0%	32.7%	21.0%
	150%		37.9%		19.2%	33.8%	40.8%	26.2%

APPENDIX E. ENVIRONMENTAL RESULTS FCPB AND BAU

Table E- 1 Yearly diesel consumption and its environmental impact of the BAU construction site

	Bobcat e10	Wacker Neuson	VOLVO FMX	VOLVO FMX	Total
Diesel consumption [L/year]	1,915	2,296	30,830	30,830	65,872
CO2 emission [kg/year]	6,237	7,477	100,383	100,383	214,480
NOx emission [kg/year]	2.7	3.2	43.2	43.2	92
NH3 emission [kg/year]	1.8	1.8	3.1	3.1	10
Total N emission [kg/year]	2.5	2.7	18.4	18.4	42

Table E- 2 Yearly WTW CO2 emission per energy source per configuration in 2025

	I-FCPB	I-PB	I-FC	II-FCPB	II-FC
Electricity grid	37,557	37,557	37,557	-	-
Fuel Cell	7,466	-	13,659	20,430	26,816
Battery	20,095	44,320	-	8,049	-
Total [kg CO₂/year]	65,118	81,877	51,216	28,479	26,816
Reduction compared to BAU	-76%	-68%	-82%	-93%	-93%

Table E- 3 Yearly TTW CO2 emission per energy source in 2025

	I-FCPB	I-PB	I-FC	II-FCPB	II-FC
Electricity grid	23,786	23,786	23,786	-	-
Fuel Cell	-	-	-	-	-
Battery	12,727	28,069	-	-	-
Total [kg CO₂/year]	36,513	51,856	23,786	-	-
Reduction compared to BAU	-78%	-68%	-85%	-100%	-78%

Table E- 4 Future yearly CO2 emission per configuration for 2030 & 2035

		Grid kg CO_2/yr	FC kg CO_2/yr	Battery kg CO_2/yr	Total kg CO_2/yr	Reduction
I-FCPB	2025	31,047	4,331	16,612	51,990	
	2030	16,024	3,188	8,574	27,787	-47%
	2035	13,833	2,976	7,402	24,211	-53%
I-PB	2025	31,047	-	36,638	67,685	
	2030	16,024	-	18,910	34,934	-48%
	2035	13,833	-	16,325	30,158	-55%
I-FC	2025	31,047	7,689	-	38,736	
	2030	16,024	5,661	-	21,685	-44%
	2035	13,833	5,283	-	19,117	-51%
II-FCPB	2025	-	11,405	4,493	15,898	
	2030	-	8,396	3,308	11,704	-26%
	2035	-	7,836	3,087	10,923	-31%
II-FC	2025	-	14,969	-	2025	
	2030	-	11,020	-	2030	-26%
	2035	0	10,286	0	2035	-31%

APPENDIX F. IMPLEMENTATION OF RENEWABLE ENERGY

Table F- 1 Yearly energy distribution FCPB-system including solar energy

Installed Solar Power [kW]	Power Source [kWh/year]	I-FCPB	I-PB	I-FC	II-FCPB	II-FC
100	Electricity grid	120,932	113,419	124,991	-	-
	Fuel Cell	65,818	-	121,062	183,659	246,054
	Battery	59,304	132,635	-	62,399	-
	Solar	11,358	11,358	11,358	11,353	11,358
250	Electricity grid	114,964	95,872	120,369	-	-
	Fuel Cell	61,004	-	109,189	174,223	229,558
	Battery	53,590	133,685	-	55,347	-
	Solar	27,854	27,854	27,854	27,842	27,854
500	Electricity grid	108,229	80,068	114,352	-	-
	Fuel Cell	57,896	-	94,314	165,098	208,666
	Battery	42,541	128,597	-	43,593	-
	Solar	48,746	48,746	48,746	48,721	48,746
1000	Electricity grid	101,818	68,344	105,844	-	-
	Fuel Cell	55,659	-	78,828	156,978	184,672
	Battery	27,217	116,351	-	27,745	-
	Solar	72,717	72,717	72,740	72,689	72,740

Table F- 2 Yearly energy distribution FCPB-system including wind energy

Installed Wind Power	Power Source	I-FCPB	I-PB	I-FC	II-FCPB	II-FC
100	Electricity grid	79,963	35,153	85,069	-	-
	Fuel Cell	12,967	-	66,662	90,886	151,731
	Battery	58,800	116,578	0	60,845	0
	Wind	105,681	105,681	105,681	105,681	105,681
250	Electricity grid	38,859	14,311	45,010	-	-
	Fuel Cell	5,903	-	52,896	43,763	97,906
	Battery	53,145	83,595	0	54,144	0
	Wind	159,505	159,505	159,505	159,505	159,505
500	Electricity grid	17,208	4,752	23,749	-	-
	Fuel Cell	2,599	-	33,937	19,359	57,686
	Battery	37,880	52,934	0	38,327	0
	Wind	199,726	199,726	199,726	199,726	199,726
1000	Electricity grid	7,970	1,386	11,880	-	-
	Fuel Cell	952	-	16,083	8,726	27,963
	Battery	19,041	26,577	0	19,237	0
	Wind	229,449	229,449	229,449	229,449	229,449

Table F- 3 Yearly production and utilization of solar energy

Installed Solar Power [kW]		I-FCPB	I-PB	I-FC	II-FCPB	II-FC
100	Total Solar Energy production [kWh/yr]	101,120	101,120	101,120	101,120	101,120
	Energy for direct charging [kWh/yr]	11,358	11,358	11,358	11,353	11,358
	Energy to battery [kWh/yr]	49,823	64,619	-	50,560	-
	Self-consumption rate	**60.5%**	**75.1%**	**11.2%**	**61.2%**	**11.2%**
250	Total Solar Energy production [kWh/yr]	252,799	252,799	252,799	252,799	252,799
	Energy for direct charging [kWh/yr]	27,854	27,854	27,854	27,842	27,854
	Energy to battery [kWh/yr]	54,471	101,029	-	55,434	-
	Self-consumption rate	**32.6%**	**51.0%**	**11.0%**	**32.9%**	**11.0%**
500	Total Solar Energy production [kWh/yr]	505,598	505,598	505,598	505,598	505,598
	Energy for direct charging [kWh/yr]	48,746	48,746	48,746	48,721	48,746
	Energy to battery [kWh/yr]	45,642	114,076	-	46,486	-
	Self-consumption rate	**18.7%**	**32.2%**	**9.6%**	**18.8%**	**9.6%**
1000	Total Solar Energy production [kWh/yr]	1,011,195	1,011,195	1,011,195	1,011,195	1,011,195
	Energy for direct charging [kWh/yr]	72,717	72,717	72,740	72,689	72,740
	Energy to battery [kWh/yr]	30,002	114,819	-	30,541	-
	Self-consumption rate	**10.2%**	**18.5%**	**7.2%**	**10.2%**	**7.2%**

Table F- 3 Yearly production and utilization of solar energy

Table F- 4 Yearly production and utilization of wind energy

Installed Wind Power [kW]		I-FCPB	I-PB	I-FC	II-FCPB	II-FC
100	Total Solar Energy production [kWh/yr]	400,398	400,398	400,398	400,398	400,398
	Energy for direct charging [kWh/yr]	105,681	105,681	105,681	105,681	105,681
	Energy to battery [kWh/yr]	64,286	88,173	-	66,076	-
	Self-consumption rate	**42.4%**	**48.4%**	**26.4%**	**42.9%**	**26.4%**
250	Total Solar Energy production [kWh/yr]	828,347	828,347	828,347	828,347	828,347
	Energy for direct charging [kWh/yr]	159,505	159,505	159,505	159,505	159,505
	Energy to battery [kWh/yr]	59,129	68,959	-	60,190	-
	Self-consumption rate	**26.4%**	**27.6%**	**19.3%**	**26.5%**	**19.3%**
500	Total Solar Energy production [kWh/yr]	1,853,909	1,853,909	1,853,909	1,853,909	1,853,909
	Energy for direct charging [kWh/yr]	199,726	199,726	199,726	199,726	199,726
	Energy to battery [kWh/yr]	42,324	45,462	-	42,809	-
	Self-consumption rate	**13.1%**	**13.2%**	**10.8%**	**13.1%**	**10.8%**
1000	Total Solar Energy production [kWh/yr]	3,873,661	3,873,661	3,873,661	3,873,661	3,873,661
	Energy for direct charging [kWh/yr]	229,449	229,449	229,449	229,449	229,449
	Energy to battery [kWh/yr]	21,275	23,100	-	21,494	-
	Self-consumption rate	**6.5%**	**6.5%**	**5.9%**	**6.5%**	**5.9%**

Table F- 4 Yearly production and utilization of wind energy

Table F- 5 Reduction of yearly energy costs by implementing solar energy

	Installed Solar Power [kW]	Reduction Direct Charge Cost Grid	Reduction Direct Charge cost FC	Reduction Battery Charge cost	Solar Energy cost	Total reduction	
I-FCPB	100	€ 2,280	€ 9,490	€ 24,326	-€ 625	€ 35,471	17.0%
	250	€ 5,476	€ 16,568	€ 29,979	-€ 1,532	€ 50,491	24.1%
	500	€ 9,083	€ 21,140	€ 32,347	-€ 2,681	€ 59,888	28.6%
	1000	€ 12,515	€ 24,429	€ 34,000	-€ 3,999	€ 66,945	32.0%
I-PB	100	€ 6,303	€ 0	€ 30,802	-€ 625	€ 36,481	25.0%
	250	€ 15,699	€ 0	€ 47,668	-€ 1,532	€ 61,835	42.3%
	500	€ 24,162	€ 0	€ 56,981	-€ 2,681	€ 78,462	53.7%
	1000	€ 30,440	€ 0	€ 64,665	-€ 3,999	€ 91,106	62.3%
I-FC	100	€ 106	€ 15,925	€ 0	-€ 625	€ 15,407	6.0%
	250	€ 2,582	€ 32,869	€ 0	-€ 1,532	€ 33,919	13.3%
	500	€ 5,804	€ 54,097	€ 0	-€ 2,681	€ 57,219	22.4%
	1000	€ 10,360	€ 76,196	€ 0	-€ 3,999	€ 82,556	32.3%
II-FCPB	100	€ 0	€ 22,968	€ 88,816	-€ 624	€ 111,160	28.5%
	250	€ 0	€ 23,659	€ 104,903	-€ 1,531	€ 127,031	32.6%
	500	€ 0	€ 37,078	€ 107,698	-€ 2,680	€ 142,096	36.4%
	1000	€ 0	€ 49,019	€ 108,575	-€ 3,999	€ 153,595	39.4%
II-FC	100	€ 0	€ 16,209	€ 0	-€ 624	€ 15,584	4.2%
	250	€ 0	€ 39,750	€ 0	-€ 1,531	€ 38,218	10.4%
	500	€ 0	€ 69,564	€ 0	-€ 4,003	€ 65,560	17.8%
	1000	€ 0	€ 103,804	€ 0	-€ 3,999	€ 99,805	27.2%

Table F- 6 Reduction of yearly energy costs by implementing wind energy

		Reduction Direct Charge Cost Grid	Reduction Direct Charge cost FC	Reduction Battery Charge cost	Wind Energy cost	Total reduction	
I-FCPB	100	€ 24,218	€ 87,211	€ 31,770	-€ 5,495	€ 137,704	65.8%
	250	€ 46,230	€ 97,601	€ 32,660	-€ 8,294	€ 168,196	80.4%
	500	€ 57,824	€ 102,460	€ 33,668	-€ 10,386	€ 183,566	87.8%
	1000	€ 62,770	€ 104,881	€ 34,763	-€ 11,931	€ 190,483	91.1%
I-PB	100	€ 48,214	€ 0	€ 51,991	-€ 5,495	€ 94,709	64.8%
	250	€ 59,375	€ 0	€ 62,435	-€ 8,294	€ 113,515	77.7%
	500	€ 64,493	€ 0	€ 69,419	-€ 10,386	€ 123,527	84.5%
	1000	€ 66,296	€ 0	€ 74,377	-€ 11,931	€ 128,741	88.1%
I-FC	100	€ 21,485	€ 93,557	€ 0	-€ 5,495	€ 109,547	42.8%
	250	€ 42,936	€ 113,202	€ 0	-€ 8,294	€ 147,844	57.8%
	500	€ 54,321	€ 140,259	€ 0	-€ 10,386	€ 184,194	72.0%
	1000	€ 60,676	€ 165,737	€ 0	-€ 11,931	€ 214,482	83.9%
II-FCPB	100	€ 0	€ 146,213	€ 104,014	-€ 5,495	€ 244,732	62.7%
	250	€ 0	€ 215,512	€ 106,895	-€ 8,294	€ 314,113	80.5%
	500	€ 0	€ 251,399	€ 108,018	-€ 10,386	€ 349,031	89.5%
	1000	€ 0	€ 267,037	€ 109,137	-€ 11,931	€ 364,242	93.4%
II-FC	100	€ 0	€ 150,813	€ 0	-€ 5,495	€ 145,318	39.6%
	250	€ 0	€ 227,624	€ 0	-€ 8,294	€ 219,330	59.7%
	500	€ 0	€ 285,021	€ 0	-€ 11,931	€ 273,090	74.3%
	1000	€ 0	€ 327,437	€ 0	-€ 11,931	€ 315,506	85.9%

Table F- 7 CO2 emission reduction by utilizing solar energy

	Installed Solar Power [kW]	Grid [kg CO$_2$]	FC [kg CO$_2$]	Battery [kg CO$_2$]	CO2 emission solar [kg]	Total CO2 reduction [kg]	
I-FCPB	100	1,056	489	11,838	-159	13,224	24.9%
	250	2,536	853	14,509	-390	17,508	33.0%
	500	4,206	1,089	15,504	-682	20,117	37.9%
	1000	5,796	1,258	16,091	-1,018	22,127	41.6%
I-PB	100	2,875	-	15,054	-159	17,771	26.3%
	250	7,258	-	23,249	-390	30,117	44.5%
	500	11,183	-	27,705	-682	38,206	56.4%
	1000	14,090	-	31,267	-1,018	44,339	65.5%
I-FC	100	49	820	-	-159	710	1.7%
	250	1,196	1,693	-	-390	2,498	6.1%
	500	2,688	2,786	-	-682	4,791	11.8%
	1000	4,798	3,924	-	-1,018	7,704	18.9%
II-FCPB	100	-	504	1,448	-159	1,793	10.4%
	250	-	1,218	1,872	-390	2,701	15.6%
	500	-	1,910	2,159	-682	3,386	19.6%
	1000	-	2,525	2,451	-1,018	3,957	22.9%
II-FC	100	-	835	-	-159	676	3.6%
	250	-	2,047	-	-390	1,657	8.8%
	500	-	3,583	-	-682	2,900	15.3%
	1000	-	5,346	-	-1,018	4,328	22.9%

Table F- 8 CO2 emission reduction by utilizing wind energy

	Installed Wind Power [kW]	Grid [kg CO_2]	FC [kg CO_2]	Battery [kg CO_2]	CO2 emission solar [kg]	Total CO2 reduction [kg]	
I-FCPB	100	11,216	4,491	12,340	-6,447	21,601	40.7%
	250	21,410	5,026	12,943	-9,730	29,650	55.8%
	500	26,780	5,277	14,030	-12,183	33,903	63.8%
	1000	29,070	5,401	15,314	-13,996	35,790	67.4%
I-PB	100	22,329	-	20,823	-6,447	36,706	54.2%
	250	27,498	-	26,370	-9,730	44,138	65.2%
	500	29,869	-	30,472	-12,183	48,157	71.1%
	1000	30,703	-	33,593	-13,996	50,300	74.3%
I-FC	100	9,950	4,818	-	-6,447	8,322	20.4%
	250	19,885	5,830	-	-9,730	15,985	39.2%
	500	25,157	7,223	-	-12,183	20,197	49.5%
	1000	28,101	8,535	-	-13,996	22,640	55.5%
II-FCPB	100	-	7,530	-1,208	-6,447	-125	-0.7%
	250	-	11,099	-788	-9,730	581	3.4%
	500	-	12,947	284	-12,183	1,048	6.1%
	1000	-	13,752	1,585	-13,996	1,341	7.7%
II-FC	100	-	7,767	-	-6,447	1,320	7.0%
	250	-	11,723	-	-9,730	1,993	10.5%
	500	-	14,679	-	-12,183	2,495	13.2%
	1000	-	16,863	-	-13,996	2,867	15.2%